Supporting Information

Synthesis of Ni^{II} Porphyrin—Ni^{II} 5,15-Diazaporphyrin Hybrid Tapes

Contents

1. Instruments and Materials

^{1}H NMR (500 MHz) spectra were taken on a Bruker AVANCE-500 spectrometer, and chemical shifts were reported as delta scale in ppm relative to internal standards; $CDCl_3$ (δ = 7.26) and Toluenen-d_8 (δ = 7.09, 7.01, 6.97, 2.08) for ^{1}H NMR. UV/Vis absorption spectra were measured at room temperature on a Shimadzu UV-3600 spectrometer. High-resolution mass spectra were obtained with a Bruker ultrafleXtreme MALDI-TOF/TOF spectrometer with matrix. X-Ray data were taken on an Agilent Supernova X-Ray diffractometer equipped with a large area CCD detector. Redox potentials were measured by cyclic voltammetry on a CHI900 scanning electrochemical microscope. EPR spectra were recorded with a Bruker Magnettech ESR5000 spectrometer. Unless otherwise noted, materials obtained from commercial suppliers were used without further purification.

2. Experimental Procedures and Compound Data

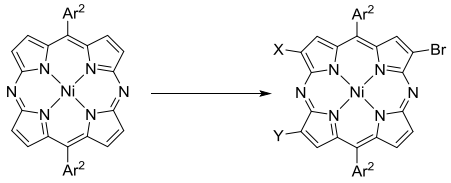

Synthesis of 2a and 2b： A solution of **Ni-DAP** (44 mg, 0.073 mmol) in $CHCl_3$ (10 mL) was added NBS (27 mg, 0.152 mmol), and the resulting mixture was heated at reflux. After 5 h, the solvent was removed under reduced pressure, and the residual was purified by column chromatography on silica gel (CH_2Cl_2/*n*-hexane as an eluent) and recrystallization with CH_2Cl_2/MeOH, a mixture of **2a** and **2b** was obtained as purple solids (38 mg, 69%). HR-MS (MALDI-TOF): *m/z* = 762.0065, calcd for $(C_{36}H_{28}Br_2N_6Ni)^+$ = 762.0068 $[M]^+$. The mixture of **2a** and **2b** was used in the next step without further purification.

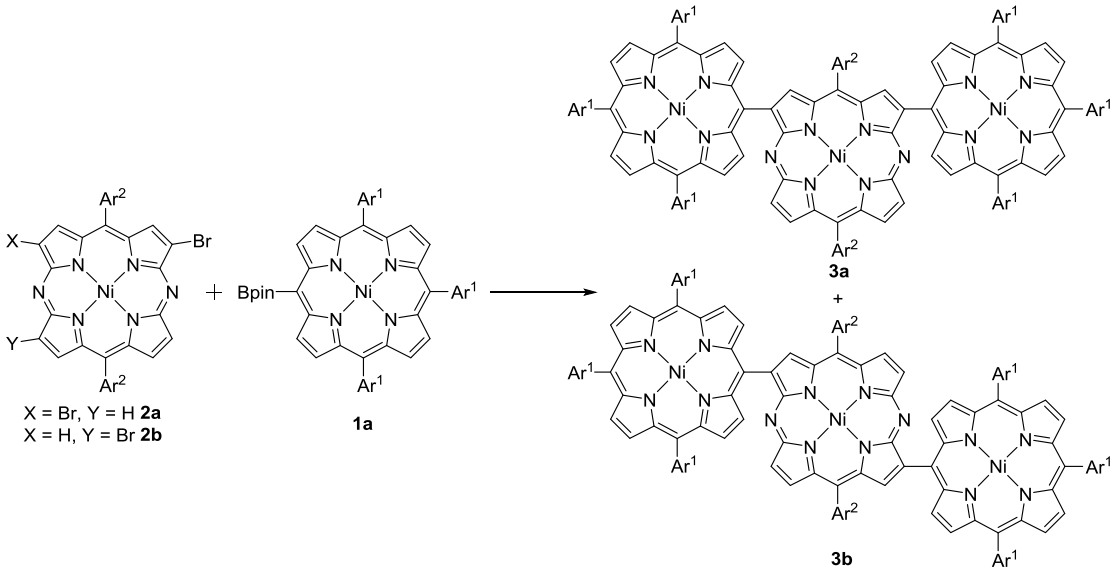

Synthesis of 3a and 3b: A solution of **2** (76.1 mg, 0.10 mmol), **1a** (211.6 mg, 0.20 mmol), $Pd_2(dba)_3$ (9.16 mg, 0.01 mmol), PPh_3 (10.5 mg, 0.04 mmol), Cs_2CO_3 (65.2 mg, 0.2 mmol), and CsF (30.4mg, 0.2 mmol) in a mixture of toluene (4 mL) and DMF (2 mL) was degassed through three freeze-pump-thaw cycles, and the reaction flask was purged with argon. The resulting mixture was refluxed for 48 h. The reaction mixture was diluted with $CHCl_3$, washed with water, and the organic layer was dried over anhydrous Na_2SO_4. After the solvent was evaporated under reduced pressure, the crude products were separated through a GPC column using $CHCl_3$ as an eluent. Separation of **3a** and **3b** was achieved by silica gel column chromatography using CH_2Cl_2/*n*-hexane as an eluent. Recrystallization with CH_2Cl_2/MeOH gave **3a** as red solids (69.0 mg, 0.028 mmol, 28% yield) and **3b** as green solids (69.0 mg, 0.028 mmol, 28% yield). The single crystals of **3a** suitable for X-ray diffraction experiments were grown from its *p*-xylene/MeOH solution.

3a: ^{1}H NMR (500 MHz, $CDCl_3$, 233 K): δ = 9.70 (s, 2H, β-H), 8.95-8.91 (m, 10H, β-H), 8.87 (d, J = 5.0 Hz, 4H, β-H), 8.58 (s, 8H, β-H), 8.15 (br, 2H, Ar-*p*-H), 8.10 (br, 4H, Ar-*o*-H), 7.79 (br, 2H, Ar-*p*-H), 7.74 (br, 6H, Ar-*o*-H (4H) and Ar-*p*-H (2H)), 7.67 (br, 4H, Ar-*o*-H), 7.24 (s, 2H, Ar-*m*-H), 7.14 (s, 2H, Ar-*m*-H), 2.49 (s, 3H, *p*-*Me*), 2.41 (s, 3H, *p*-*Me*), 2.31 (s, 6H, *o*-*Me*), 1.71 (s, 6H, *o*-*Me*), 1.55 (s, 18H, *t*-Bu), 1.47 (s, 18H, *t*-Bu), 1.46 (s, 36H, *t*-Bu), and 1.42 (s, 36H, *t*-Bu) ppm; ^{13}C NMR (125 MHz, $CDCl_3$): δ = 151.7, 151.6, 149.0, 148.9, 146.2, 144.6, 144.2, 143.1, 142.8, 142.7, 142.2, 140.18, 140.16, 139.0, 138.9, 138.5, 138.3, 137.2, 135.5, 135.2, 135.0, 133.2, 132.7, 132.6, 132.4, 132.2, 128.8, 128.7, 128.3, 127.9, 121.9, 121.1, 121.08, 120.7, 120.5, 120.4, 111.7, 35.1, 35.0, 31.8, and 31.7 ppm; UV/Vis (CH_2Cl_2): λ_{max} (ε [$M^{-1}cm^{-1}$]) = 374 (71200), 422 (327000), 532 (54200), and 577 (40300) nm; HR-MS (MALDI-TOF): *m/z* = 2462.1635, calcd for $(C_{160}H_{171}N_{14}Ni_3)^+$ = 2462.1866 ([*M*+H]$^+$).

3b: ^{1}H NMR (500 MHz, $CDCl_3$, 233 K): δ = 9.54 (s, 2H, β-H), 8.93 (d, J = 5.0 Hz, 4H, β-H), 8.90 (d, J = 5.0 Hz, 4H, β-H), 8.85 (d, J = 5.0 Hz, 4H, β-H), 8.83 (d, J = 5.0 Hz, 4H, β-H), 8.70 (d, J = 5.0 Hz, 2H, β-H), 8.62 (d, J = 5.0 Hz, 2H, β-H), 8.12 (br, 2H, Ar-*p*-H), 8.07 (br, 4H, Ar-*o*-H), 7.77 (br, 2H, Ar-*p*-H), 7.72 (br, 2H, Ar-*p*-H), 7.71 (br, 4H, Ar-*o*-H), 7.64 (br, 4H, Ar-*o*-H), 7.17 (s, 4H, Ar-*m*-H), 2.43 (s, 6H, *p*-*Me*), 1.99 (s, 12H, *o*-*Me*), 1.53 (s, 18H, *t*-Bu), 1.46 (s, 18H, *t*-Bu), 1.44 (s, 36H, *t*-Bu), and 1.39 (s, 36H, *t*-Bu) ppm; ^{13}C NMR (125 MHz, $CDCl_3$): δ = 151.7, 151.6, 149.0, 148.9, 146.3, 144.6, 144.1, 143.1, 142.7, 142.65, 142.2, 140.2, 140.1, 139.0, 138.4, 137.2, 135.3, 134.9, 133.3, 132.7, 132.5, 132.4, 132.2, 128.7, 128.6, 128.1, 121.2, 121.1, 121.06, 120.7, 120.4, 111.7, 35.1, 35.0, 31.8, and 31.7 ppm; UV/Vis (CH_2Cl_2): λ_{max} (ε [$M^{-1}cm^{-1}$]) = 373 (73700), 424 (363000), 531 (51000), and 595 (47700) nm; HR-MS (MALDI-TOF): *m/z* = 2462.1656, calcd for $(C_{160}H_{171}N_{14}Ni_3)^+$ = 2462.1866 ([*M*+H]$^+$).

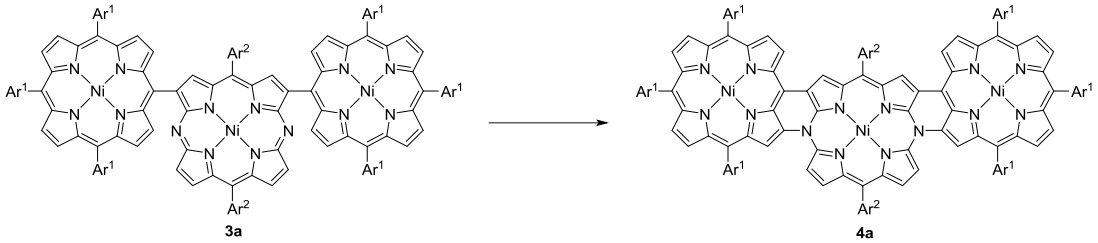

3a **4a**

Synthesis of 4a: To a solution of **3a** (12.3 mg, 0.005 mmol) and AgOTf (128.5 mg, 0.5 mmol) in degassed anhydrous CH_2Cl_2 (10 mL) was added a solution of $FeCl_3$ (8.1 mg, 0.05 mmol) and DDQ (11.4 mg, 0.05 mmol) in nitromethane (1 mL). The reaction mixture was stirred at room temperature for 1 h and the reaction was quenched by addition of a saturated $NaHCO_3$ solution. The reaction mixture was washed with water, and dried over anhydrous sodium sulfate. Evaporation of the solvent followed by silica-gel column chromatography (CH_2Cl_2/*n*-hexane as an eluent) and recrystallization with CH_2Cl_2/MeOH, **4a** obtained as a brown solid (4 mg, 0.0015 mmol, 30% yield).

4a: ^{1}H NMR (500 MHz, Toluene-d_8, 298 K): δ = 9.19 (d, J = 5.0 Hz, 2H, β-H), 9.04 (s, 2H, β-H), 8.83 (d, J = 5.0 Hz, 2H, β-H), 8.77 (d, J = 5.0 Hz, 2H, β-H), 8.72 (d, J = 5.0 Hz, 2H, β-H), 8.68 (d, J = 5.0 Hz, 2H, β-H), 8.62 (d, J = 5.0 Hz, 2H, β-H), 8.17 (br, 4H, Ar-*o*-H), 7.95 (br, 4H, Ar-*o*-H), 7.92 (br, 4H, Ar-*o*-H), 7.84 (br, 2H, Ar-*p*-H), 7.82 (br, 2H, Ar-*p*-H), 7.79 (br, 2H, Ar-*p*-H), 7.56 (s, 2H, β-H), 7.11 (br, 2H, β-H), 6.90 (s, 2H, Ar-*m*-H), 6.85 (s, 2H, Ar-*m*-H), 6.37 (d, J = 5.0 Hz, 2H, β-H), 2.45 (s, 6H, *o*-*Me*), 2.37 (s, 6H, *o*-*Me*), 2.25 (s, 3H, *p*-*Me*), 2.22 (s, 3H, *p*-*Me*), 1.46 (s, 36H, *t*-Bu), 1.40 (s, 36H, *t*-Bu), and 1.37(s, 36H, *t*-Bu) ppm; ^{13}C NMR (125 MHz, $CDCl_3$): δ = 151.1, 149.5, 149.01, 148.98, 148.9, 144.0, 143.6, 142.7, 141.4, 139.9, 139.8, 138.2, 138.0, 137.7, 137.4, 137.2, 136.5, 133.0, 132.9, 132.6, 132.5, 132.4, 131.1, 129.9, 129.4, 128.7, 128.6, 128.5, 128.34, 128.26, 128.1, 125.1, 121.7, 121.1, 121.0, 120.9, 119.5, 118.2, 109.4, 106.9, 106.3, 35.1, 35.0, 31.73, 31.70, and 31.69 ppm; UV/Vis (CH_2Cl_2): λ_{max} (ε [$M^{-1}cm^{-1}$]) = 412 (109800), 473 (78200), 564 (71800), 815 (96800), and 1054 (94900) nm; HR-MS (MALDI-TOF): *m/z* = 2459.1427, calcd for $(C_{160}H_{168}N_{14}Ni_3)^+$ = 2459.1631 ($[M]^+$).

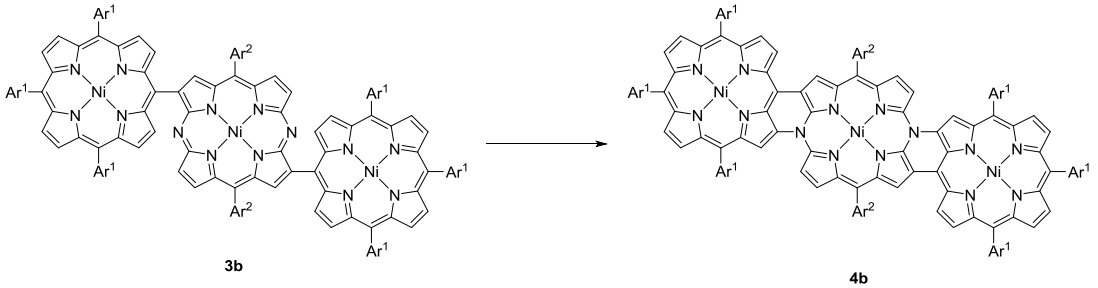

3b **4b**

Synthesis of 4b: To a solution of **3b** (12.3 mg, 0.005 mmol) and AgOTf (128.5 mg, 0.5 mmol) in degassed anhydrous DCM (10 mL) was added a solution of $FeCl_3$ (8.1 mg, 0.05 mmol) and DDQ (11.3 mg, 0.05 mmol) in nitromethane (1 mL). The reaction mixture was carried out at room temperature for 1 h and quenched by addition of a saturated $NaHCO_3$ solution. The

reaction mixture was washed with water, and dried over anhydrous sodium sulfate. Evaporation of the solvent followed by silica-gel column chromatography (CH_2Cl_2/*n*-hexane as an eluent) and recrystallization with CH_2Cl_2/MeOH, **4b** obtained as a brown solid (5 mg, 0.0016 mmol, 32% yield).

4b: ^{1}H NMR (500 MHz, toluene-d_8, 298 K): δ = 9.28 (d, J = 5.0 Hz, 2H, β-H), 9.01 (s, 2H, β-H), 8.81 (d, J = 5.0 Hz, 2H, β-H), 8.77 (d, J = 5.0 Hz, 2H, β-H), 8.74 (d, J = 5.0 Hz, 2H, β-H), 8.72 (d, J = 5.0 Hz, 2H, β-H), 8.65 (d, J = 5.0 Hz, 2H, β-H), 8.15 (br, 4H, Ar-*o*-H), 7.96 (br, 4H, Ar-*o*-H), 7.95 (br, 4H, Ar-*o*-H), 7.84 (t, J = 1.5 Hz, 2H, Ar-*p*-H), 7.80 (m, 4H, Ar-*p*-H), 7.62 (s, 2H, β-H), 7.07 (br, 2H, β-H), 6.90 (s, 4H, Ar-*m*-H), 6.38 (d, J = 5.0 Hz, 2H, β-H), 2.42 (s, 12H, *o-Me*), 2.25 (s, 6H, *p-Me*), 1.42 (s, 36H, *t*-Bu), 1.40 (s, 36H, *t*-Bu), and 1.39 (s, 36H, *t*-Bu) ppm; ^{13}C NMR (125 MHz, toluene-d_8): δ = 153.3, 150.3, 149.8, 149.7, 148.1, 145.4, 144.9, 144.0, 142.7, 142.1, 141.7, 141.64, 141.57, 141.1, 141.0, 139.4, 138.5, 137.0, 136.2, 135.9, 134.1, 133.43, 133.38, 133.3, 133.1, 132.5, 131.8, 130.3, 130.0, 123.8, 122.6, 121.7, 121.6, 121.5, 120.3, 118.7, 117.7, 109.43, 109.38, 108.7, 35.6, 35.53, 35.52, 32.22, 32.18, and 32.15 ppm; UV/Vis (CH_2Cl_2): λ_{max} (ε [$M^{-1}cm^{-1}$]) = 409 (81000), 473 (51500), 560 (50600), 624 (24700), and 857 (138000) nm; HR-MS (MALDI-TOF): *m/z* = 2459.1584, calcd for $(C_{160}H_{168}N_{14}Ni_3)^+$ = 2459.1631 ($[M]^+$).

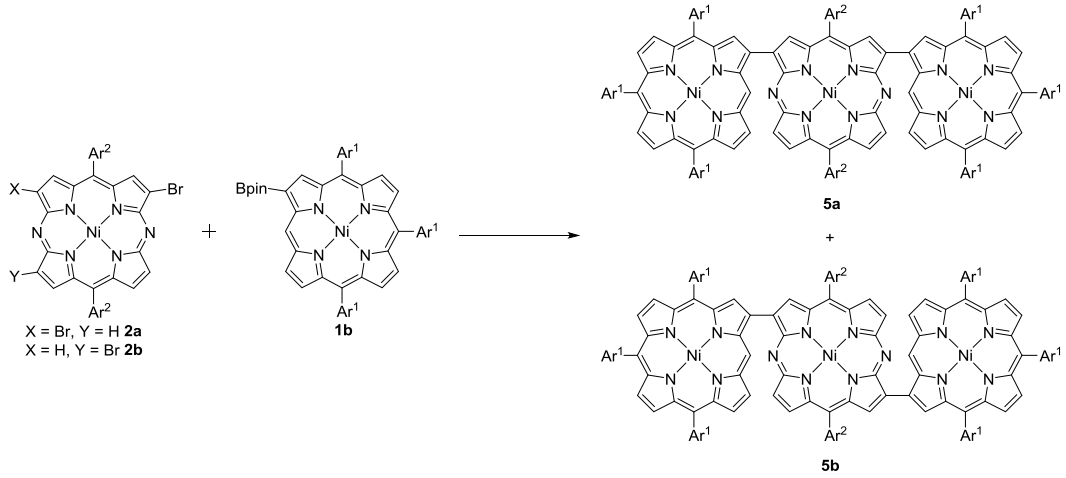

Synthesis of 5a and 5b: A solution of **2** (76.1 mg, 0.10 mmol, 1.0 equiv.), **1b** (211.6 mg, 0.20 mmol, 2.0 equiv.), $Pd_2(dba)_3$ (9.16 mg, 0.01 mmol, 10 mol %), PPh_3 (10.5 mg, 0.04 mmol, 40 mol %), Cs_2CO_3 (65.2 mg, 0.2 mmol, 2.0 equiv.) and CsF (30.4 mg, 0.2 mmol, 2.0 equiv.) in a mixture of toluene (4 mL) and DMF (2 mL) was degassed through three freeze-pump-thaw cycles, and the reaction flask was purged with argon. The resulting mixture was refluxed for 48 h. The reaction mixture was diluted with $CHCl_3$, and the organic extract was washed with water and dried over anhydrous Na_2SO_4. After the solvent was evaporated under reduced pressure, the crude products were separated through a GPC column using $CHCl_3$ as an eluent. Separation of **5a** and **5b** was achieved by silica gel column chromatography using CH_2Cl_2/*n*-hexane as an eluent. Recrystallization with CH_2Cl_2/MeOH gave **5a** as green solids (80.0 mg, 0.032 mmol, 33% yield) and **5b** as green solids (90.5 mg, 0.037 mmol, 37% yield).

5a: ^{1}H NMR (500 MHz, $CDCl_3$, 298 K): δ = 10.46 (s, 2H, *meso*-H)，10.11 (s, 2H, β-H)，9.51

(s, 2H, *β*-H), 9.05-9.02 (m, 4H, *β*-H), 8.97-8.95 (m, 4H, *β*-H), 8.92-8.87 (m, 6H, *β*-H), 8.80 (d, *J* = 5.0 Hz, 2H, *β*-H), 8.19 (d, *J* = 2.0 Hz, 4H, Ar-*o*-H), 7.97 (d, *J* = 2.0 Hz, 4H, Ar-*o*-H), 7.96 (d, *J* = 2.0 Hz, 4H, Ar-*o*-H), 7.81 (t, *J* = 2.0 Hz, 2H, Ar-*p*-H), 7.77 (br, 4H, Ar-*p*-H), 7.39 (s, 2H, Ar-*m*-H), 7.30 (s, 2H, Ar-*m*-H), 2.63 (s, 3H, *p*-*Me*), 2.55 (s, 3H, *p*-*Me*), 2.33 (s, 6H, *o*-*Me*), 1.90 (s, 6H, *o*-*Me*), 1.57 (s, 36H, *t*-Bu), 1.52 (s, 72H, *t*-Bu) ppm; ^{13}C NMR (125 MHz, $CDCl_3$): δ = 151.5, 149.6, 149.1, 149.05, 149.0, 144.1, 143.9, 143.5, 143.4, 143.38, 143.13, 143.05, 142.9, 142.5, 142.3, 141.2, 140.5, 140.3, 140.2, 139.3, 139.1, 138.8, 138.5, 138.0, 135.6, 135.4, 134.7, 133.3, 133.2, 132.7, 132.5, 132.4, 132.3, 132.2, 129.1, 128.9, 128.8, 128.5, 128.1, 121.2, 121.14, 121.11, 120.7, 120.6, 120.0, 105.2, 35.2, 35.1, 31.9, 31.8 ppm; UV/Vis (CH_2Cl_2): λ_{max} (ε [$M^{-1}cm^{-1}$]) = 415 (322000), 532 (54400), 584 (51000) nm; HR-MS (MALDI-TOF): *m/z* = 2462.2041, calcd for $(C_{160}H_{171}N_{14}Ni_3)^+$ = 2462.1866 ([*M*+H]$^+$).

5b: ^{1}H NMR (500 MHz, $CDCl_3$, 298 K): δ = 10.39 (s, 2H, *meso*-H), 10.07 (s, 2H, *β*-H), 9.41 (s, 2H, *β*-H), 9.03 (d, *J* = 5.0 Hz, 2H, *β*-H), 9.00 (d, *J* = 5.0 Hz, 2H, *β*-H), 8.94-8.91 (m, 4H, *β*-H), 8.89 (d, *J* = 5.0 Hz, 2H, *β*-H), 8.86-8.83 (m, 6H, *β*-H), 8.16 (d, *J* = 2.0 Hz, 4H, Ar-*o*-H), 7.95 (d, *J* = 1.5 Hz, 4H, Ar-*o*-H), 7.94 (d, *J* = 2.0 Hz, 4H, Ar-*o*-H), 7.79 (t, *J* = 1.75 Hz, 2H, Ar-*p*-H), 7.74 (t, *J* = 1.75 Hz, 4H, Ar-*p*-H), 7.32 (s, 4H, Ar-*m*-H), 2.57 (s, 6H, *p*-*Me*), 2.09 (s, 12H, *o*-*Me*), 1.54 (s, 36H, *t*-Bu), 1.50 (s, 72H, *t*-Bu) ppm; ^{13}C NMR (125 MHz, $CDCl_3$): δ = 151.5, 149.4, 149.0, 148.98, 148.9, 144.3, 143.5, 143.4, 143.31, 143.30, 143.0, 142.97, 142.8, 142.4, 142.2, 140.9, 140.4, 140.3, 140.1, 139.1, 138.6, 138.0, 135.4, 135.3, 134.9, 133.4, 133.0, 132.6, 132.5, 132.3, 132.2, 132.17, 129.1, 128.9, 128.8, 128.2, 121.2, 121.10, 121.08, 120.6, 120.5, 119.9, 105.1, 35.1, 35.0, 31.9, 31.7 ppm; UV/Vis (CH_2Cl_2): λ_{max} (ε [$M^{-1}cm^{-1}$]) = 417 (220000), 526 (29800), 638 (44100) nm; HR-MS (MALDI-TOF): *m/z* = 2462.2031, calcd for $(C_{160}H_{171}N_{14}Ni_3)^+$ = 2462.1866 ([*M*+H]$^+$).

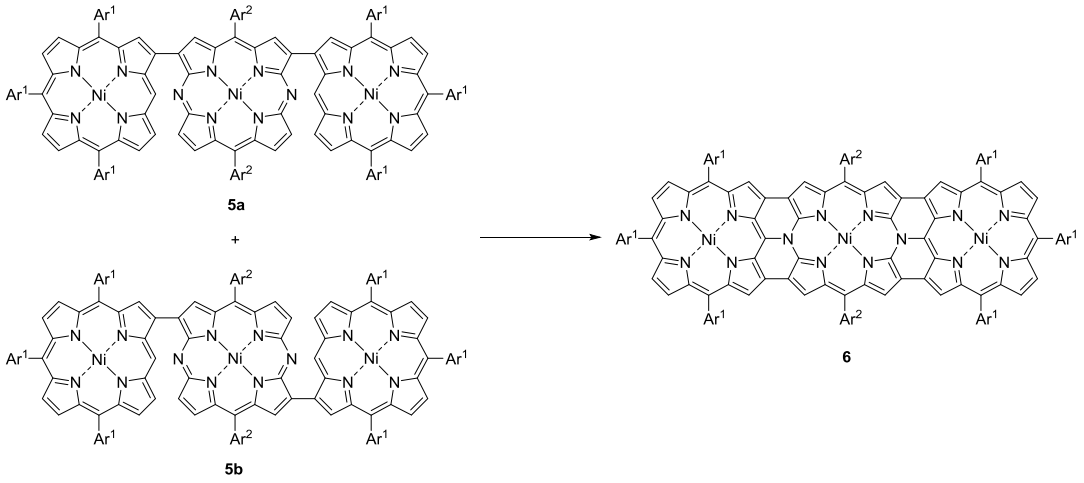

Synthesis of 6: To a solution of a ca. 1:1 mixture of **5a** and **5b** (12.3 mg, 0.005 mmol, 1.0 equiv.) and AgOTf (128.5 mg, 0.5 mmol, 100.0 equiv.) in degassed anhydrous CH_2Cl_2 (10 mL) was added a solution of $FeCl_3$ (8.1 mg, 0.05 mmol, 10 equiv.) and DDQ (11.4 mg, 0.05 mmol, 10 equiv.) in nitromethane (1 mL). The reaction mixture was stirred at room temperature for 1

h and the reaction was quenched by addition of a saturated $NaHCO_3$ solution. The product was extracted with CH_2Cl_2 and the organic extract was washed with water, and dried over anhydrous Na_2SO_4. Evaporation of the solvent followed by silica-gel column chromatography (CH_2Cl_2/*n*-hexane as an eluent) and recrystallization with CH_2Cl_2/MeOH gave **6** as green solids (5.5 mg, 0.0022 mmol, 45% yield). Oxidation of **5a** and **5b** with DDQ and $FeCl_3$ under the similar conditions gave **6** in 25% yield along with *β*-chlorinated products **6-Cl** in ca. 10%. Oxidations of pure **5a** and **5b** under the optimized conditions **6** in ca. 25% yield.

6: ^{1}H NMR (500 MHz, toluene-d_8, 298 K): δ = 9.14 (s, 4H, *β*-H), 8.81 (d, J = 3.8 Hz, 4H, *β*-H), 8.76 (d, J = 3.8 Hz, 4H, *β*-H), 8.13 (s, 8H, Ar), 8.02 (s, 4H, *β*-H), 7.85(br, 10H, Ar), 6.93 (s, 4H, Ar-*m*-H), 2.45 (s, 12H, *o-Me*), 2.36 (s, 6H, *p-Me*), 1.41 (d, J = 6.3 H, 108H, *t*-Bu)ppm; ^{13}C NMR (125 MHz, Toluene-d_8): δ = 149.9, 149.8, 146.8, 145.0, 144.0, 142.1, 141.9, 139.8, 138.4, 135.6, 135.3, 133.7, 132.2, 131.5, 121.9, 121.8, 121.5, 121.1, 118.7, 117.8, 116.7, 114.1, 35.5, 32.2, and 32.1 ppm; UV/Vis (CH_2Cl_2): λ_{max} (ε [$M^{-1}cm^{-1}$]) = 315 (44200), 427 (94800), 672 (239000), and 953 (290000) nm; HR-MS (MALDI-TOF): *m/z* = 2455.1405, calcd for $(C_{160}H_{164}N_{14}Ni_3)^+$ = 2455.1318 ($[M]^+$).
6-Cl: ^{1}H NMR (500 MHz, $CDCl_3$, 298 K): δ = 8.75 (d, 1H, J = 5.0 Hz, *β*-H), 8.69 (d, 1H, J = 5.0 Hz, *β*-H), 8.65-8.58 (m, 6H, *β*-H), 8.11 (s, 1H, *β*-H), 7.92 (m, 4H, *β*-H), 7.90 (m, 2H, *β*-H), 7.85-7.68 (m, 18H, Ar-H), 7.29 (s, 4H, $C_6H_2Me_3$), 2.65 (s, 3H, Me), 2.63 (s, 3H, Me), 2.46-2.44 (m, 12 H, Me), 1.54-1.52 (m, 54H, ^{t}Bu), 1.48-1.46 (m, 54H, ^{t}Bu)

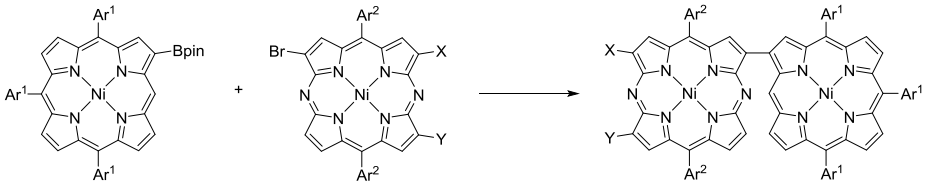

Synthesis of 7: A solution of **1b** (105.8 mg, 0.10 mmol, 1.0 equiv.), **2** (a mixture of **2a** and **2b**) (218.9 mg, 0.30 mmol, 3.0 equiv.), $Pd_2(dba)_3$ (2.8 mg, 0.003 mmol, 3 mol %), PPh_3 (3.2 mg, 0.012 mmol, 12 mol %), Cs_2CO_3 (37.6 mg, 0.10 mmol, 1.0 equiv.), and CsF (15.2 mg, 0.10 mmol, 1.0 equiv.) in a mixture of toluene (4 mL) and DMF (2 mL) was degassed through three freeze-pump-thaw cycles, and the reaction flask was purged with argon. The resulting mixture was stirred at 110 °C for 24 h. The reaction mixture was diluted with $CHCl_3$, and the organic layer was dried over anhydrous Na_2SO_4. After the solvent was evaporated under reduced pressure, the crude products were separated through a GPC column using $CHCl_3$ as an eluent and through a silica gel column using CH_2Cl_2/*n*-hexane as an eluent. Recrystallization with CH_2Cl_2/MeOH gave **7** as dark green solids (82.2 mg, 0.051 mmol, 51% yield).

7 (a mixture of **7a** and **7b**): ^{1}H NMR (500 MHz, $CDCl_3$, 298 K): δ = 10.36-10.32 (*meso*-H), 10.06-10.02 (*β*-H), 9.41-9.29 (*β*-H), 9.00-8.70 (*β*-H), 8.16-7.71 (Ar) 7.35-7.27 (Ar-*m*-H), 2.64-2.56 (*p-Me*), 2.10-1.83 (*o-Me*), and 1.54-1.49 (*t*-Bu) ppm; UV/Vis (CH_2Cl_2): λ_{max} (ε [$M^{-1}cm^{-1}$]) = 416 (257000), 531 (32000), and 588 (47500) nm; HR-MS (MALDI-TOF): *m/z* =

1611.5995, calcd for $(C_{98}H_{100}BrN_{10}Ni_2)^+$ = 1611.6017 $[M+H]^+$.

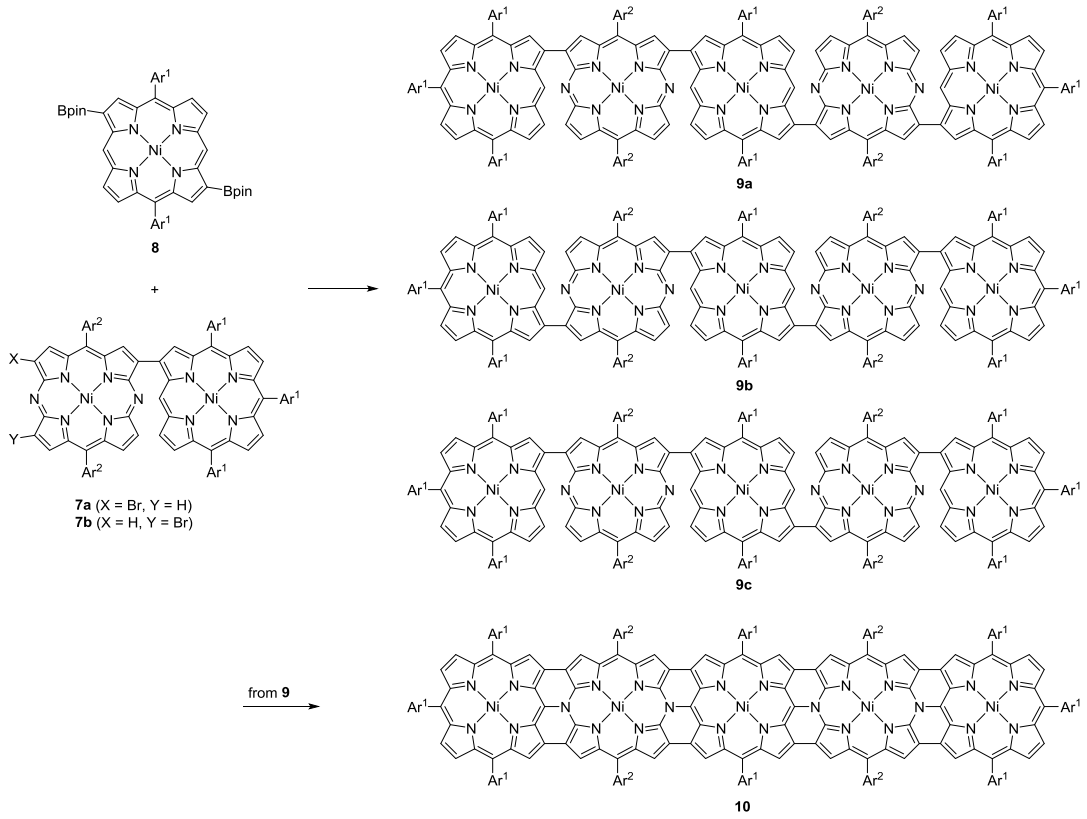

Synthesis of 9: A solution of **8** (39.8 mg, 0.04 mmol, 1.0 equiv.), **7** (a mixture of **7a** and **7b**) (129.1 mg, 0.08 mmol, 2.0 equiv.), $Pd_2(dba)_3$ (3.6 mg, 0.004 mmol, 10 mol %), PPh_3 (4.2 mg, 0.016 mmol, 40 mol %), Cs_2CO_3 (30.0 mg, 0.08 mmol, 2.0 equiv.), and CsF (12.1 mg, 0.08 mmol, 2.0 equiv.) in a mixture of toluene (4 mL) and DMF (2 mL) was degassed through three freeze-pump-thaw cycles, and the reaction flask was purged with argon. The resulting mixture was refluxed for 48 h. The reaction mixture was diluted with $CHCl_3$, and the products were extracted with CH_2Cl_2. The organic extract was washed with water and dried over anhydrous Na_2SO_4. After concentrating under reduced pressure, the crude product was separated by GPC (eluent: $CHCl_3$) and silica gel column chromatography (eluent: CH_2Cl_2/*n*-hexane). Precipitation with CH_2Cl_2/MeOH gave **9** obtained as dark green solids (92 mg, 0.024 mmol, 61% yield).

9 (a mixture of **9a**, **9b**, and **9c**): ^{1}H NMR (500 MHz, $CDCl_3$, 298 K): δ = 10.59-10.42 (*meso*-H), 10.23-8.80 (β-H), 8.47-7.76 (Ar), 7.40-7.31 (Ar-*m*-H), 2.63-1.91 (*o*-*Me* and *p*-*Me*), 1.59-1.51 (*t*-Bu) ppm; UV/Vis (CH_2Cl_2): λ_{max} (ε [$M^{-1}cm^{-1}$]) = 414(484000), 529 (89600), 627 (107000) nm; HR-MS (MALDI-TOF): *m/z* = 3804.6956, calcd for $(C_{244}H_{249}N_{24}Ni_5)^+$ = 3804.6984 ($[M+H]^+$).

Synthesis of 10: To a solution of **9** (15.2 mg, 0.004 mmol) and AgOTf (205.5 mg, 0.8 mmol) in degassed anhydrous DCM (10 mL) was added a solution of $FeCl_3$ (26.0 mg, 0.16 mmol) and DDQ (36.3 mg, 0.16 mmol) in nitromethane (1 mL). The reaction mixture was carried out

at room temperature for 1 h and quenched by addition of a saturated $NaHCO_3$ solution. The reaction mixture was washed with water, and dried over anhydrous sodium sulfate. Evaporation of the solvent followed by silica-gel column chromatography (CH_2Cl_2/*n*-hexane as an eluent) and recrystallization with CH_2Cl_2/MeOH, **10** obtained as a brown solid (2.4 mg, 0.0006 mmol, 16% yield).

10: ^{1}H NMR (500 MHz, Toluene-d_8, 298 K): δ = 9.17 (s, 4H, β-H), 9.05 (s, 4H, β-H), 8.82 (d, J = 5.0 Hz, 4H, β-H), 8.76 (d, J = 5.0 Hz, 4H, β-H), 8.20 (br, 4H, β-H), 8.12 (d, J = 1.0 Hz, 8H, Ar), 8.00 (br, 4H, β-H), 7.86-7.79 (m, 24H, Ar), 2.43 (s, 24H, *o*-*Me*), 2.34 (s, 12H, *p*-*Me*), 1.40 (s, 36H, *t*-Bu), 1.39 (s, 72H, *t*-Bu), 1.36 (s, 36H, *t*-Bu) ppm; UV/Vis (CH_2Cl_2): λ_{max} (ε [$M^{-1}cm^{-1}$]) = 326 (75200), 405 (116000), 737 (287000), 1037 (66600), 1168 (558000) nm; HR-MS (MALDI-TOF): *m/z* = 3791.5733, calcd for $(C_{244}H_{236}N_{24}Ni_5)^+$ = 3791.5966 ([*M*]$^+$).

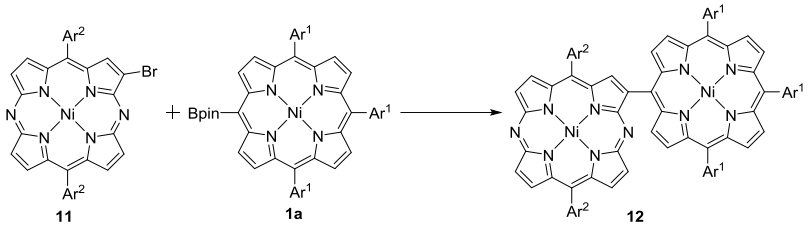

Synthesis of 12: A solution of **11** (68.4 mg, 0.10 mmol, 1.0 equiv.), **1a** (105.8 mg, 0.10 mmol, 1.0 equiv.), $Pd_2(dba)_3$ (4.58 mg, 0.005 mmol, 5 mol %), PPh_3 (5.24 mg, 0.02 mmol, 20 mol %), Cs_2CO_3 (32.6 mg, 0.10 mmol, 1.0 equiv.), and CsF (15.2 mg, 0.10 mmol, 1.0 equiv.) in a mixture of toluene (4 mL) and DMF (2 mL) was degassed through three freeze-pump-thaw cycles, and the reaction flask was purged with argon. The resulting mixture was refluxed for 48 h. The reaction mixture was diluted with $CHCl_3$, and the organic layer was washed with water, and dried over anhydrous Na_2SO_4. After the solvent was evaporated under reduced pressure, the crude products were separated through a GPC column using CH_2Cl_2/*n*-hexane as an eluent. Recrystallization with CH_2Cl_2/MeOH gave **12** as dark green solids (108.5 mg, 0.071mmol, 71% yield).

12: ^{1}H NMR (500 MHz, $CDCl_3$, 233 K): δ = 9.58 (s, 1H, β-H), 9.31 (d, J = 5.0 Hz, 1H, β-H), 9.26 (d, J = 5.0 Hz, 1H, β-H), 9.00 (d, J = 5.0 Hz, 1H, β-H), 8.96 (d, J = 5.0 Hz, 2H, β-H), 8.93 (d, J = 5.0 Hz, 2H, β-H), 8.87 (d, J = 5.0 Hz, 1H, β-H), 8.83 (br, 4H, β-H), 8.60 (d, J = 5.0 Hz, 1H, β-H), 8.57 (d, J = 5.0 Hz, 1H, β-H), 8.15 (br, 1H, Ar-*p*-H), 8.08 (br, 2H, Ar-*o*-H), 7.79 (br, 1H, Ar-*p*-H), 7.74 (br, 1H, Ar-*p*-H), 7.73 (br, 2H, Ar-*o*-H), 7.66 (br, 2H, Ar-*o*-H), 7.27 (s, 2H, Ar-*m*-H), 7.22 (s, 2H, Ar-*m*-H), 2.56 (s, 3H, *p*-*Me*), 2.52 (s, 3H, *p*-*Me*), 2.07 (s, 6H, *o*-*Me*), 1.77 (s, 6H, *o*-*Me*), 1.55 (s, 9H, *t*-Bu), 1.47 (s, 9H, *t*-Bu), 1.45 (s, 18H, *t*-Bu), and 1.41 (s, 18H, *t*-Bu) ppm; UV/Vis (CH_2Cl_2): λ_{max} (ε [$M^{-1}cm^{-1}$]) = 372 (94800), 421 (317000), 532 (38400), and 581 (60600) nm; HR-MS (MALDI-TOF): *m/z* = 1533.6948, calcd for $(C_{98}H_{101}N_{10}Ni_2)^+$ = 1533.6912 ([*M*+H]$^+$).

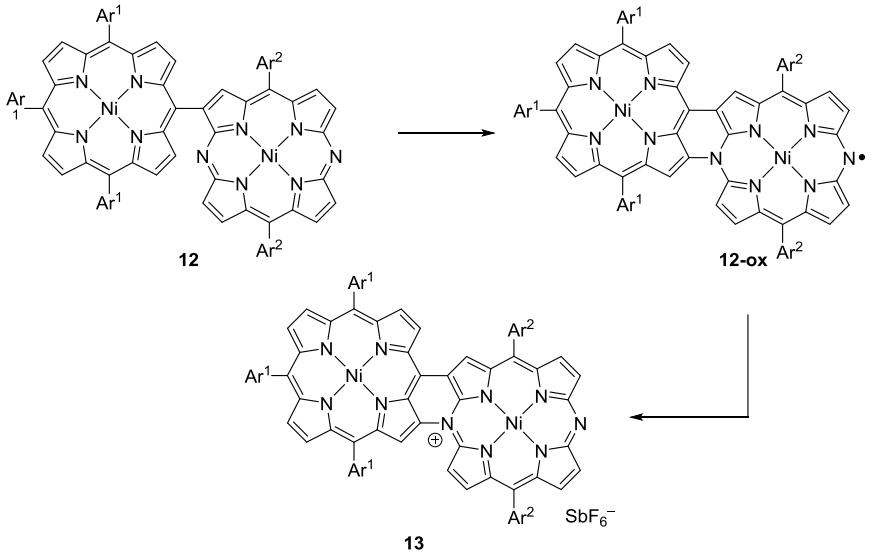

Synthesis of 13: To a solution of **12** (15.3 mg, 0.01 mmol, 1.0 equiv.) in degassed anhydrous CH_2Cl_2 (10 mL) was added a solution of $FeCl_3$ (8.1 mg, 0.05 mmol, 5 equiv.) and DDQ (11.4 mg, 0.05 mmol, 5 equiv.) in nitromethane (1 mL). The reaction mixture was stirred at room temperature for 1 h and the reaction was quenched by addition of a saturated $NaHCO_3$ solution. The product was extracted with CH_2Cl_2 and the organic extract was washed with water, and dried over anhydrous Na_2SO_4. After concentrating under reduced pressure, the residue was dissolved in CH_2Cl_2 under N_2, to which TBPA·SbF_6 (7.90 mg, 0.011 mmol, 1.1 equiv.) was added and the reaction mixture was further stirred for 1 h at room temperature. The reaction mixture was passed through a short Celite pad with CH_2Cl_2 as an eluent. Recrystallization from CH_2Cl_2/*n*-hexane afforded **13** (10 mg, 0.006 mmol, 60%).

12-ox: UV/Vis (CH_2Cl_2): λ_{max} (ε [$M^{-1}cm^{-1}$]) = 316 (32500), 430 (63100), 472 (67500), 543 (37600), 776 (30900), and 1357 (7860) nm; HR-MS (MALDI-TOF): *m/z* = 1531.6771, calcd for $(C_{98}H_{99}N_{10}Ni_2)^+$ = 1531.6756 ($[M]^+$).

13: ^{1}H NMR (500 MHz, $CDCl_3$, 298 K): δ = 9.07 (s, 1H, β-H), 8.52 (br, 6H, β-H), 8.28-8.25 (m, 5H, β-H), 7.81-7.70 (m, 11H, β-H and Ar), 7.29 (s, 2H, Ar-*m*-H), 7.27 (s, 2H, Ar-*m*-H), 2.60 (s, 6H, *p*-*Me*), 2.03 (s, 6H, *o*-*Me*), 1.95 (s, 6H, *o*-*Me*), 1.49 (s, 18H, *t*-Bu), 1.48 (s, 18H, *t*-Bu), and 1.45 (s, 18H, *t*-Bu) ppm; UV/Vis (CH_2Cl_2): λ_{max} (ε [$M^{-1}cm^{-1}$]) = 436 (57100), 748 (11700), and 1020 (24600) nm; HR-MS (MALDI-TOF): *m/z* = 1531.6747, calcd for $(C_{98}H_{99}N_{10}Ni_2)^+$ = 1531.6756 ($[M$-$SbF_6]^+$).

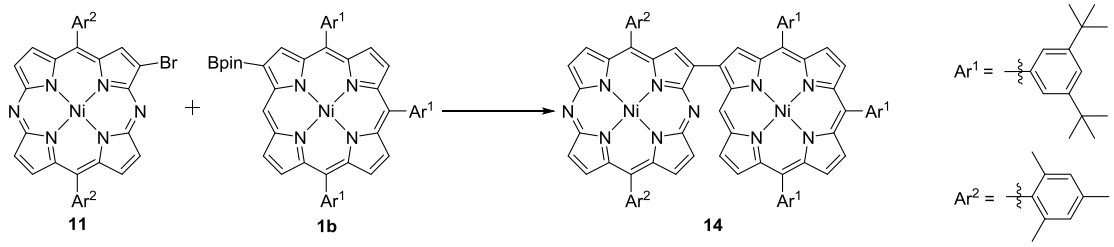

Synthesis of 14: A solution of **11** (68.4 mg, 0.10 mmol, 1.0 equiv.), **1b** (105.8 mg, 0.10 mmol, 1.0 equiv.), $Pd_2(dba)_3$ (4.58 mg, 0.005 mmol, 5 mol %), PPh_3 (5.24 mg, 0.02 mmol, 20 mol %), Cs_2CO_3 (32.6 mg, 0.10 mmol, 1.0 equiv.), and CsF (15.2 mg, 0.10 mmol, 1.0 equiv.) in a mixture of toluene (4 mL) and DMF (2 mL) was degassed through three freeze-pump-thaw cycles, and the reaction flask was purged with argon. The resulting mixture was refluxed for 48 h. The reaction mixture was diluted with $CHCl_3$, and the organic extract was washed with water and dried over anhydrous Na_2SO_4. After the solvent was evaporated under reduced pressure, the crude product was separated through a GPC column using $CHCl_3$ as an eluent and through a silica gel column using CH_2Cl_2/*n*-hexane as an eluent. Recrystallization with CH_2Cl_2/MeOH gave **14** obtained as dark green solids (115.1 mg, 0.075 mmol, 75% yield).

14: ^{1}H NMR (500 MHz, $CDCl_3$, 298 K): δ = 10.35 (s, 1H, *meso*-H), 10.03 (s, 1H, β-H), 9.39 (s, 1H, β-H), 9.24 (d, J = 5.0 Hz, 1H, β-H), 9.21 (d, J = 5.0 Hz, 1H, β-H), 8.98-8.96 (m, 2H, β-H), 8.93-8.83 (m, 7H, β-H), 8.75 (d, J = 5.0 Hz, 1H, β-H), 8.14 (d, J = 1.5 Hz, 2H, Ar-*o*-H), 7.94 (d, J = 1.5 Hz, 2H, Ar-*o*-H), 7.93 (d, J = 1.5 Hz, 2H, Ar-*o*-H), 7.76 (br, 1H, Ar-*p*-H), 7.74 (br, 2H, Ar-*p*-H), 7.32 (s, 2H, Ar-*m*-H), 7.28 (s, 2H, Ar-*m*-H), 2.61 (s, 3H, *p*-*Me*), 2.57 (s, 3H, *p*-*Me*), 2.05 (s, 6H, *o*-*Me*), 1.84 (s, 6H, *o*-*Me*), 1.52 (s, 18H, *t*-Bu), and 1.49 (s, 36H, *t*-Bu) ppm; UV/Vis (CH_2Cl_2): λ_{max} (ε [$M^{-1}cm^{-1}$]) = 416 (272000), 532 (35200), and 592 (48700) nm; HR-MS (MALDI-TOF): *m/z* = 1532.6794, calcd for $(C_{98}H_{100}N_{10}Ni_2)^+$ = 1532.6834 ($[M]^+$).

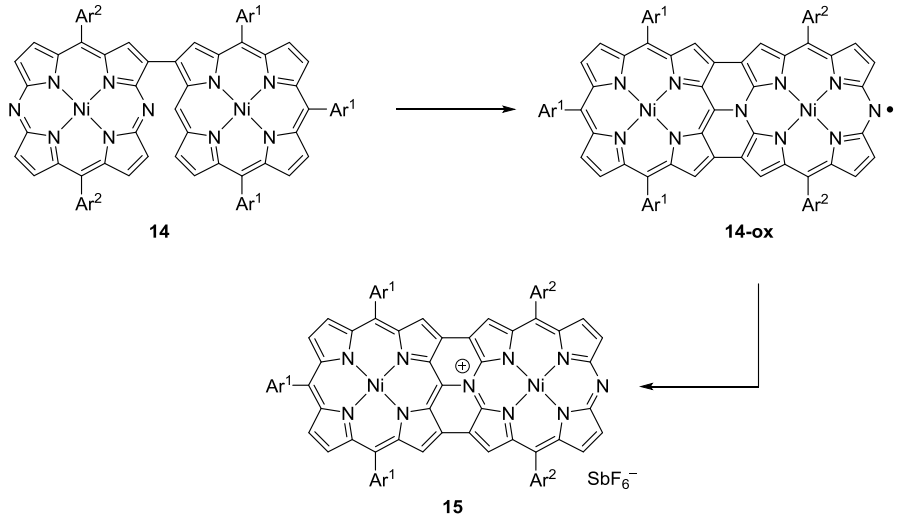

Synthesis of 15: To a solution of **14** (15.3 mg, 0.01 mmol, 1.0 equiv.) in degassed anhydrous CH_2Cl_2 (10 mL) was added a solution of $FeCl_3$ (16.2 mg, 0.1 mmol, 10 equiv.) and DDQ (22.7 mg, 0.1 mmol, 10 equiv.) in nitromethane (1 mL). The reaction mixture was stirred at room temperature for 1 h and the reaction was quenched by addition of a saturated $NaHCO_3$ solution. The product was extracted with CH_2Cl_2 and the organic extract was washed with water, and dried over anhydrous Na_2SO_4. After concentrating under reduced pressure, the residue was dissolved in CH_2Cl_2 under N_2, TBPA·SbF_6 (7.90 mg, 0.011 mmol, 1.1 equiv.) was added and the reaction mixture was further stirred for 1 h at room temperature. The reaction mixture was passed through a short Celite pad with CH_2Cl_2 as an eluent. Recrystallization

from CH_2Cl_2/*n*-hexane afforded **15** (14 mg, 0.008 mmol, 80%). The single crystals of **15** suitable for X-ray diffraction experiments were grown from its PhCl/Octane solution.

14-ox: UV/Vis (CH_2Cl_2): λ_{max} (ε [$M^{-1}cm^{-1}$]) = 390 (64200), 444 (72700), 583 (153000), 783 (35300), 1000 (12800), 1200 (14500) nm; HR-MS (MALDI-TOF): *m/z* = 1530.6597, calcd for $(C_{98}H_{98}N_{10}Ni_2)^+$ = 1530.6677 ([*M*+H]$^+$).
15: ^{1}H NMR (500 MHz, $CDCl_3$, 213 K): δ = 7.84 (br, 2H, β-H), 7.55-7.32 (m, 15H, Ar and β-H), 7.06 (s, 4H, Ar-*m*-H), 6.74 (br, 2H, β-H), 6.70 (br, 2H, β-H), 2.43 (s, 6H, *p-Me*), 1.91 (s, 12H, *o-Me*), 1.36 (s, 36H, *t*-Bu), and 1.31 (s, 18H, *t*-Bu) ppm (signals are very broad and difficult to assign); UV/Vis (CH_2Cl_2): λ_{max} (ε [$M^{-1}cm^{-1}$]) = 381 (61700), 444 (65400), 563 (61800), 766 (14900), 834 (15800), and 974 (36500) nm; HR-MS (MALDI-TOF): *m/z* = 1529.6697, calcd for $(C_{98}H_{97}N_{10}Ni_2)^+$ = 1529.6599 ([*M*-SbF_6]$^+$).

3. NMR and EPR Spectra

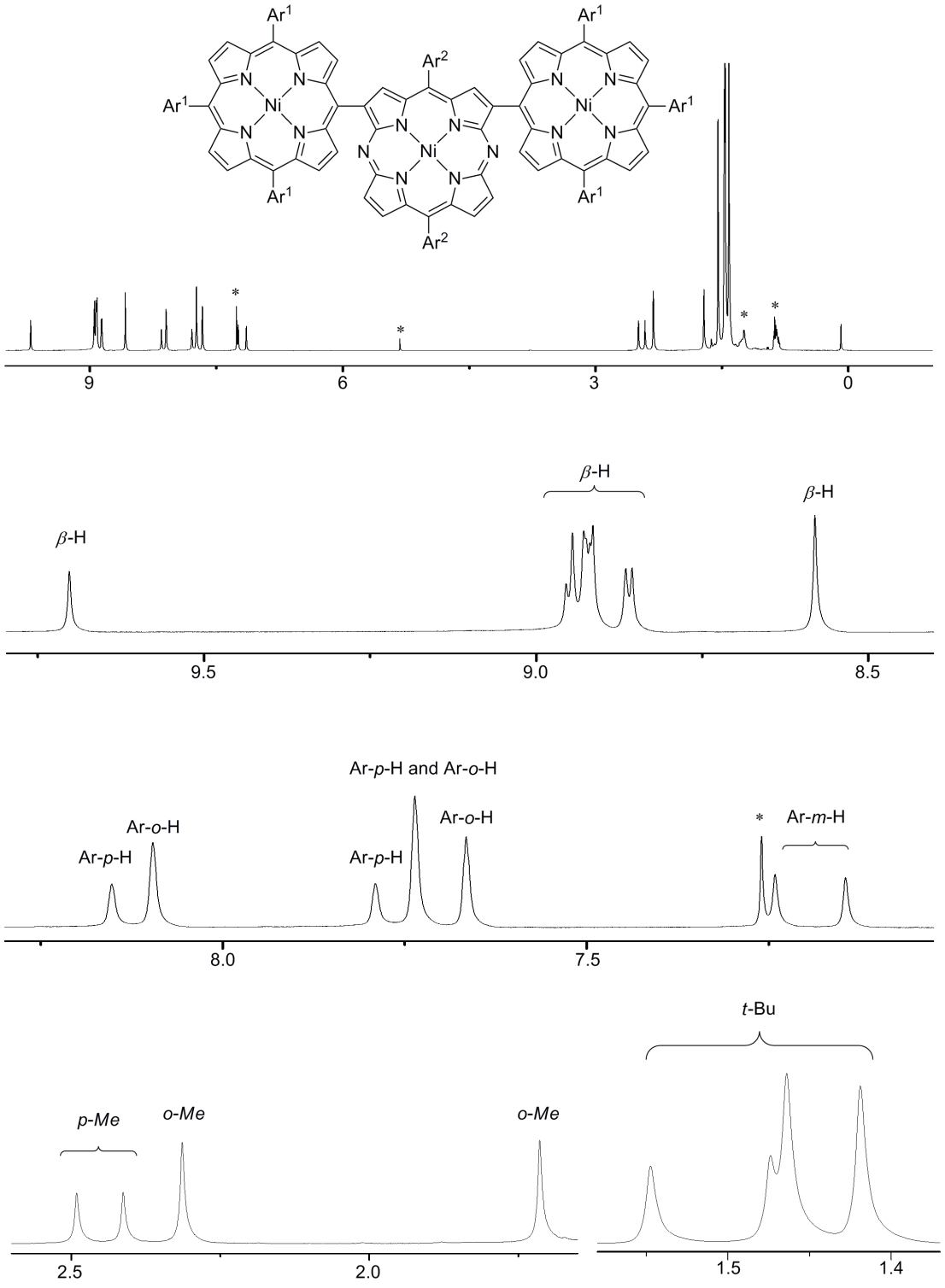

Figure S1-1. ^{1}H NMR spectrum of **3a** in $CDCl_3$ at 233 K.

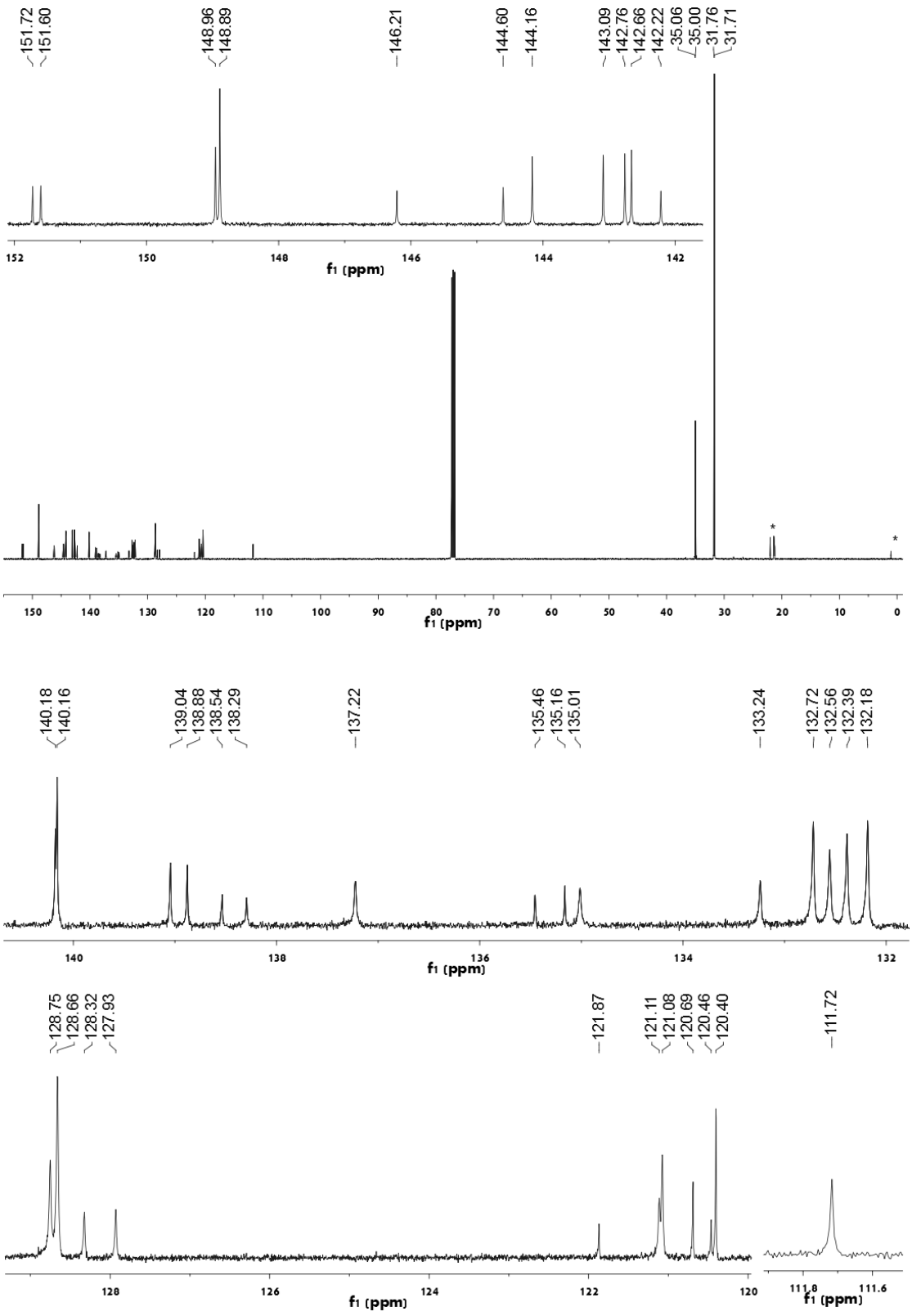

Figure S1-2. ^{13}C NMR spectrum of **3a** in $CDCl_3$ at 298 K.

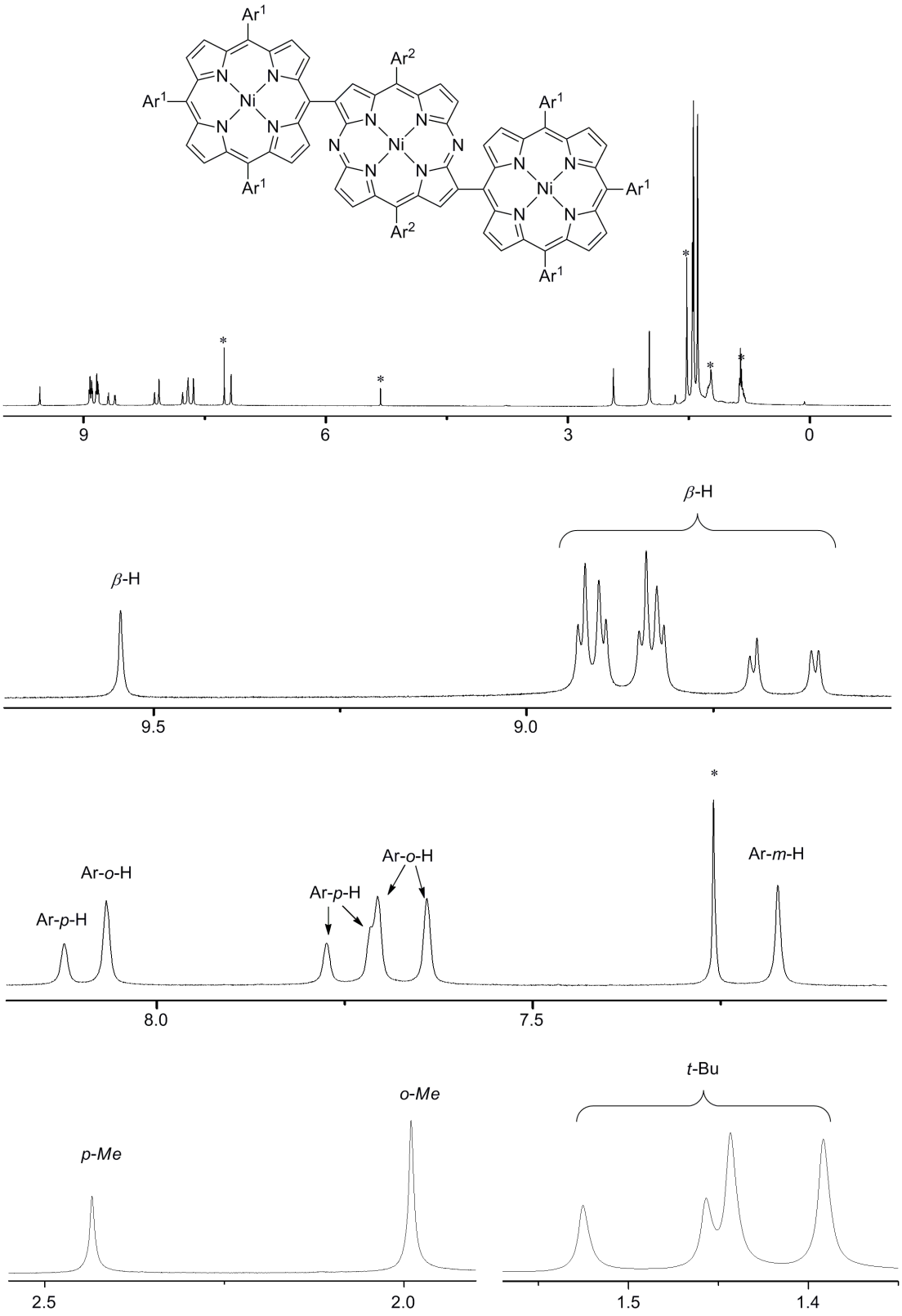

Figure S1-3. ^{1}H NMR spectrum of **3b** in $CDCl_3$ at 233 K.

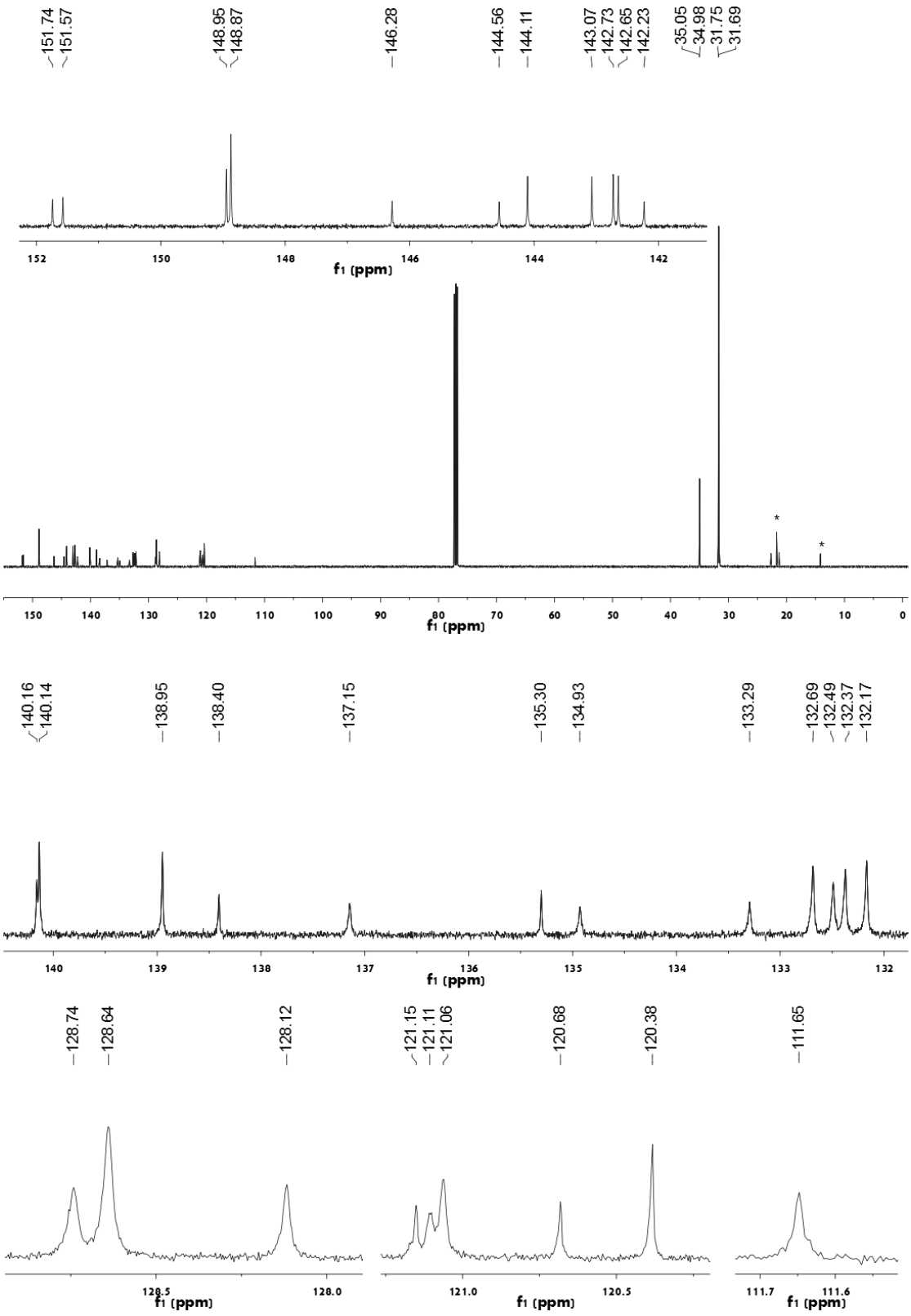

Figure S1-4. ^{13}C NMR spectrum of **3b** in $CDCl_3$ at 298 K.

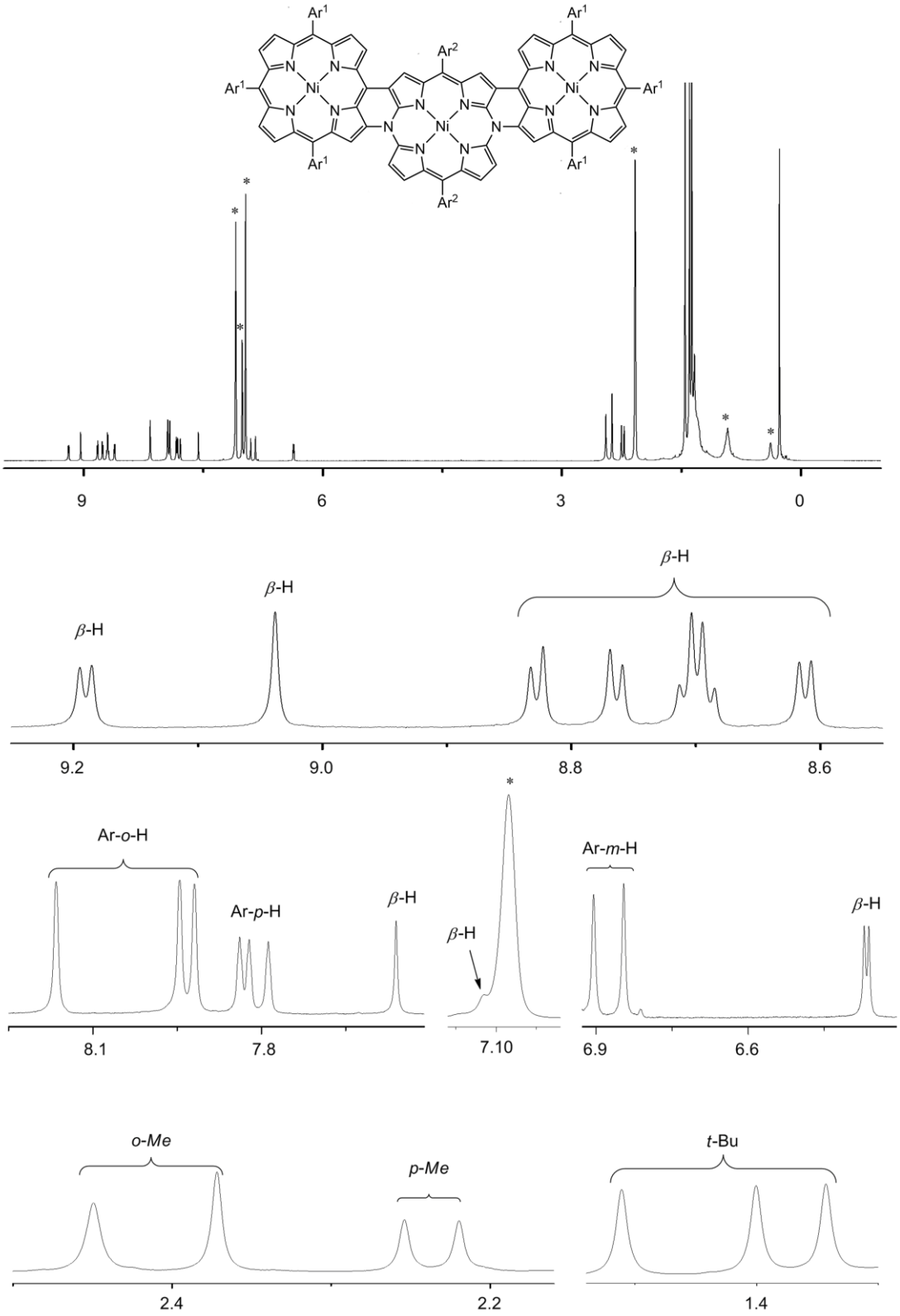

Figure S1-5. ^{1}H NMR spectrum of **4a** in Toluene-d_8 at 298 K.

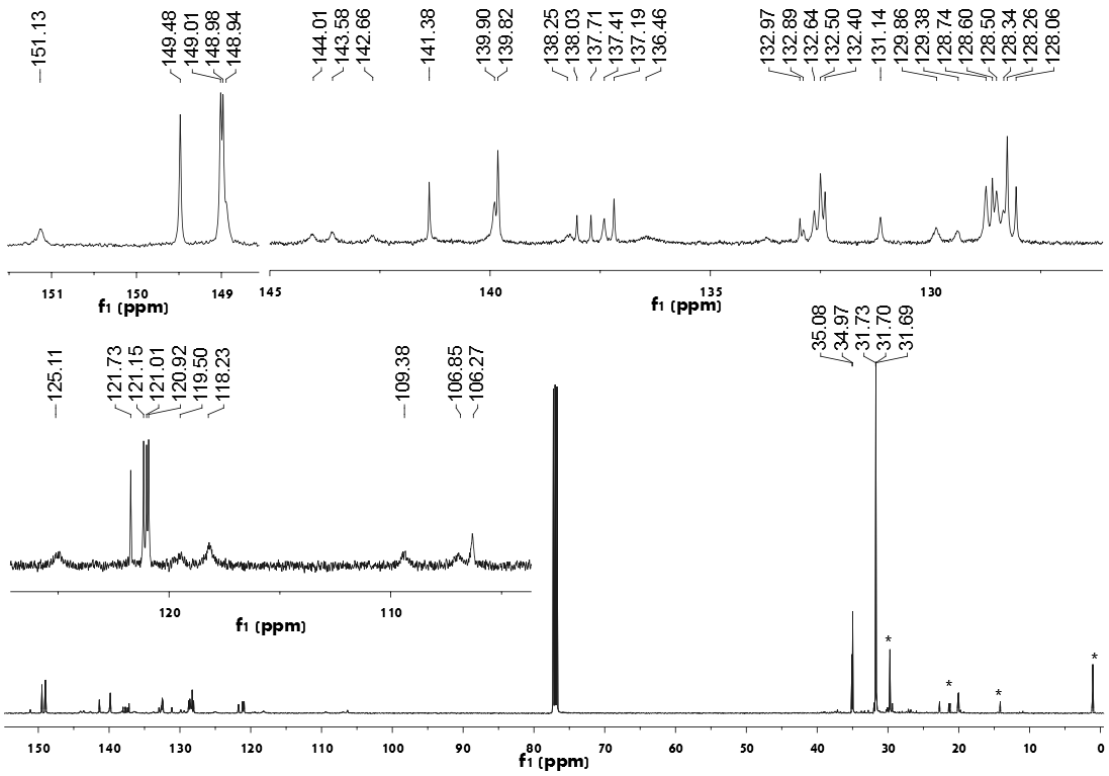

Figure S1-6. ^{13}C NMR spectrum of **4a** in $CDCl_3$.

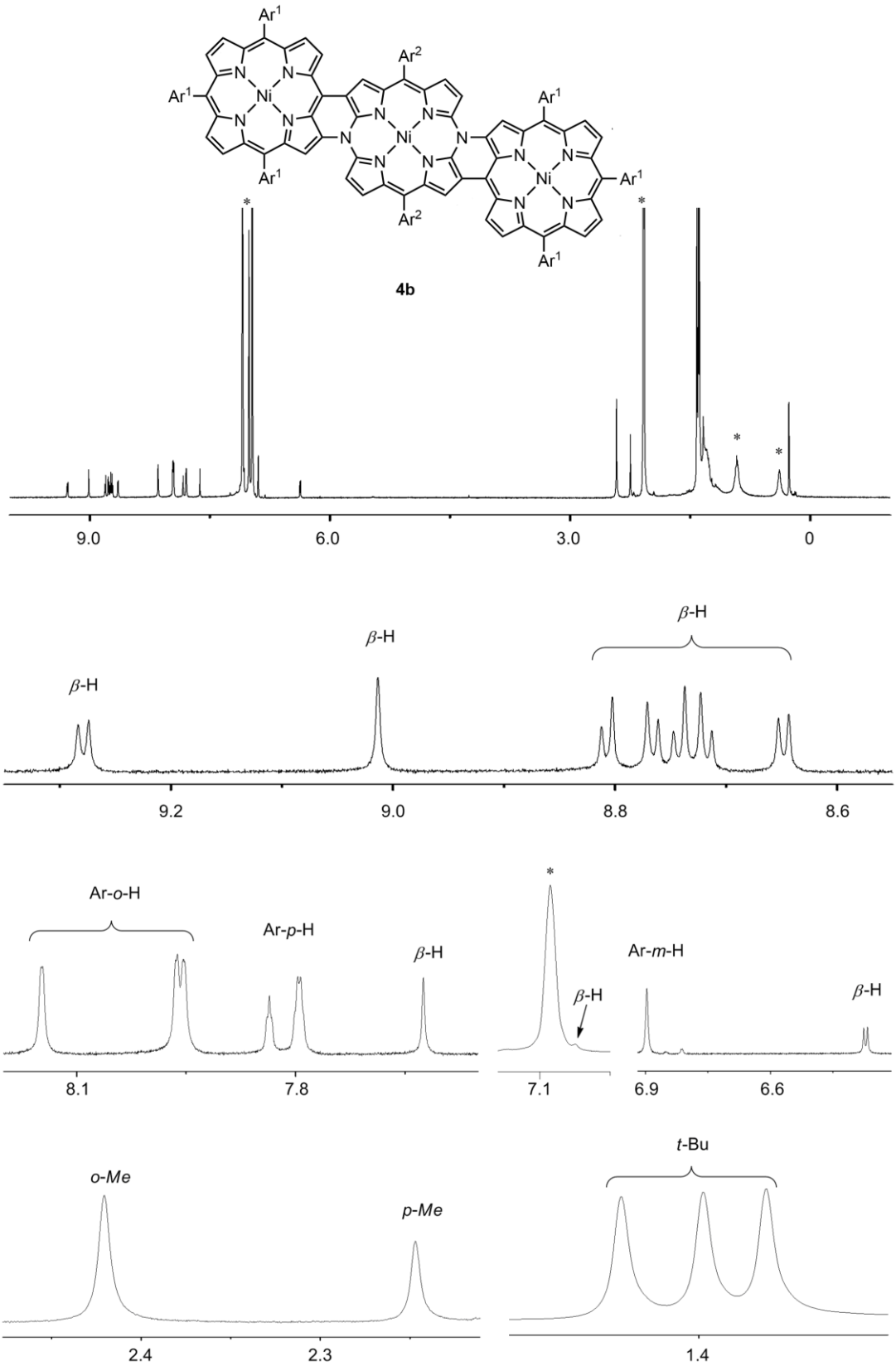

Figure S1-7. ^{1}H NMR spectrum of **4b** in Toluene-d_8 at 298 K.

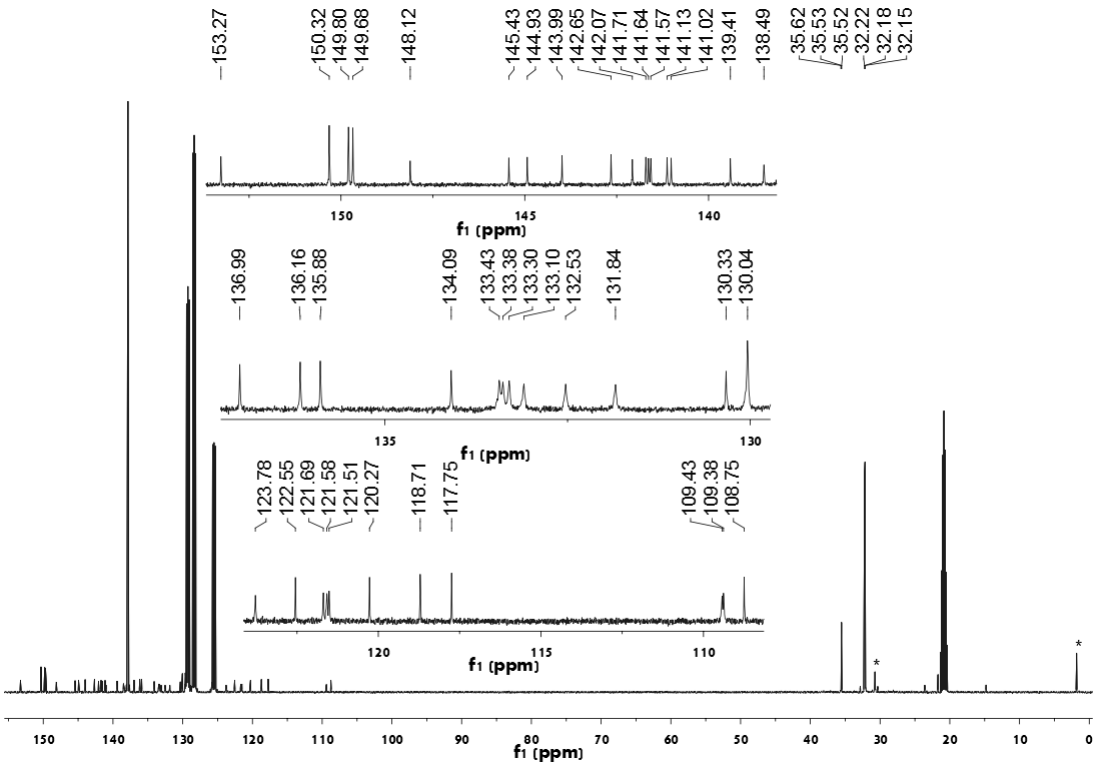

Figure S1-8. ^{13}C NMR spectrum of **4b** in toluene-d_8.

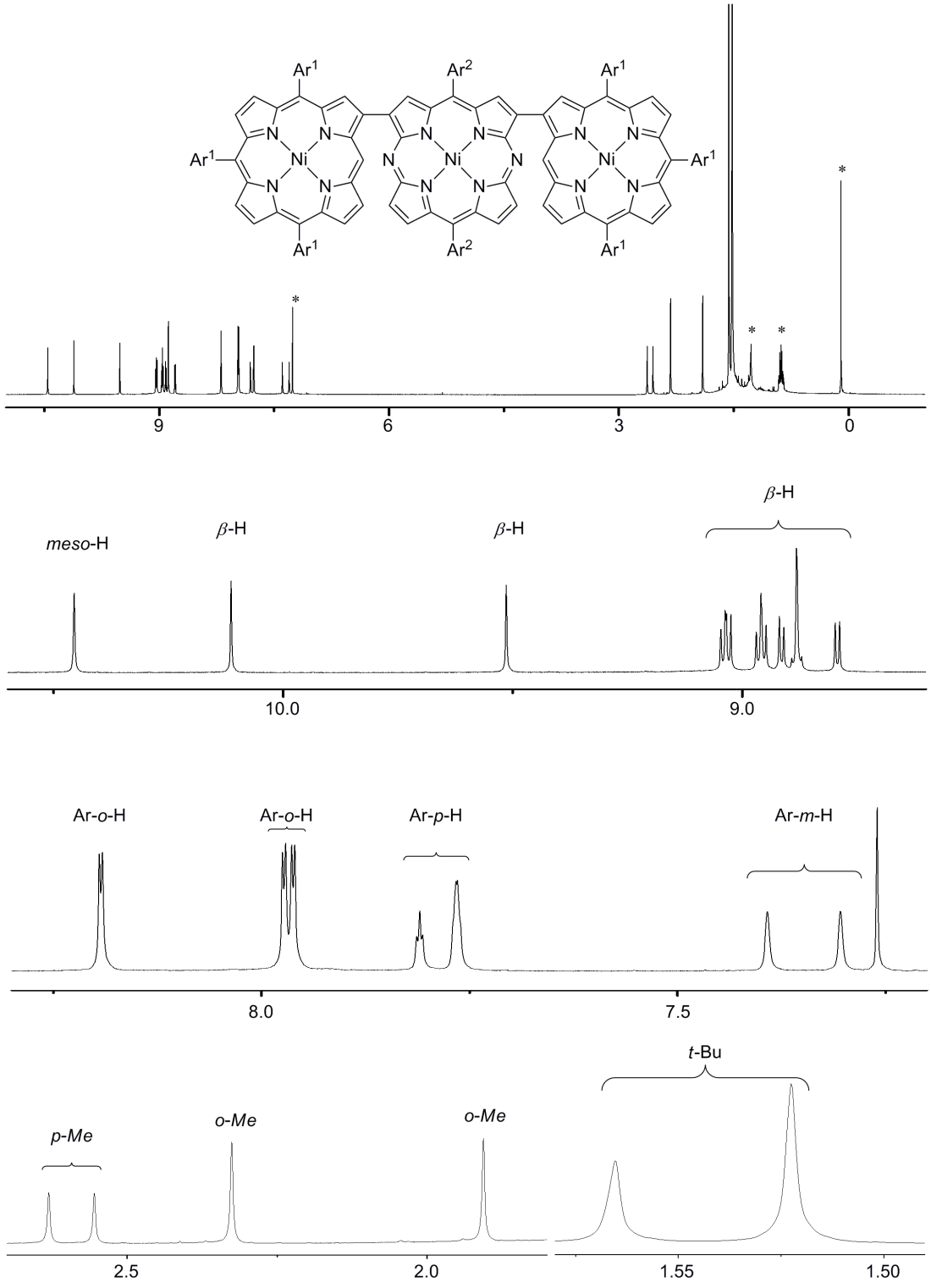

Figure S1-9. ^{1}H NMR spectrum of **5a** in $CDCl_3$ at 298 K.

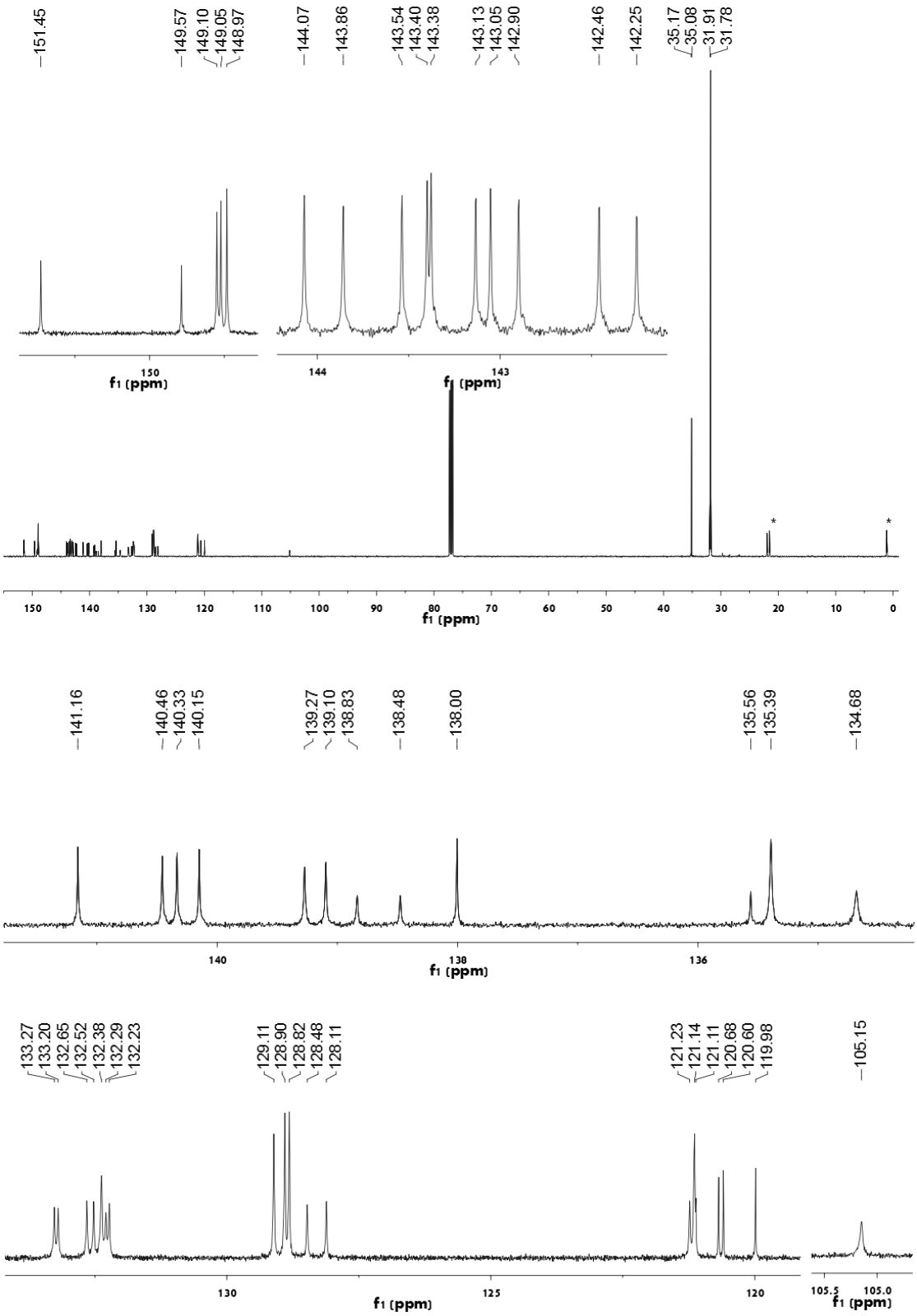

Figure S1-10. ^{13}C NMR spectrum of **5a** in $CDCl_3$ at 298 K.

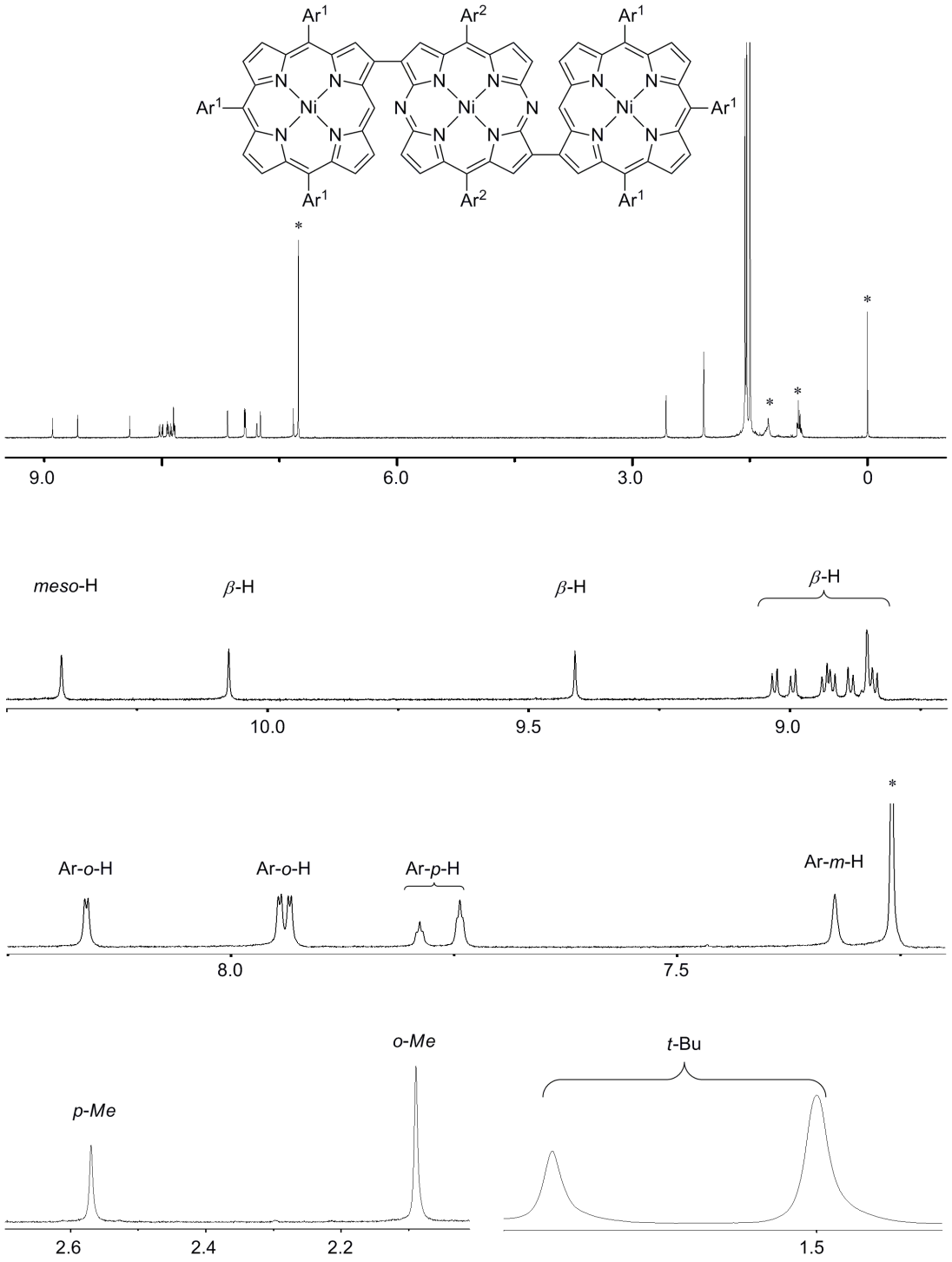

Figure S1-11. ^{1}H NMR spectrum of **5b** in $CDCl_3$ at 298 K.

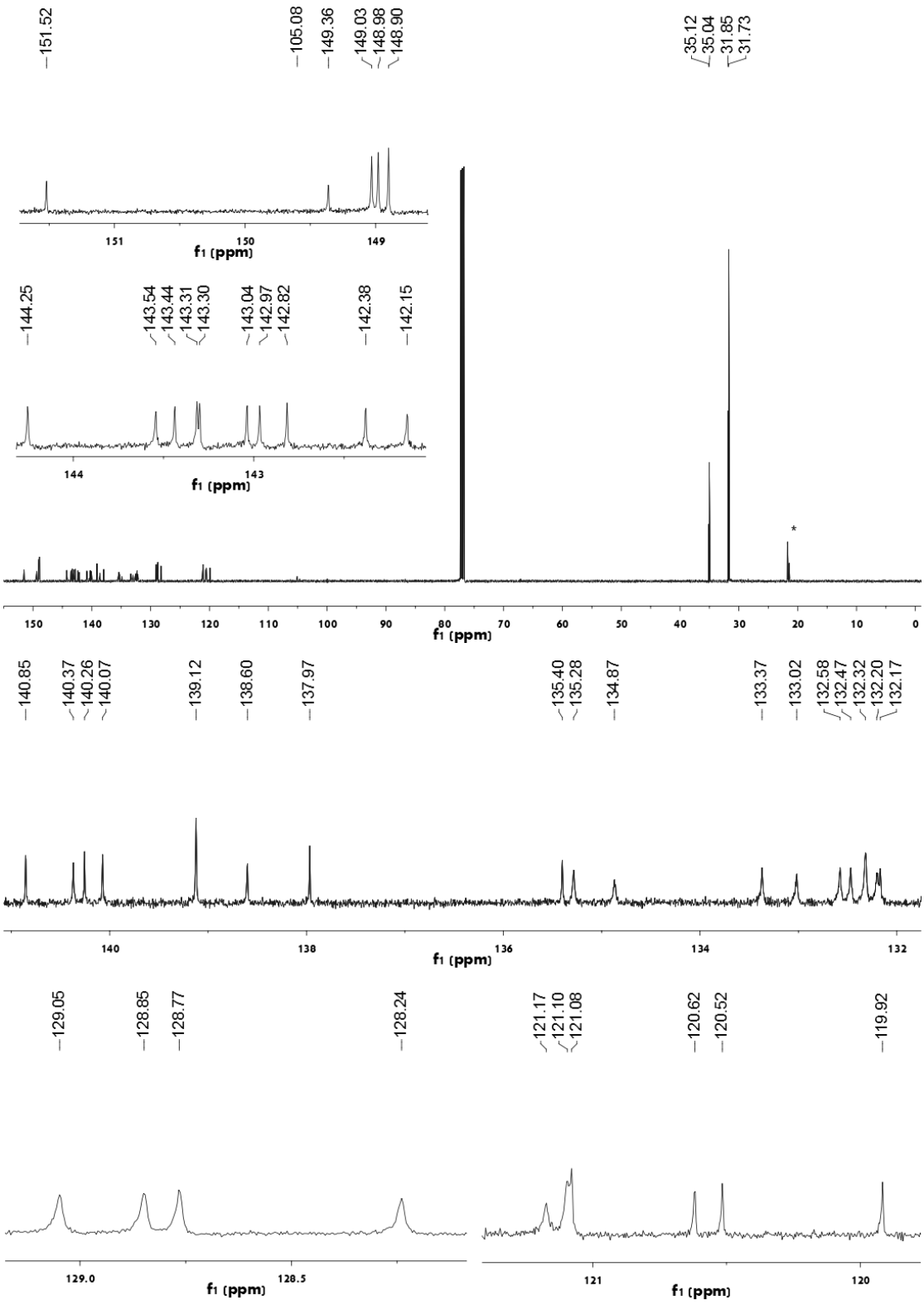

Figure S1-12. ^{13}C NMR spectrum of **5b** in $CDCl_3$ at 298 K.

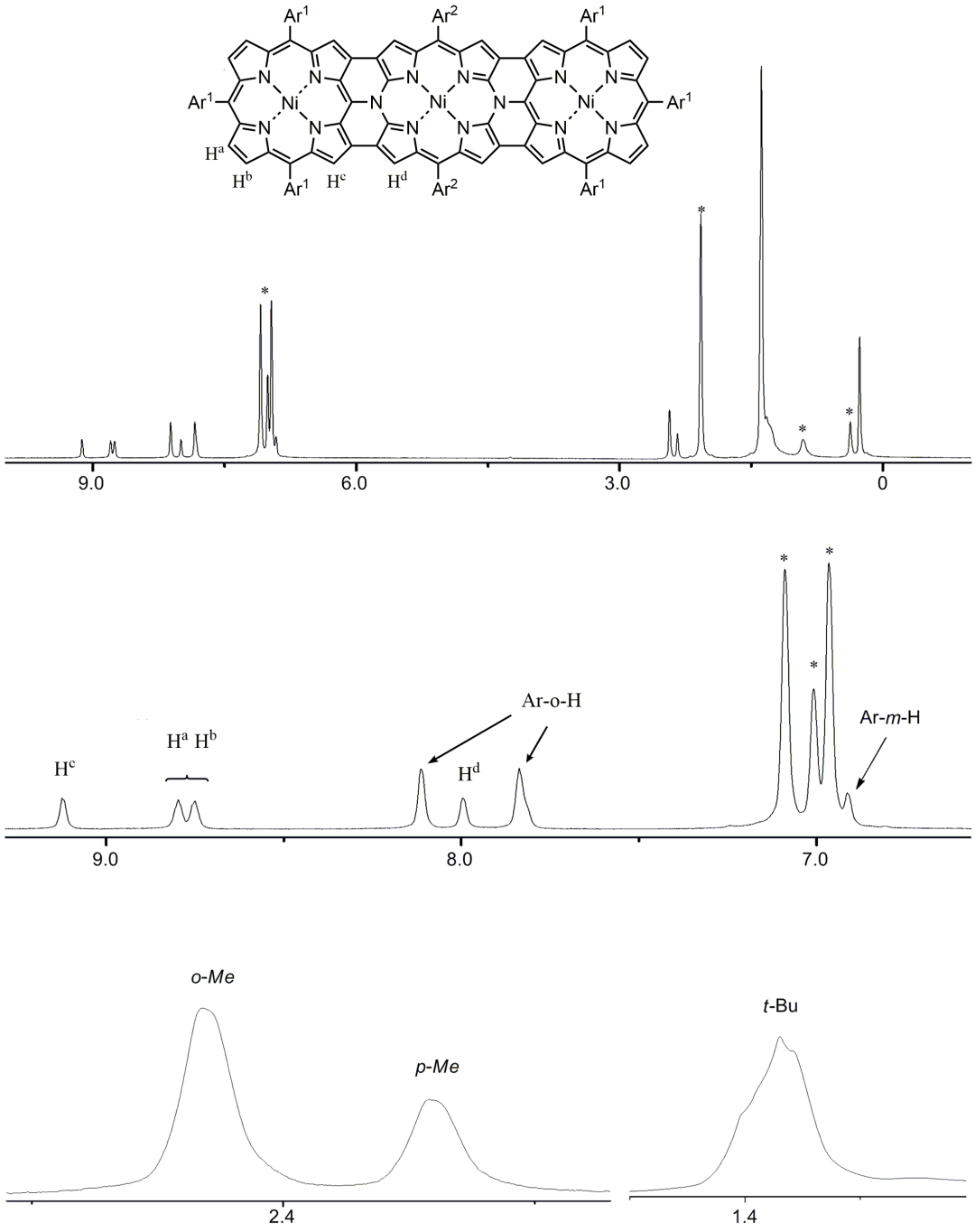

Figure S1-13. ^{1}H NMR spectrum of **6** in toluene-d_8 at 298 K.

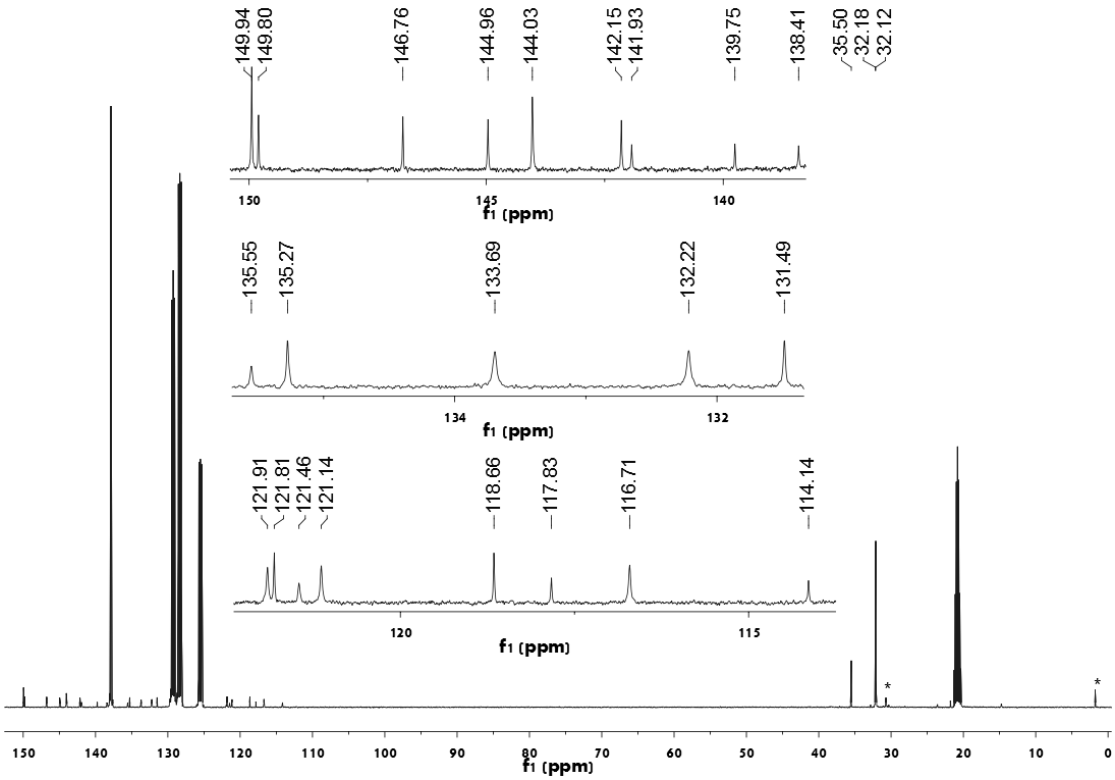

Figure S1-14. ^{13}C NMR spectrum of **6** in toluene-d_8.

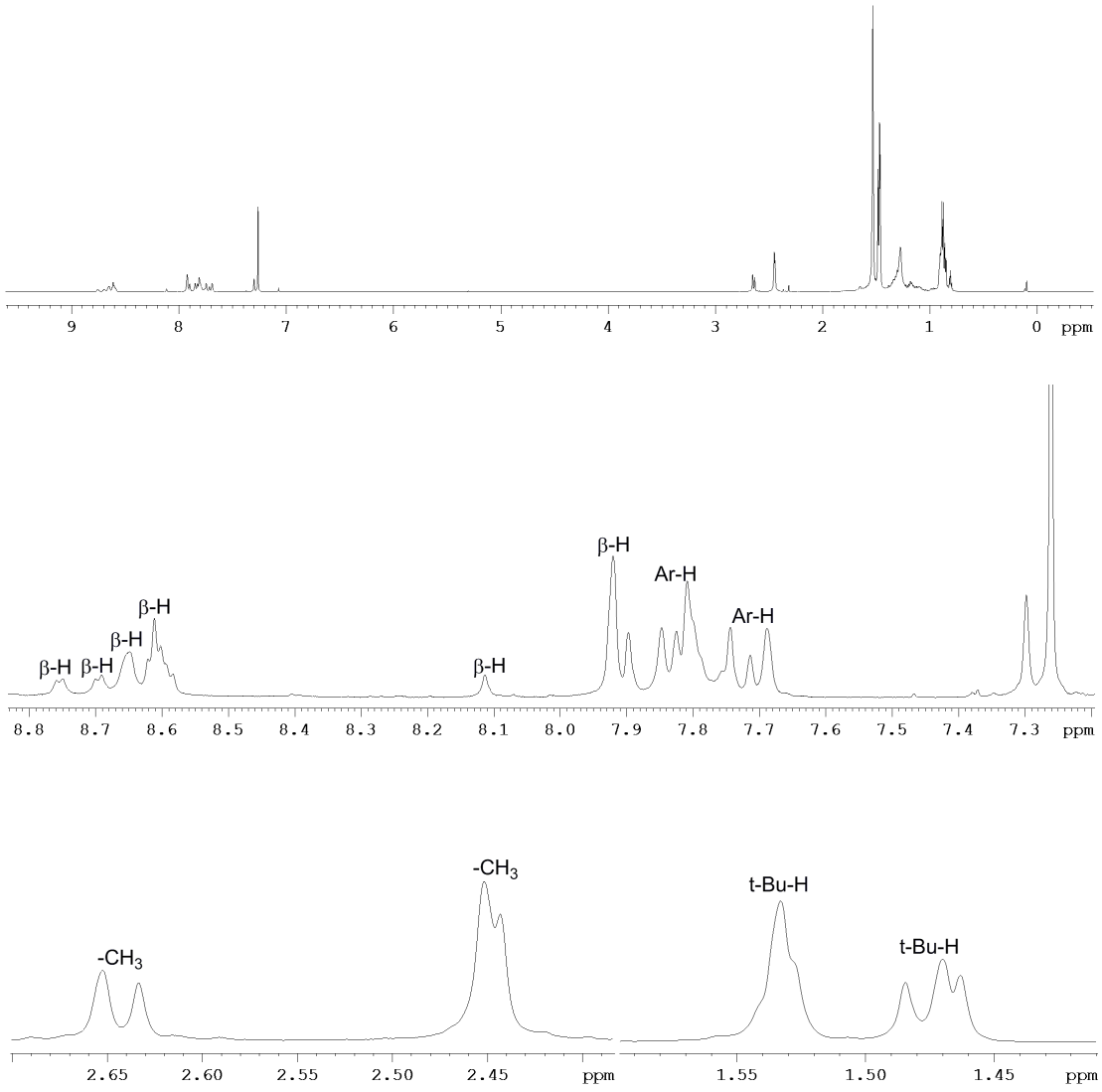

Figure S1-15. ^{1}H NMR spectrum of **6-Cl** in $CDCl_3$ at 298 K.

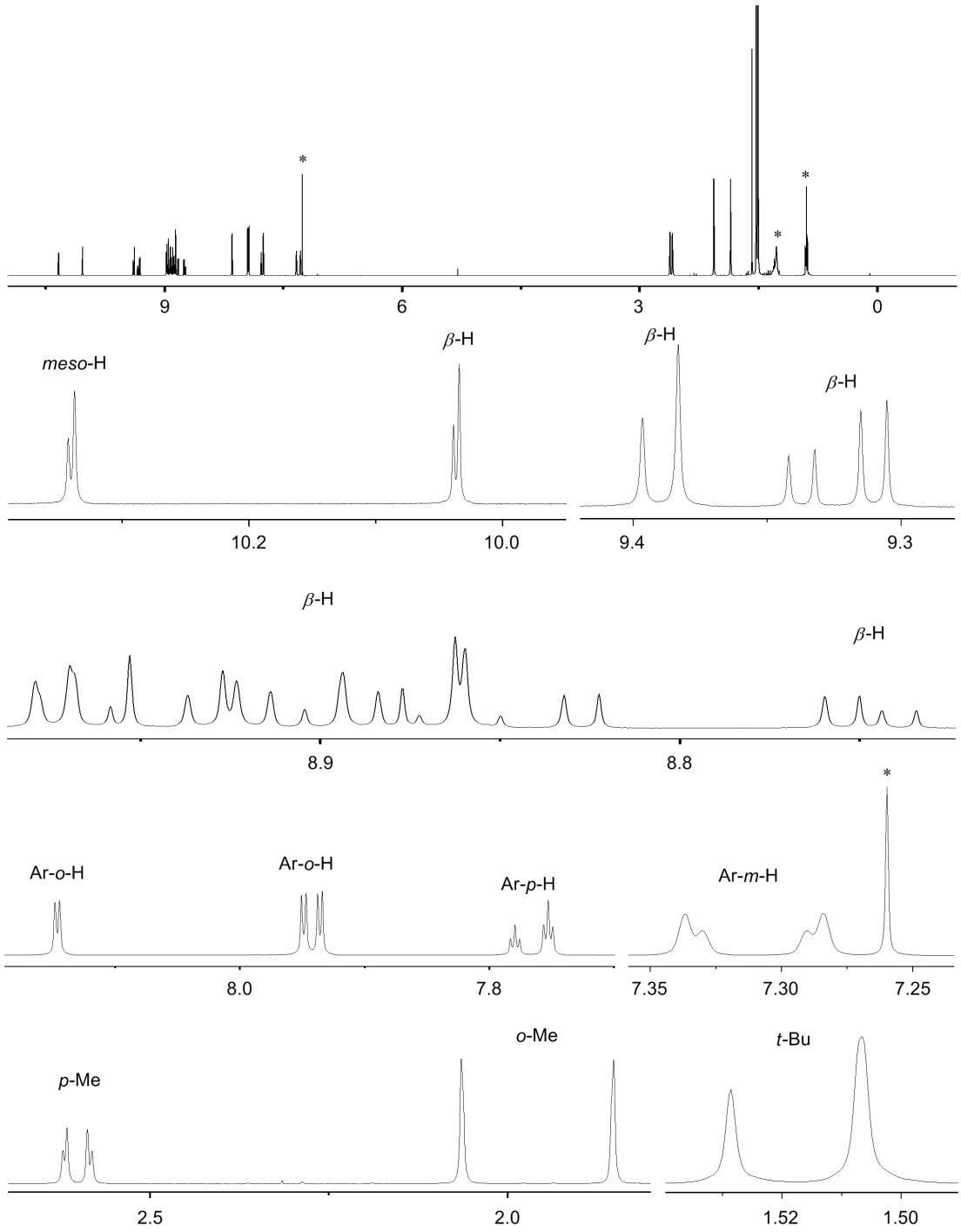

Figure S1-16. ^{1}H NMR spectrum of **7** in $CDCl_3$ at 298 K.

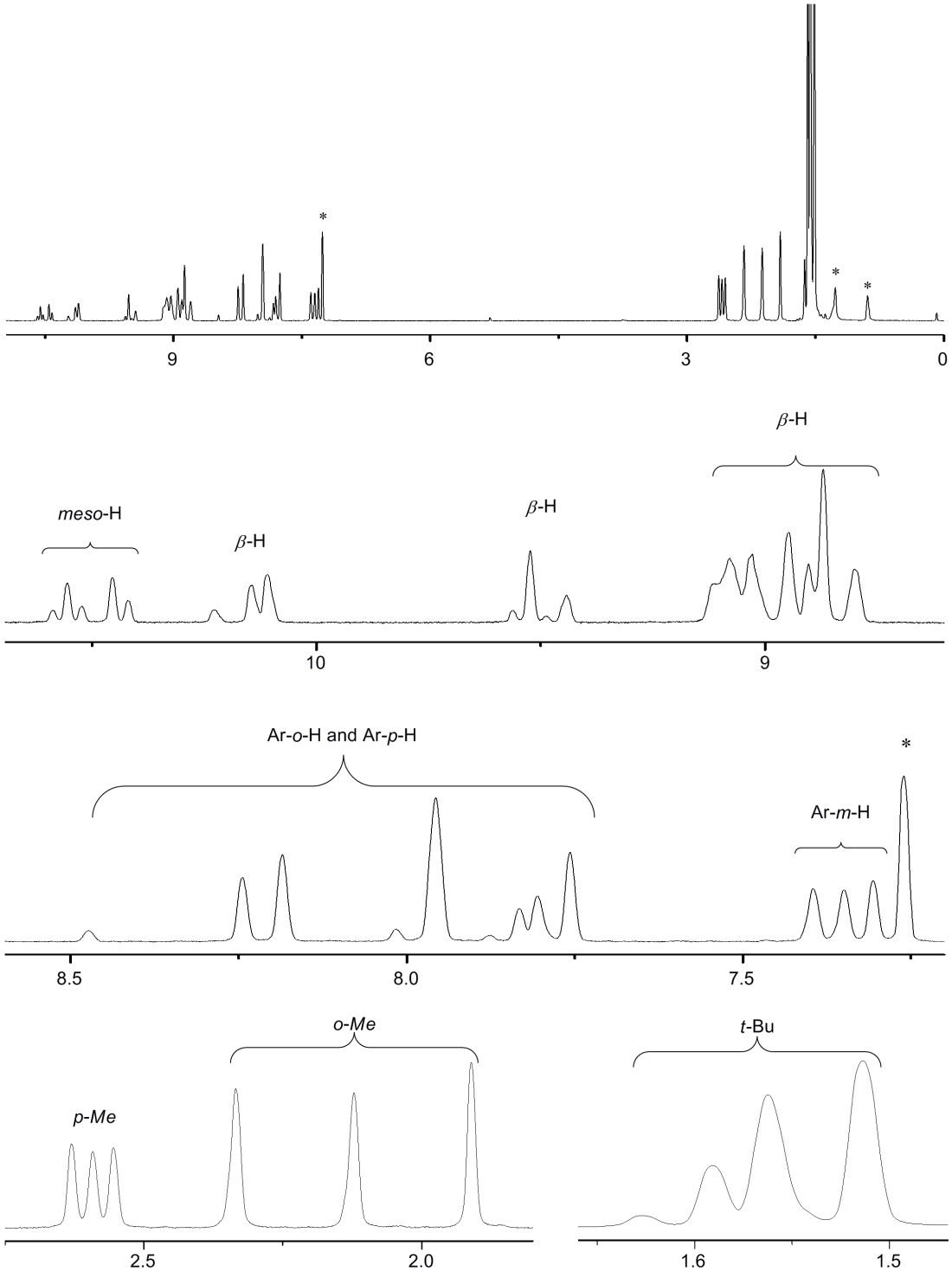

Figure S1-17. ^{1}H NMR spectrum of **9** in $CDCl_3$ at 298 K.

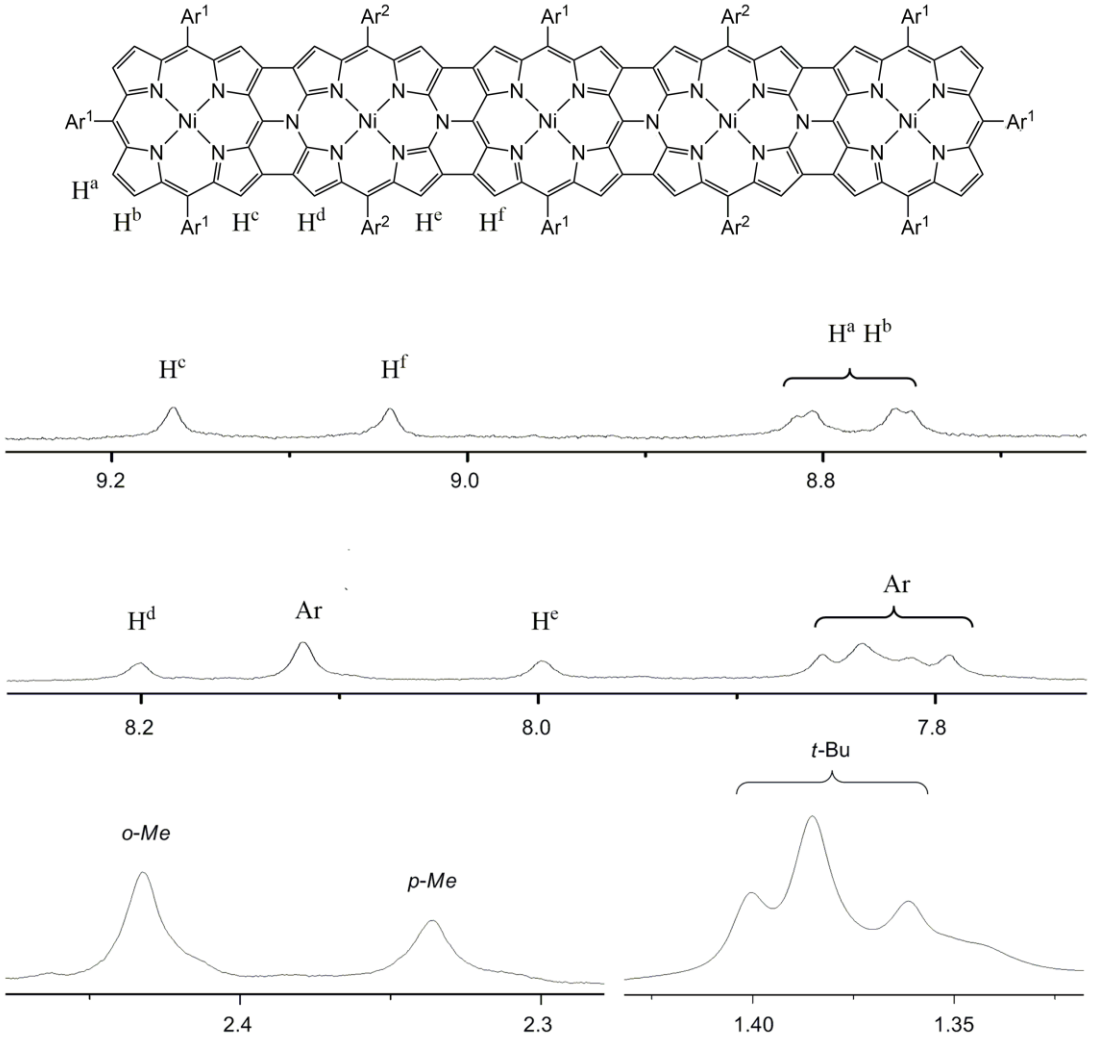

Figure S1-18. ^{1}H NMR spectrum of **10** in toluene-d_8 at 298 K.

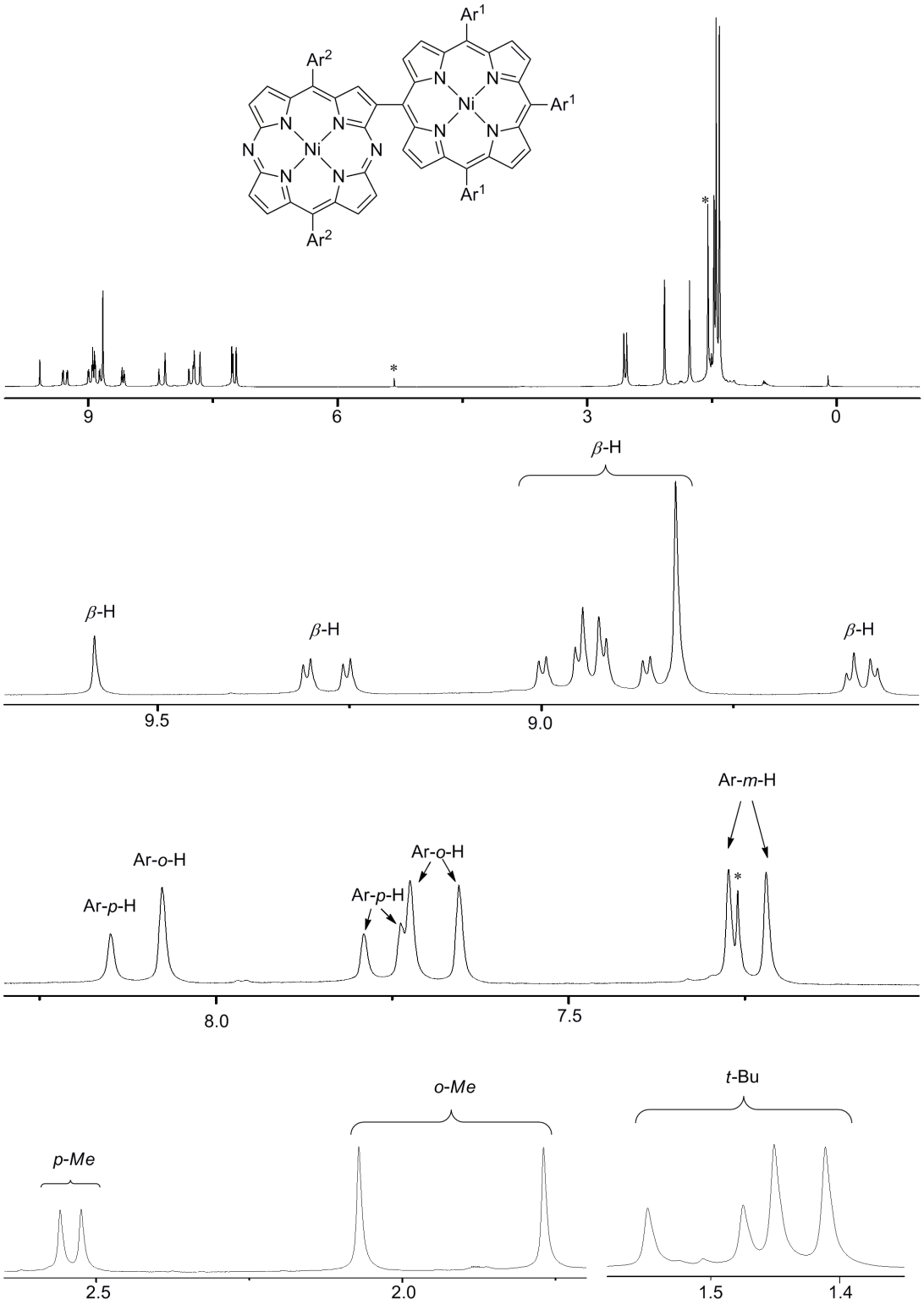

Figure S1-19. ^{1}H NMR spectrum of **12** in $CDCl_3$ at 233 K.

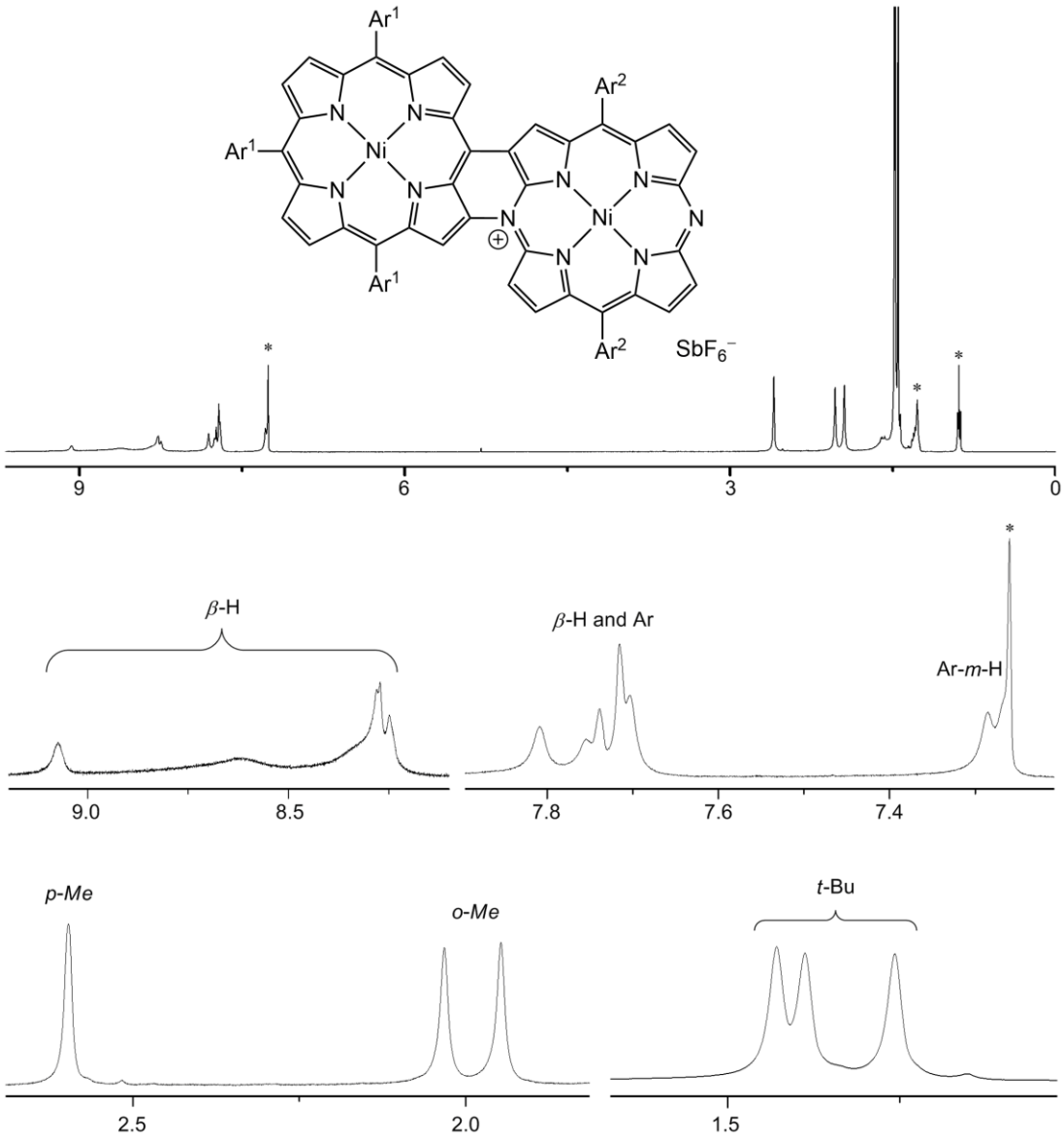

Figure S1-20. ^{1}H NMR spectrum of **13** in $CDCl_3$ at 298 K.

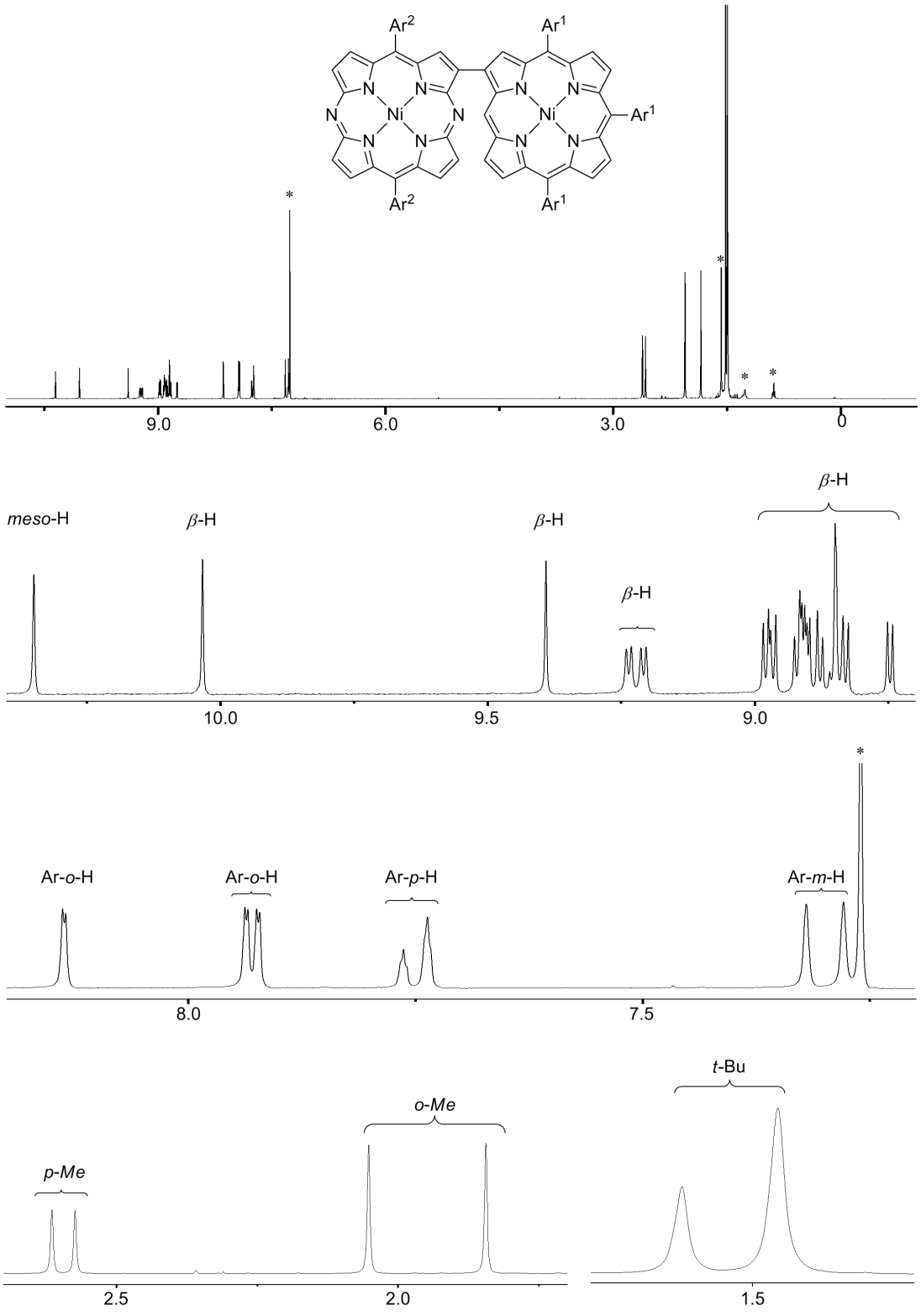

Figure S1-21. ^{1}H NMR spectrum of **14** in $CDCl_3$ at 298 K.

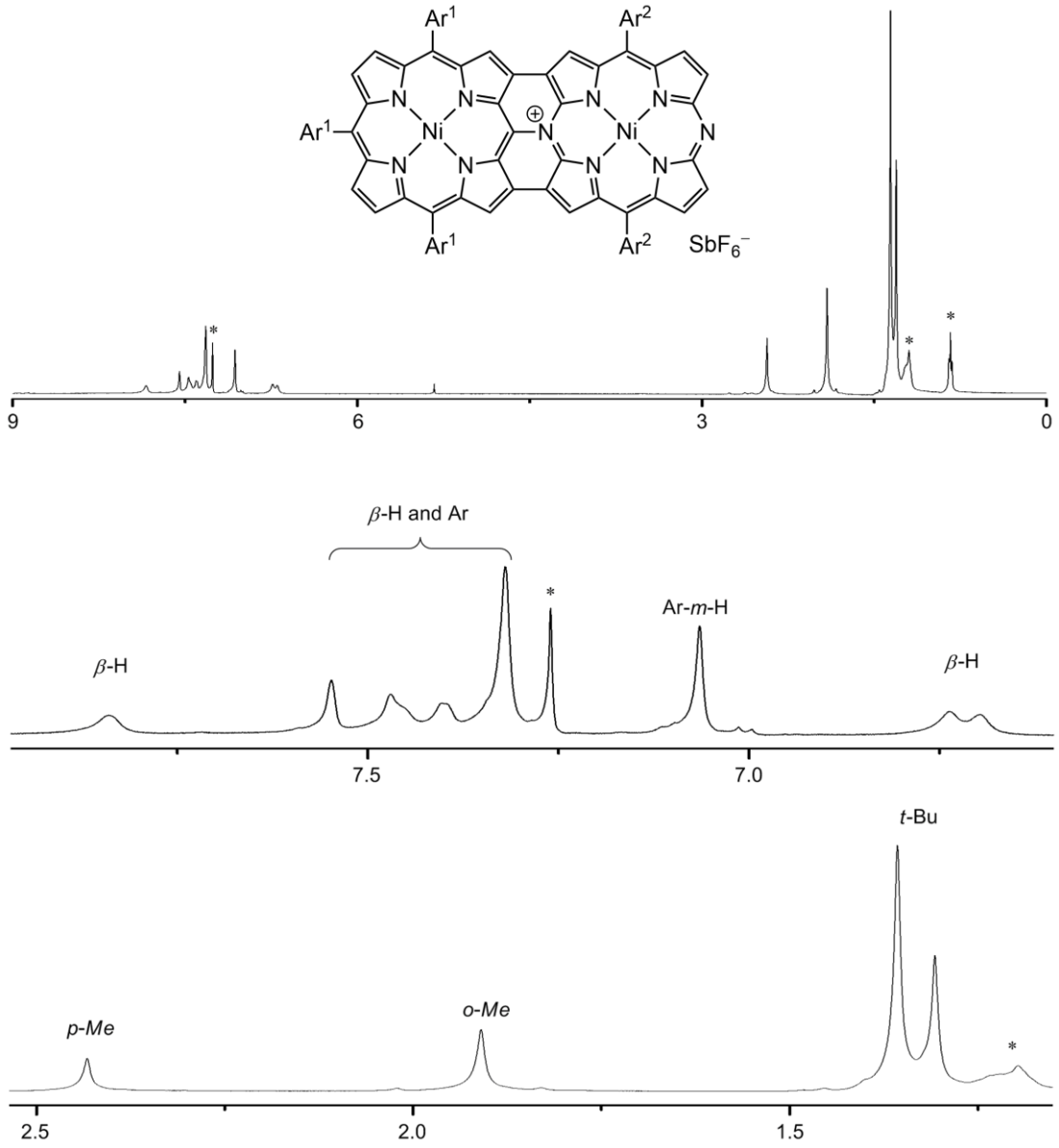

Figure S1-22. ^{1}H NMR spectrum of **15** in $CDCl_3$ at 213 K.

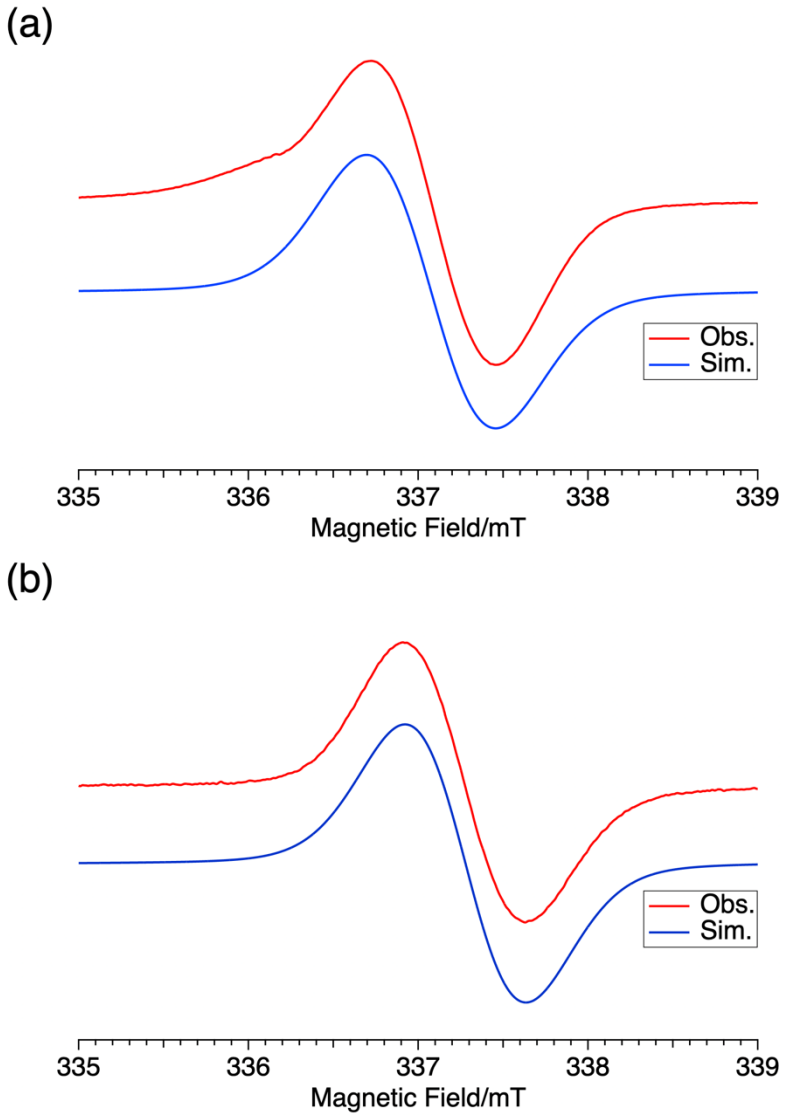

Figure S1-23. EPR spectra of (a) **12-ox** and (b) **14-ox** (0.1 mM in degassed toluene) at room temperature.

4. High Resolution Mass Spectra

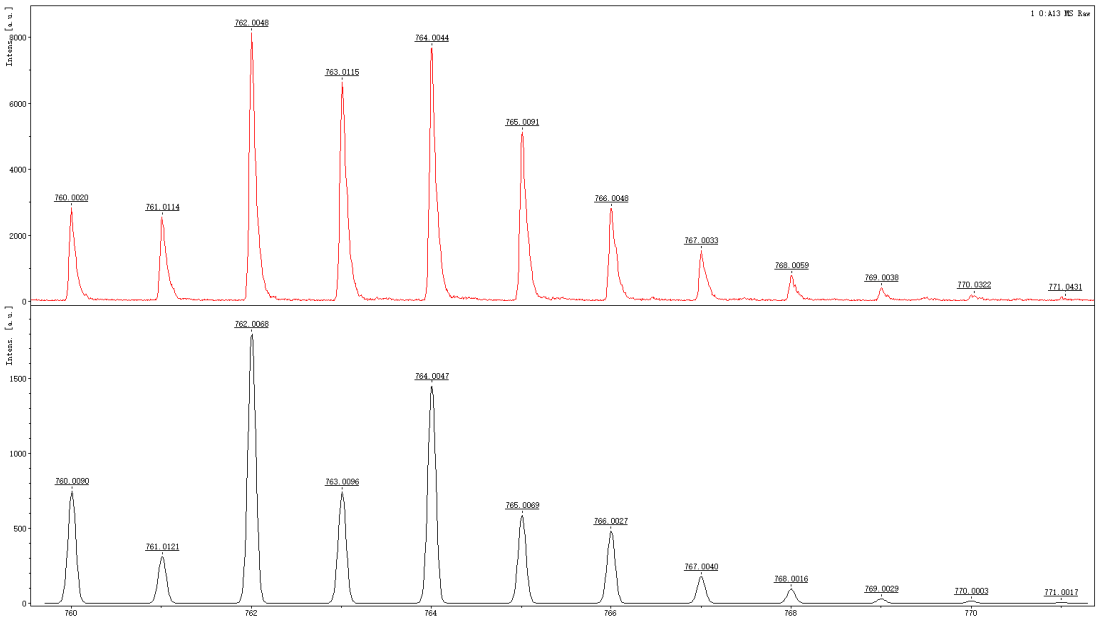

Figure S2-1. Observed (top) and simulated (bottom) MALDI-TOF mass spectrum of **2a** and **2b**.

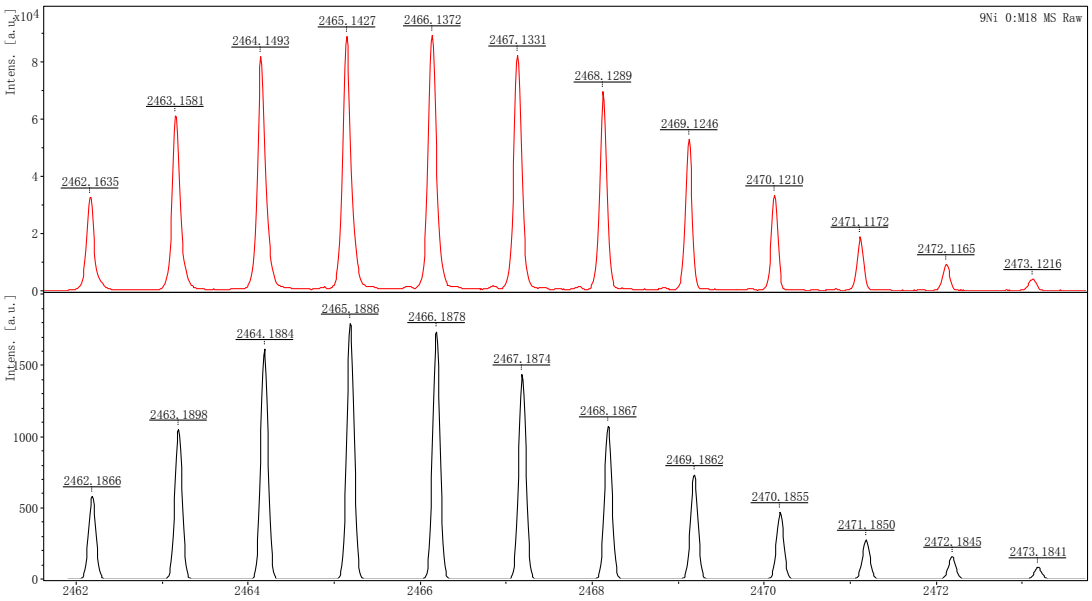

Figure S2-2. Observed (top) and simulated (bottom) MALDI-TOF mass spectrum of **3a**.

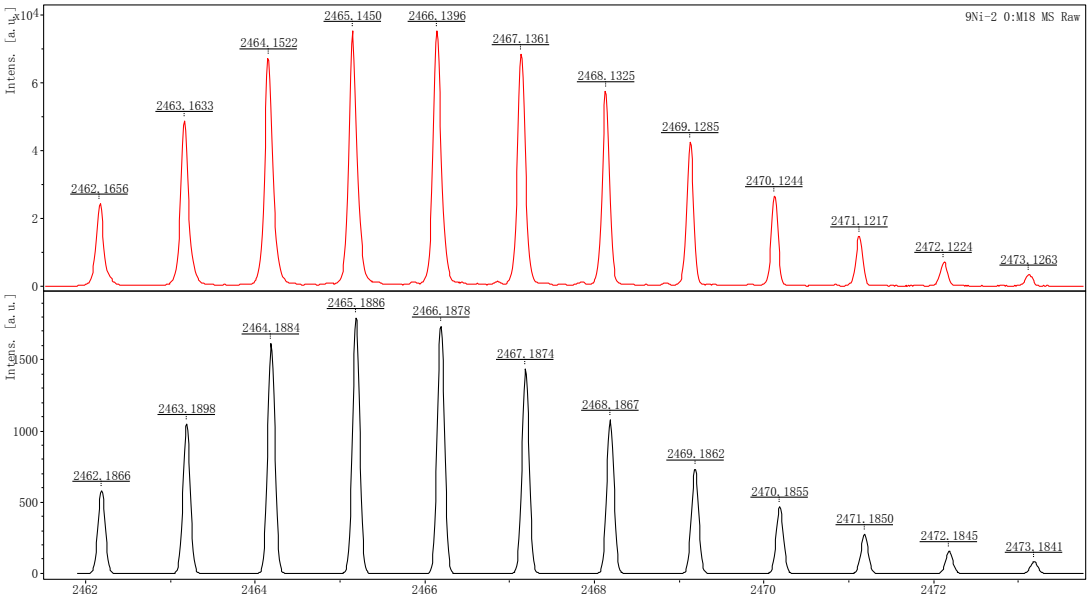

Figure S2-3. Observed (top) and simulated (bottom) MALDI-TOF mass spectrum of **3b**.

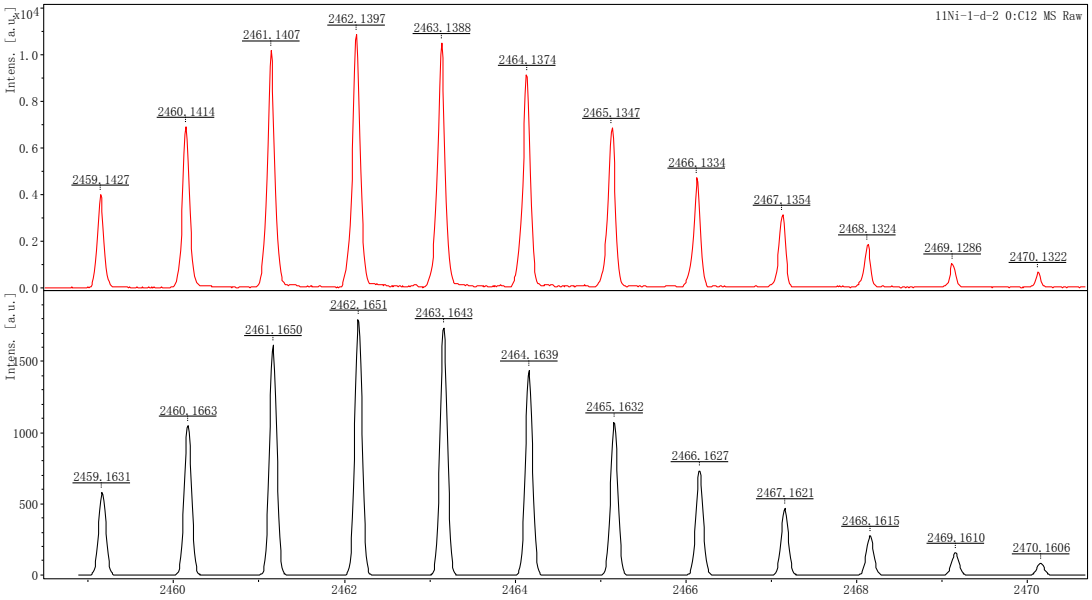

Figure S2-4. Observed (top) and simulated (bottom) MALDI-TOF mass spectrum of **4a**.

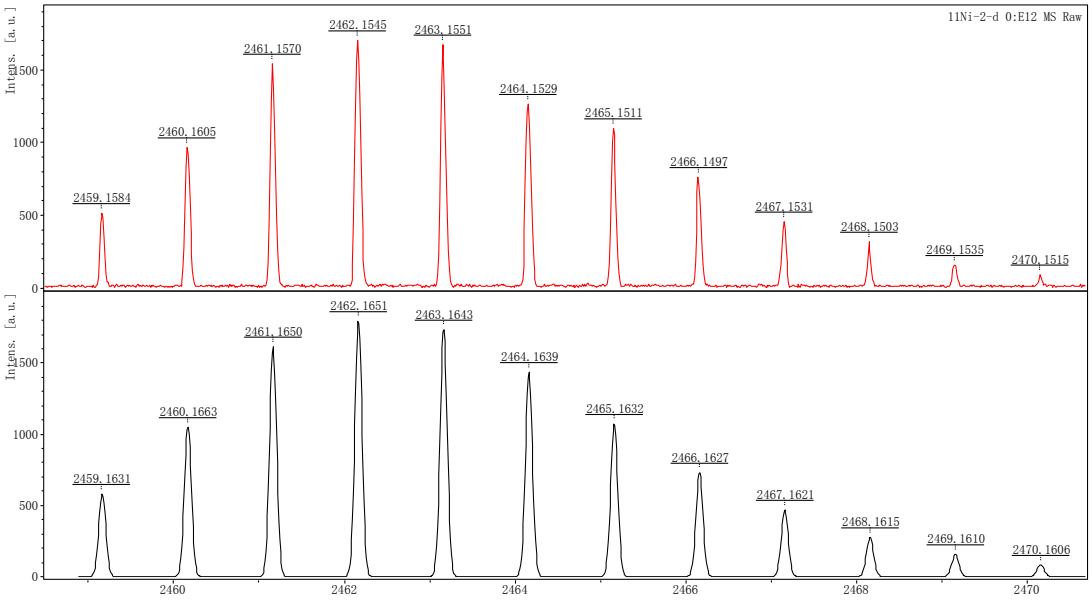

Figure S2-5. Observed (top) and simulated (bottom) MALDI-TOF mass spectrum of **4b**.

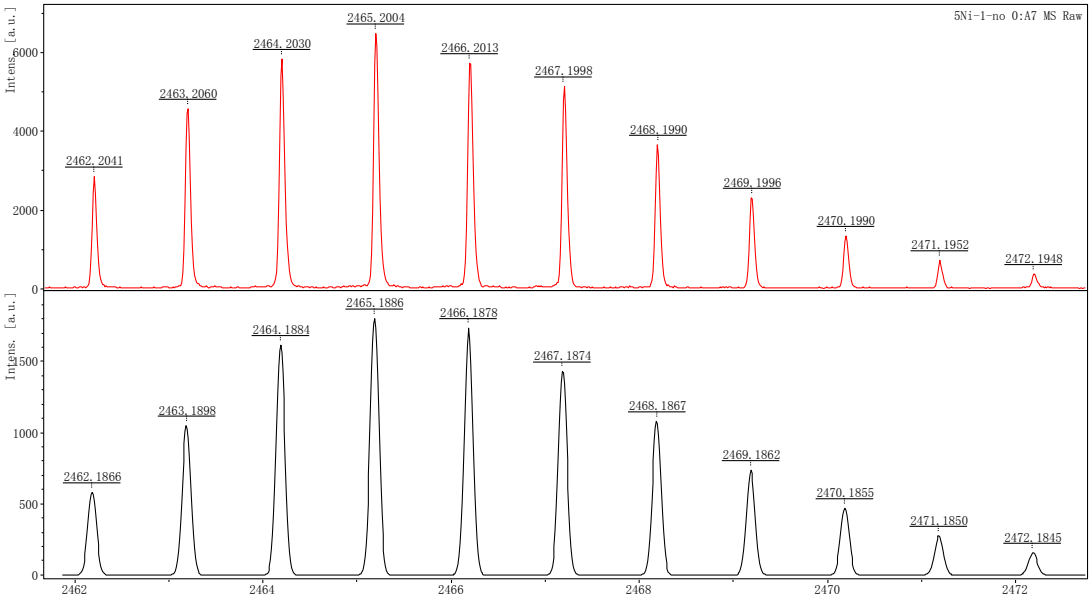

Figure S2-6. Observed (top) and simulated (bottom) MALDI-TOF mass spectrum of **5a**.

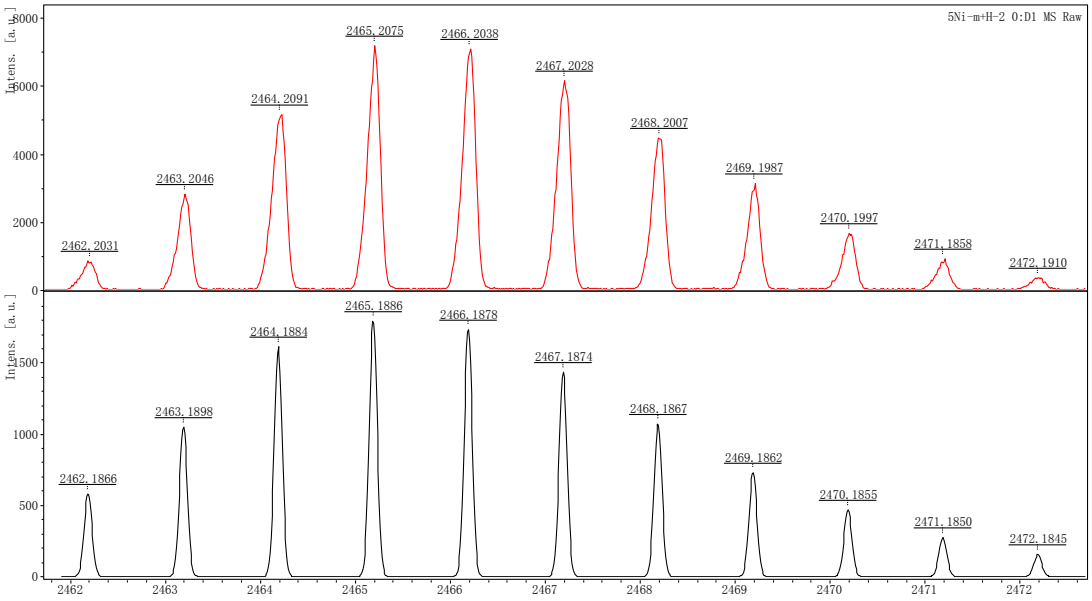

Figure S2-7. Observed (top) and simulated (bottom) MALDI-TOF mass spectrum of **5b**.

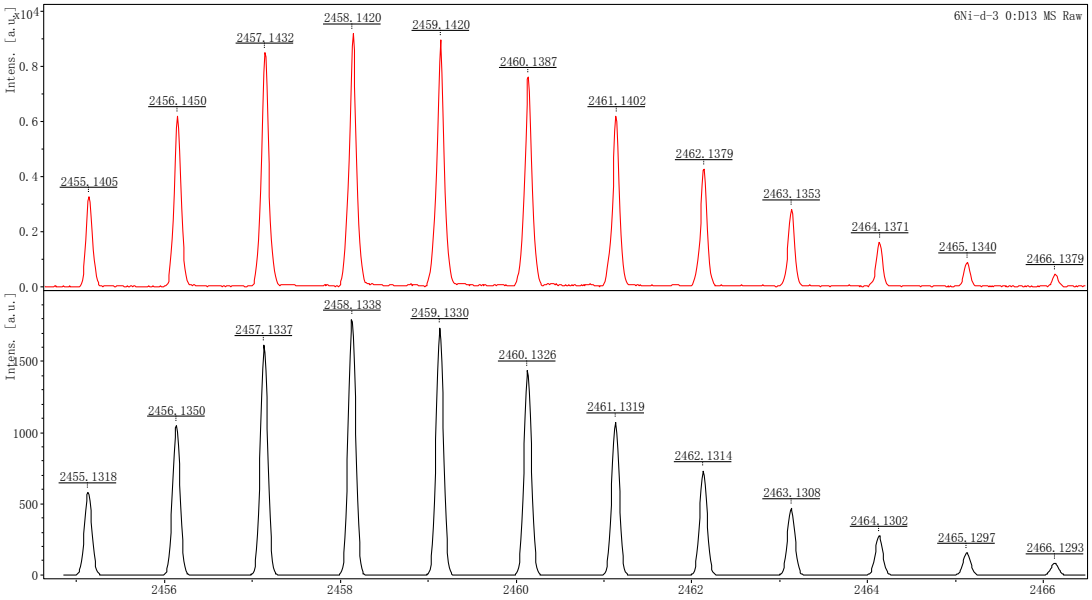

Figure S2-8. Observed (top) and simulated (bottom) MALDI-TOF mass spectrum of **6**.

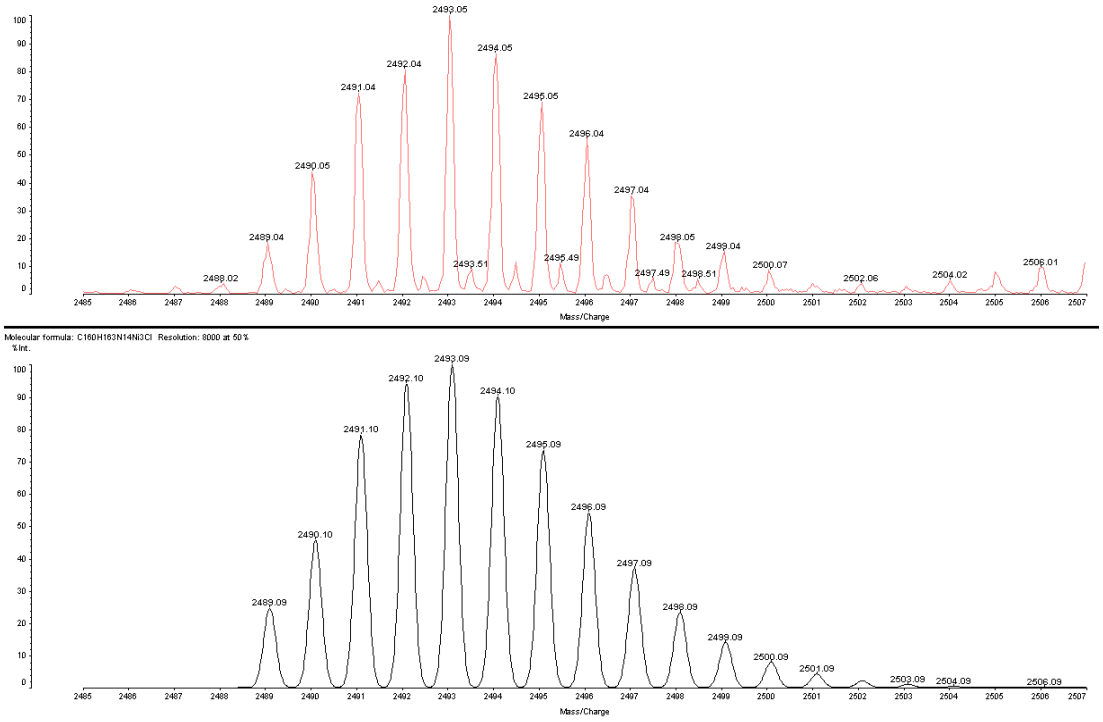

Figure S2-9. Observed (top) and simulated (bottom) MALDI-TOF mass spectrum of **6-Cl**.

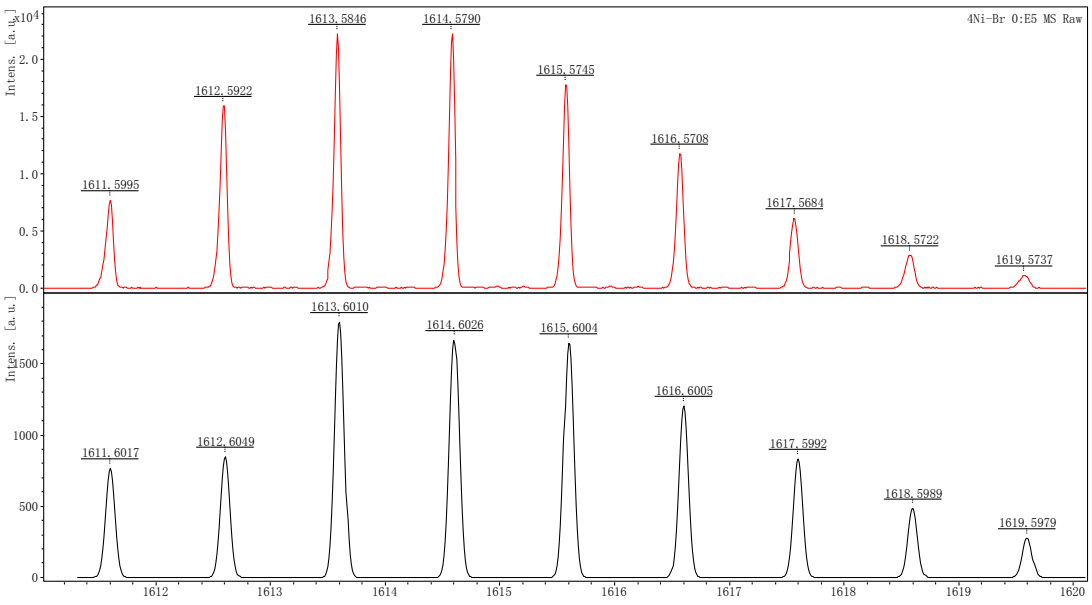

Figure S2-10. Observed (top) and simulated (bottom) MALDI-TOF mass spectrum of **7**.

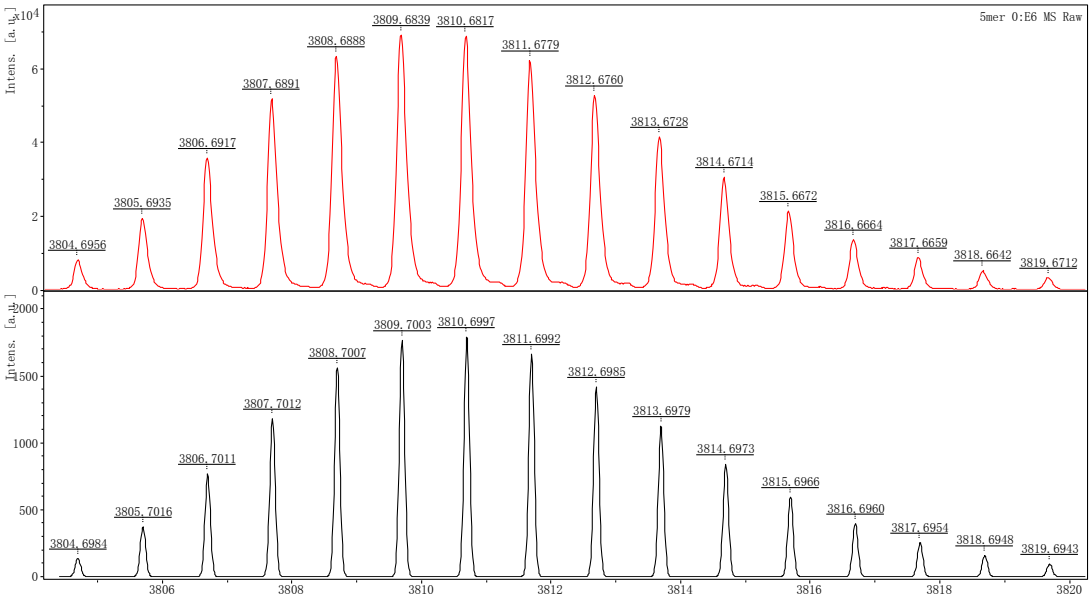

Figure S2-11. Observed (top) and simulated (bottom) MALDI-TOF mass spectrum of **9**.

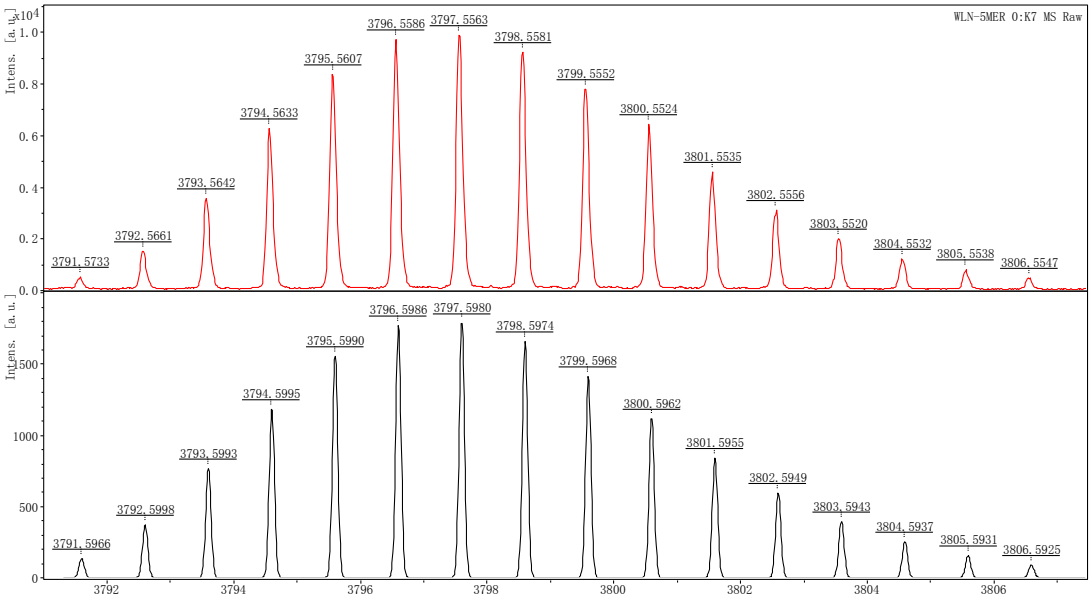

Figure S2-12. Observed (top) and simulated (bottom) MALDI-TOF mass spectrum of **10**.

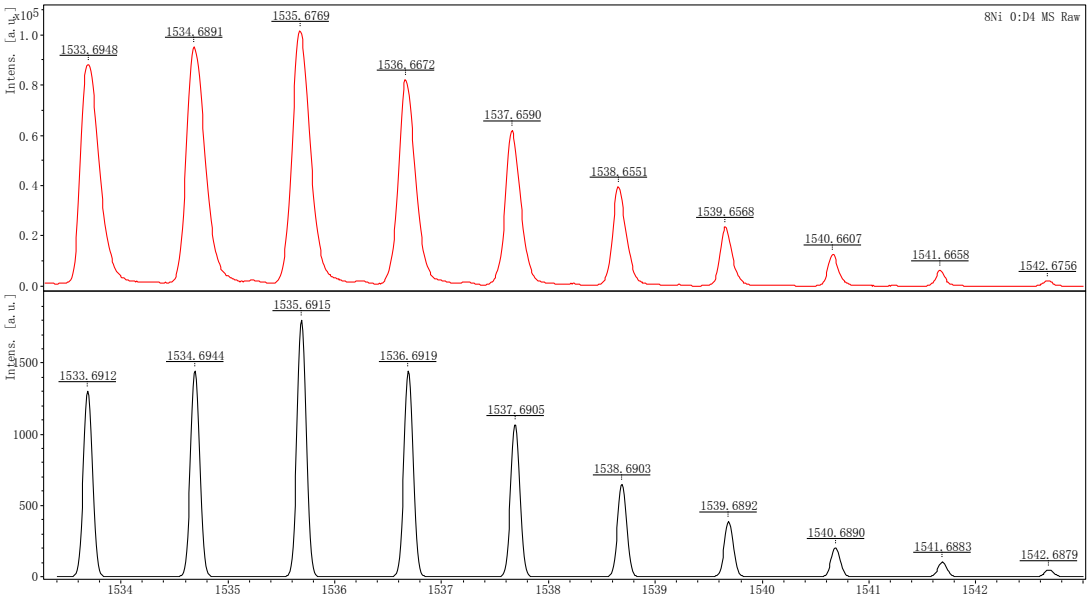

Figure S2-13. Observed (top) and simulated (bottom) MALDI-TOF mass spectrum of **12**.

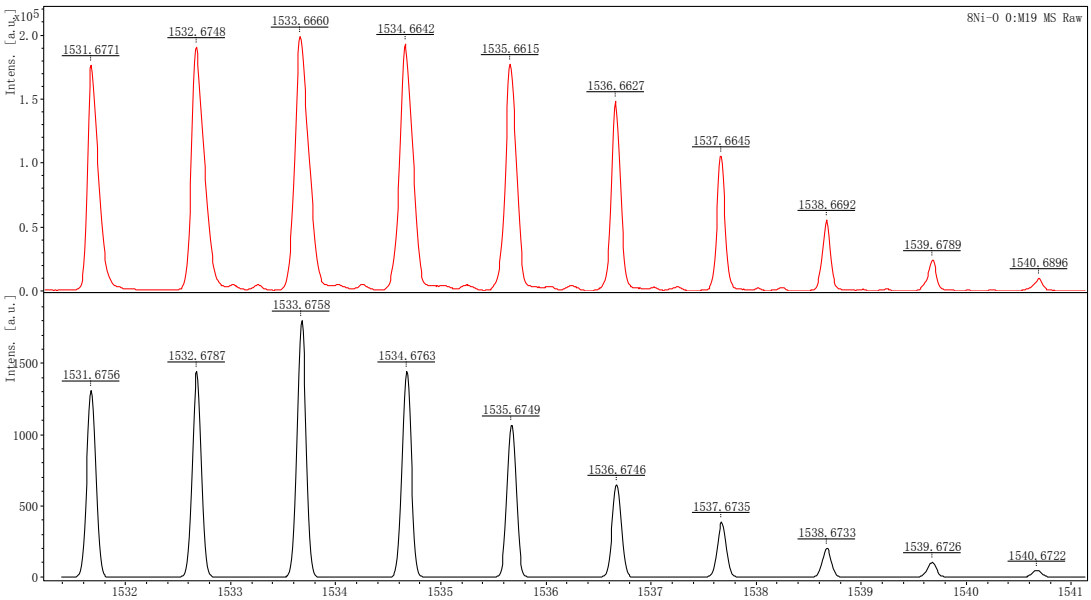

Figure S2-14. Observed (top) and simulated (bottom) MALDI-TOF mass spectrum of **12-ox**.

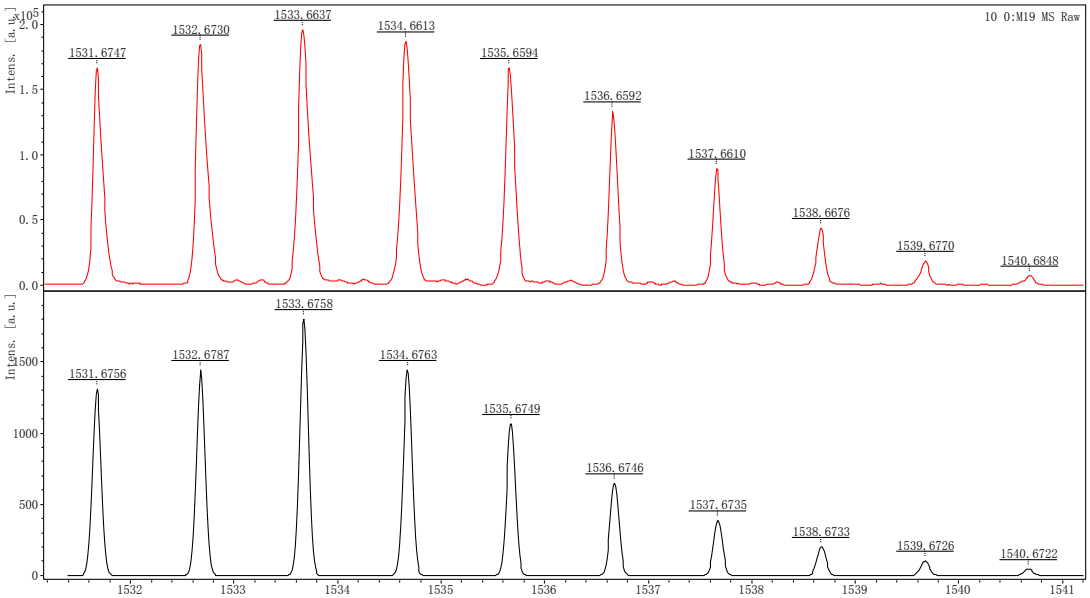

Figure S2-15. Observed (top) and simulated (bottom) MALDI-TOF mass spectrum of **13**.

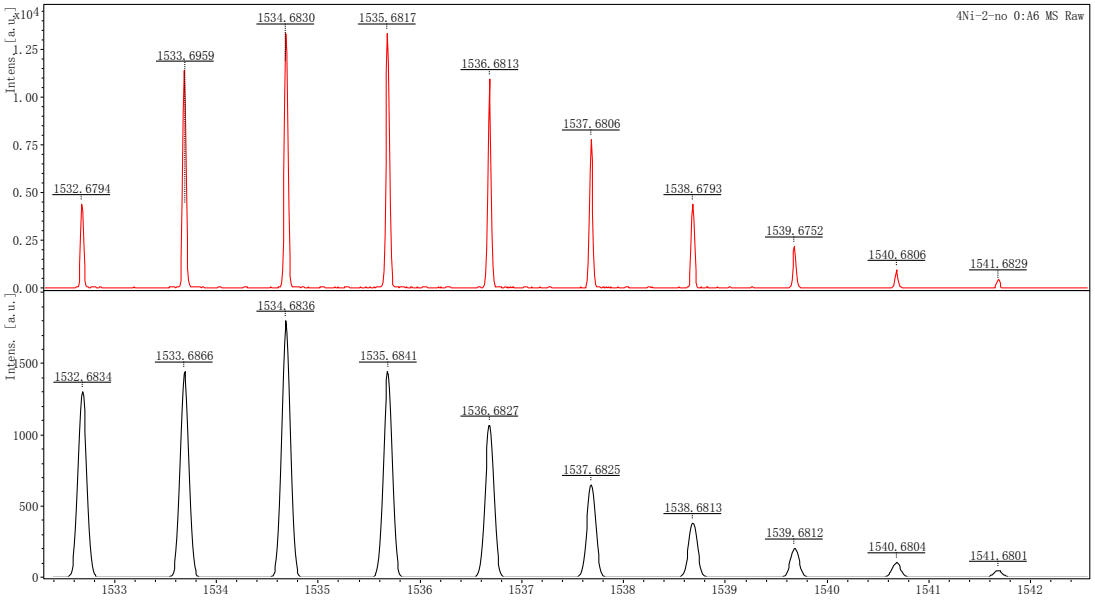

Figure S2-16. Observed (top) and simulated (bottom) MALDI-TOF mass spectrum of **14**.

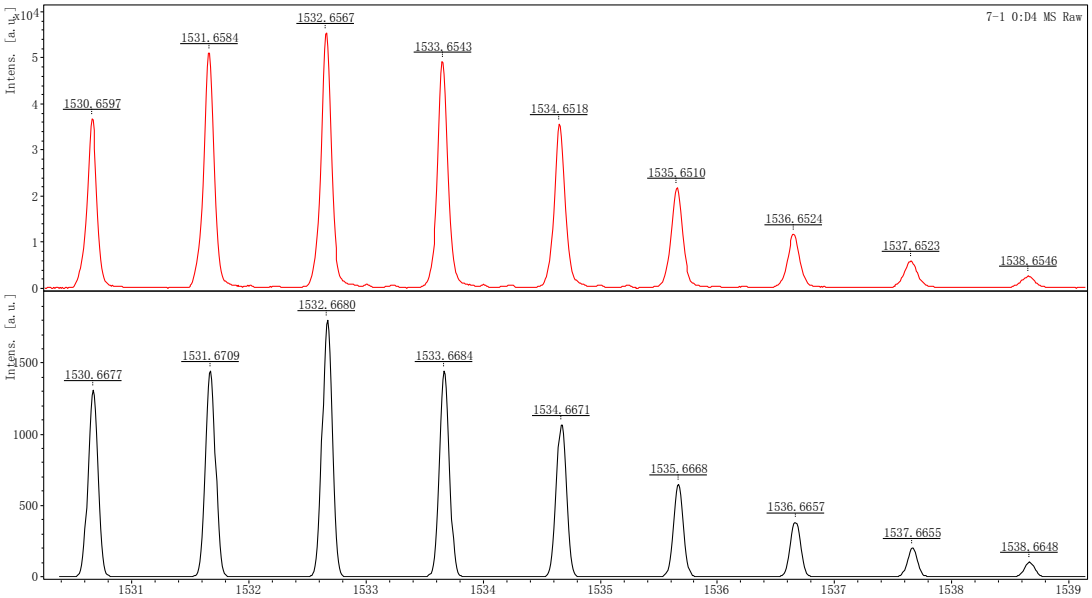

Figure S2-17. Observed (top) and simulated (bottom) MALDI-TOF mass spectrum of **14-ox**.

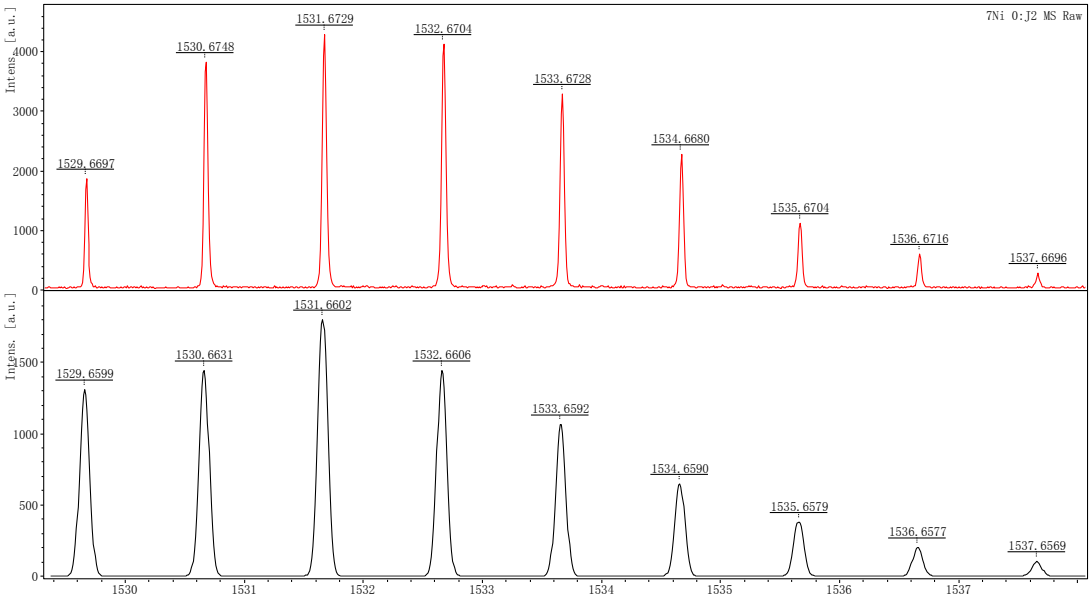

Figure S2-18. Observed (top) and simulated (bottom) MALDI-TOF mass spectrum of **15**.

5. UV/Vis/NIR Absorption Spectra

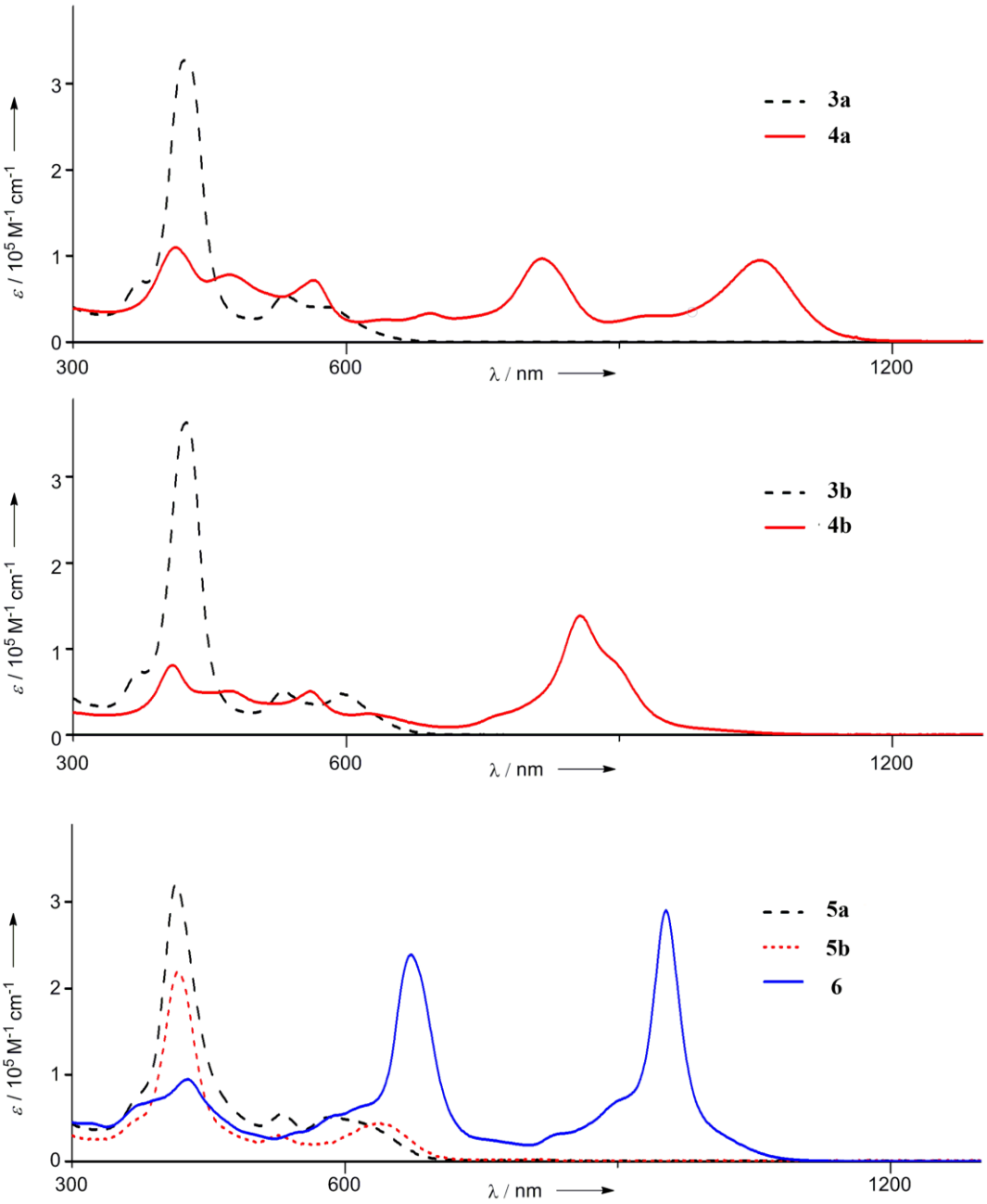

Figure S3-1. UV/Vis absorption spectra of **3a**, **3b**, **4a**,**4b**, **5a**, **5b**, and **6** in CH_2Cl_2.

Table S1-1. UV/Vis absorptions recorded in CH_2Cl_2.

Compound	λ [nm] (log ε)
3a	374 (4.86), 422 (5.51), 532 (4.71), 577 (4.61)
3b	373 (4.87), 425 (5.56), 532 (4.71), 595 (4.68)
4a	412 (5.04), 473 (4.89), 565 (4.86), 814 (4.99), 1054 (4.98)
4b	409 (4.91), 473 (4.89), 560 (4.70), 624 (4.39), 857 (5.14)
5a	415 (5.51), 532 (4.74), 584 (4.71)
5b	417 (5.34), 526 (4.47), 638 (4.64)
6	316 (4.65), 427 (4.98), 672 (5.38), 953 (5.46)

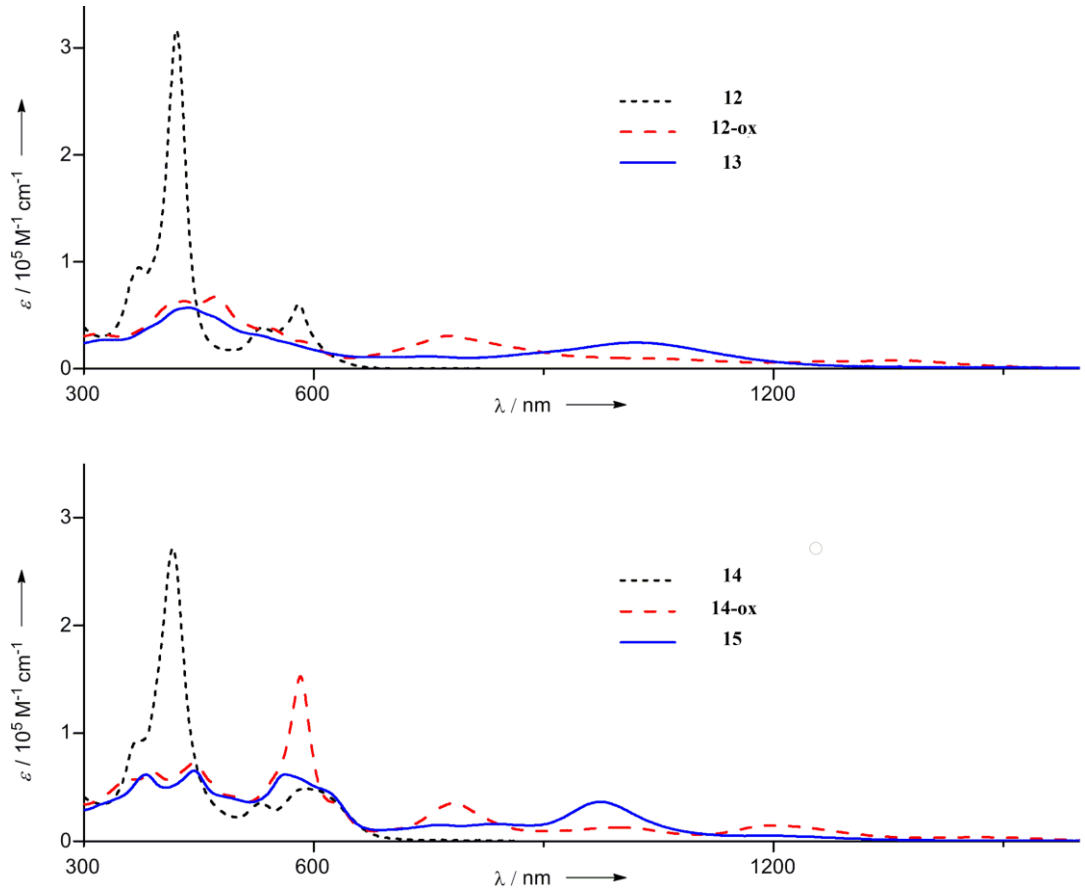

Figure S3-2. UV/Vis absorption spectra of **12**, **12-ox**,**13**,**14**, **14-ox**, and **15** in CH_2Cl_2.

Table S1-2. UV/Vis absorptions recorded in CH_2Cl_2.

Compound	λ [nm] (log ε)
12	372 (4.98), 421 (5.50), 532 (4.58), 581 (4.78)
12-ox	316 (4.51), 430 (4.80), 472 (4.83), 543 (4.58), 776 (4.49), 1357 (3.90)
13	436 (4.64), 748 (3.95), 1020 (4.27)
14	416 (5.43), 532 (4.55), 592 (4.69)
14-ox	390 (4.81), 444 (4.86), 583 (5.18), 783 (4.55), 1000 (4.11), 1200 (4.16)
15	381 (4.79), 444 (4.82), 563 (4.79), 766 (4.17), 834 (4.20), 974 (4.56)

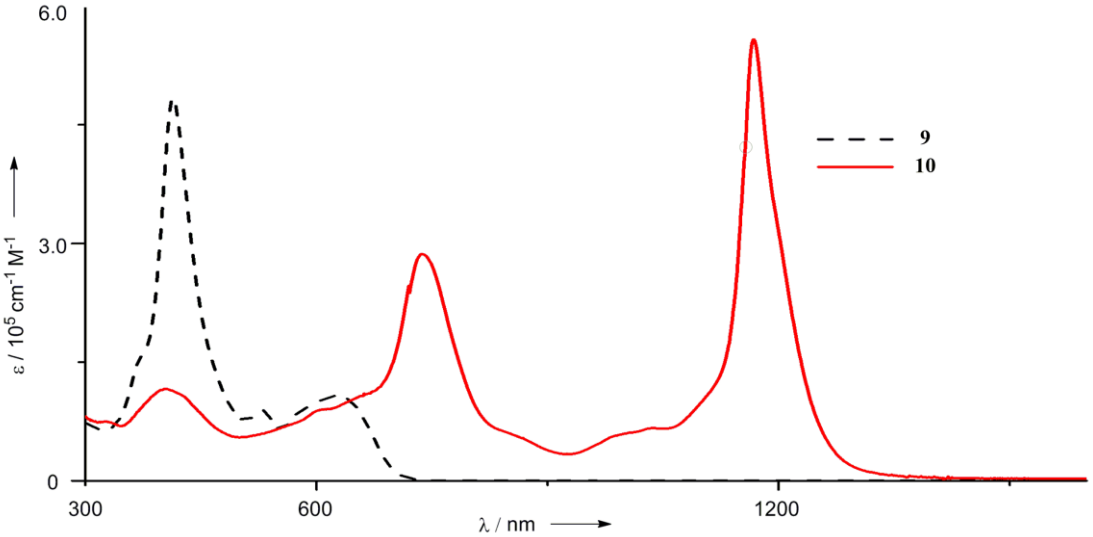

Figure S3-3. UV/Vis absorption spectra of **9** and **10** in CH_2Cl_2.

Table S1-3. UV/Vis absorptions recorded in CH_2Cl_2.

Compound	λ [nm] (log ε)
9	414 (5.68), 529 (4.95), 627 (5.03)
10	326 (4.88), 405 (5.06), 737 (5.46), 1037 (4.82), 1168 (5.75)

6. Electrochemical Data

Cyclic voltammograms and differential pulse voltammograms were measured in benzonitrile with 0.1 M $^{n}Bu_4NPF_6$; potentials were determined *vs* ferrocene/ferrocenium ion by differential pulse voltammograms; working electrode: glassy carbon; counter electrode: Pt wire; reference electrode: $Ag/AgNO_3$.

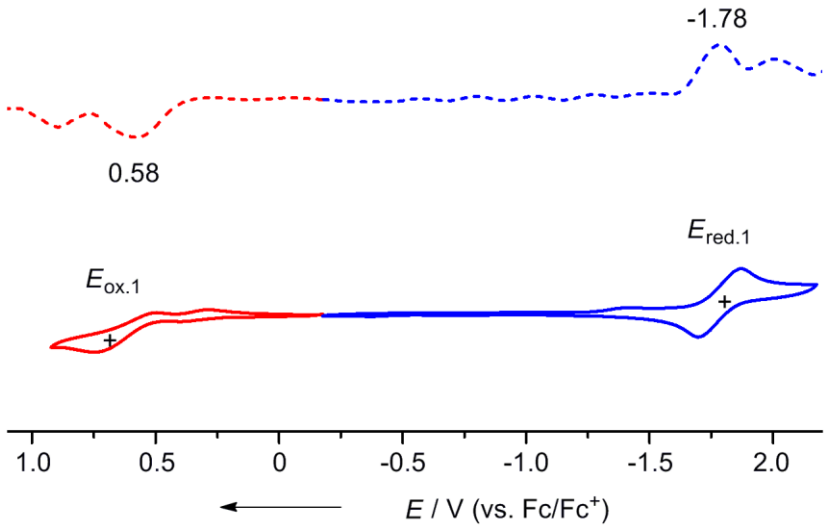

Figure S4-1. Cyclic voltammogram and differential pulse voltammogram of Ni^{II} porphyrin (P).

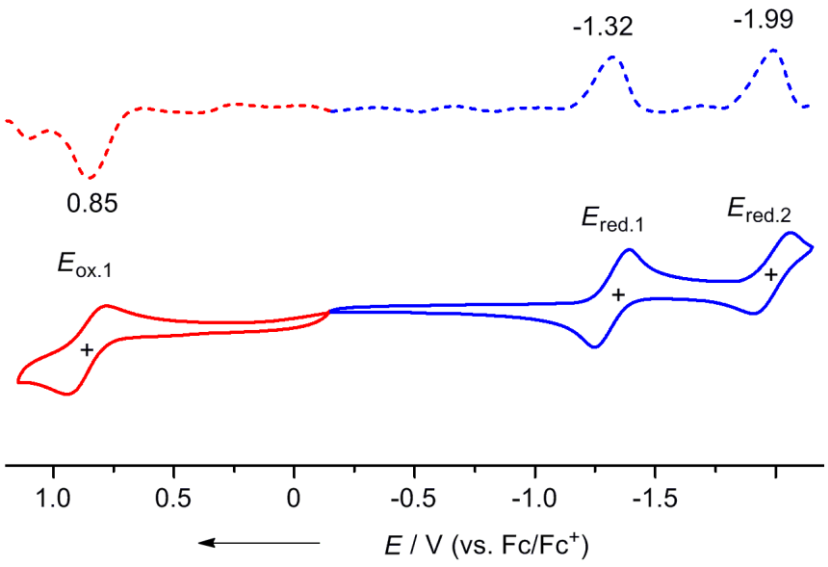

Figure S4-2. Cyclic voltammogram and differential pulse voltammogram of Ni^{II} diazaporphyrin (DAP).

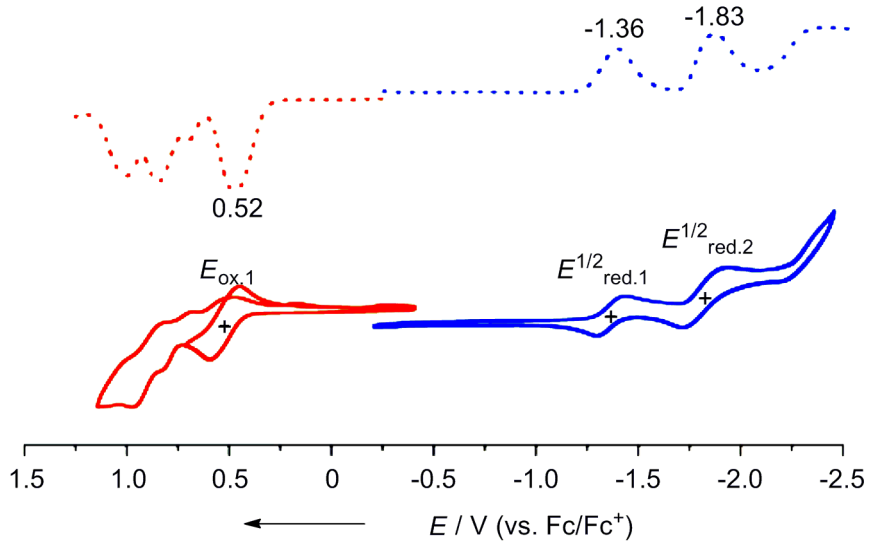

Figure S4-3. Cyclic voltammogram and differential pulse voltammogram of **3a**.

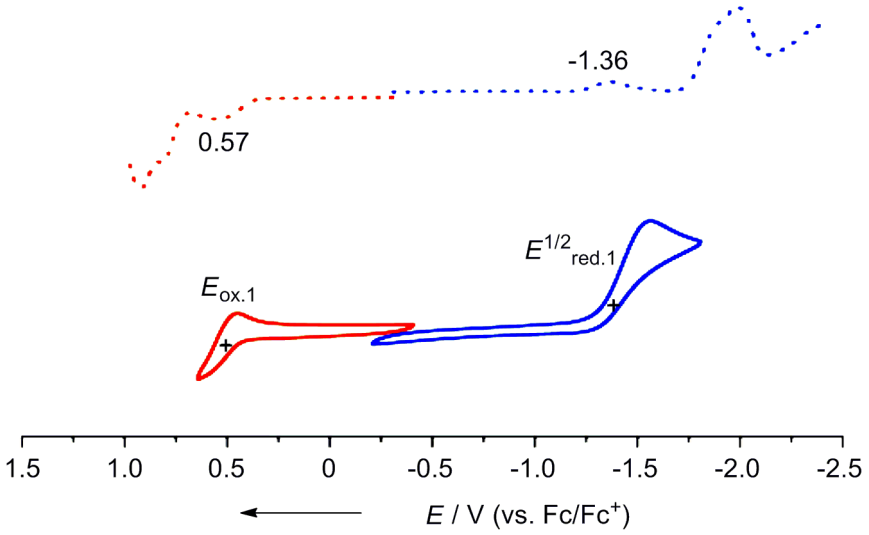

Figure S4-4. Cyclic voltammogram and differential pulse voltammogram of **3b**.

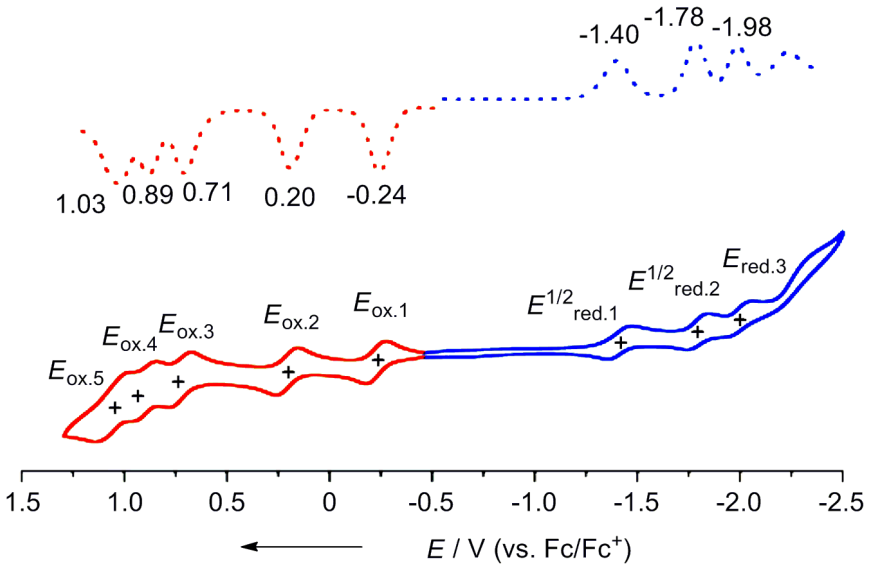

Figure S4-5. Cyclic voltammogram and differential pulse voltammogram of **4a**.

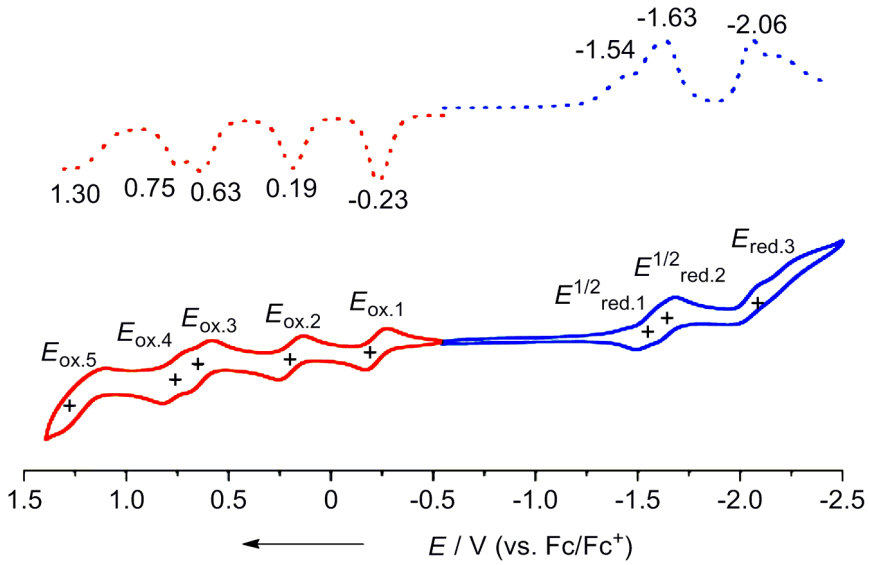

Figure S4-6. Cyclic voltammogram and differential pulse voltammogram of **4b**.

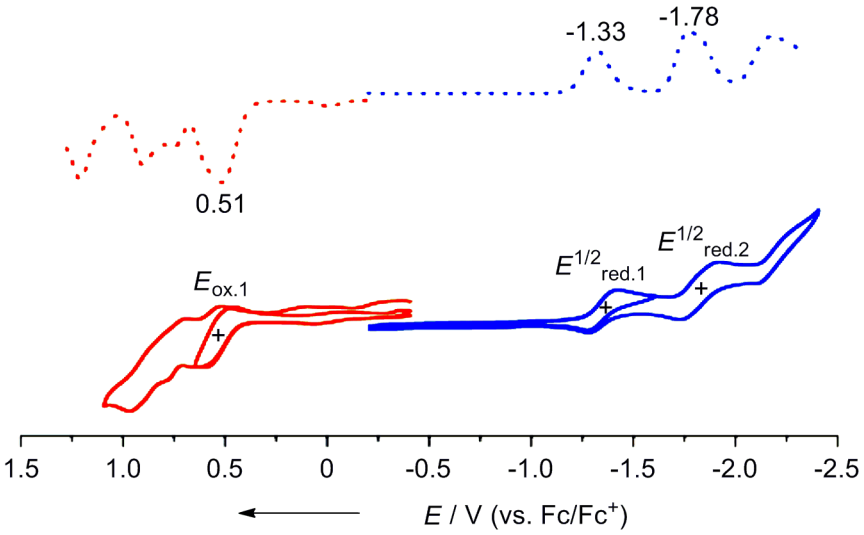

Figure S4-7. Cyclic voltammogram and differential pulse voltammogram of **5a**.

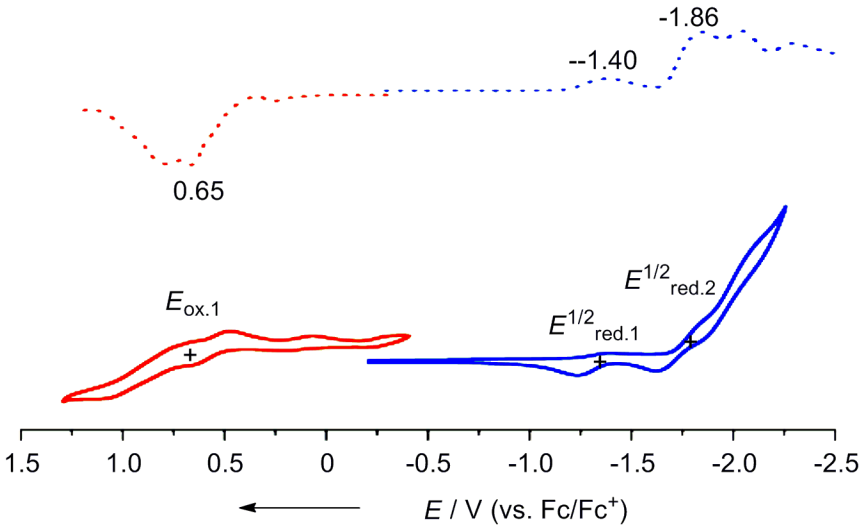

Figure S4-8. Cyclic voltammogram and differential pulse voltammogram of **5b**.

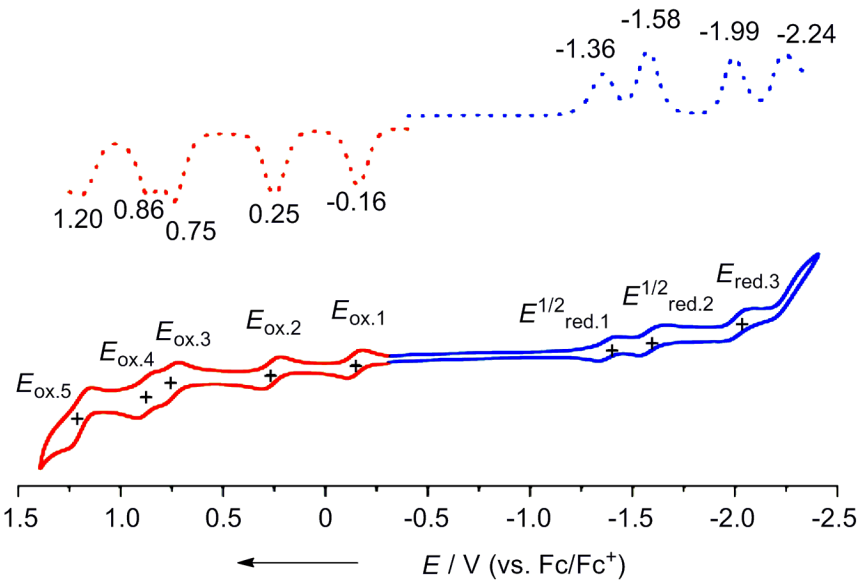

Figure S4-9. Cyclic voltammogram and differential pulse voltammogram of **6**.

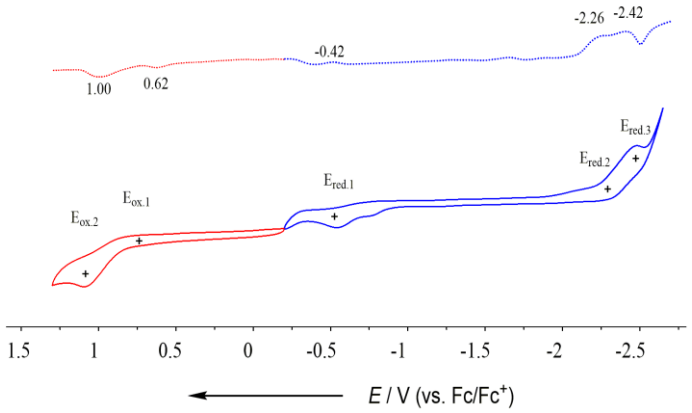

Figure S4-10. Cyclic voltammogram and differential pulse voltammogram of **10**.

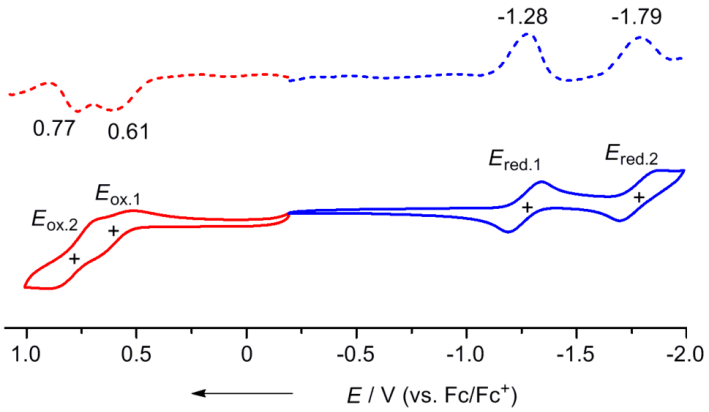

Figure S4-11. Cyclic voltammogram and differential pulse voltammogram of **12**.

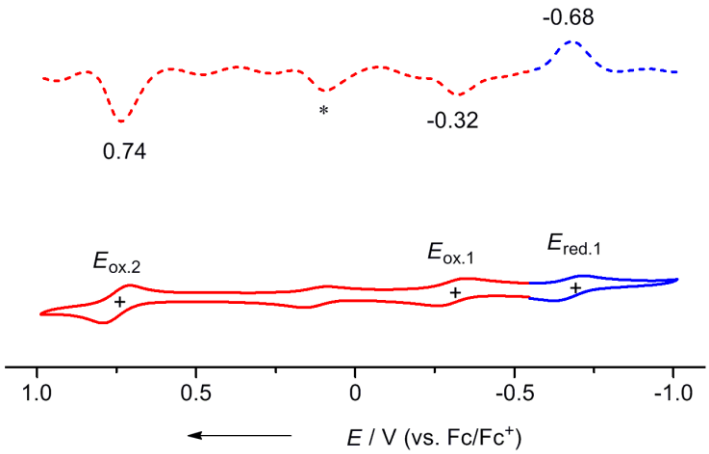

Figure S4-12. Cyclic voltammogram and differential pulse voltammogram of **12-ox**.

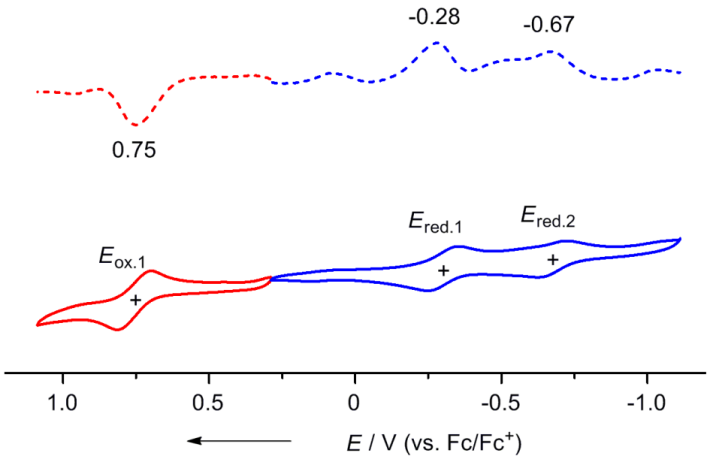

Figure S4-13. Cyclic voltammogram and differential pulse voltammogram of **13**.

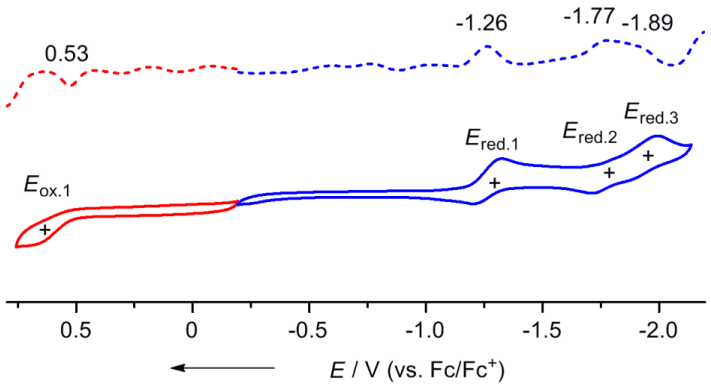

Figure S4-14. Cyclic voltammogram and differential pulse voltammogram of **14**.

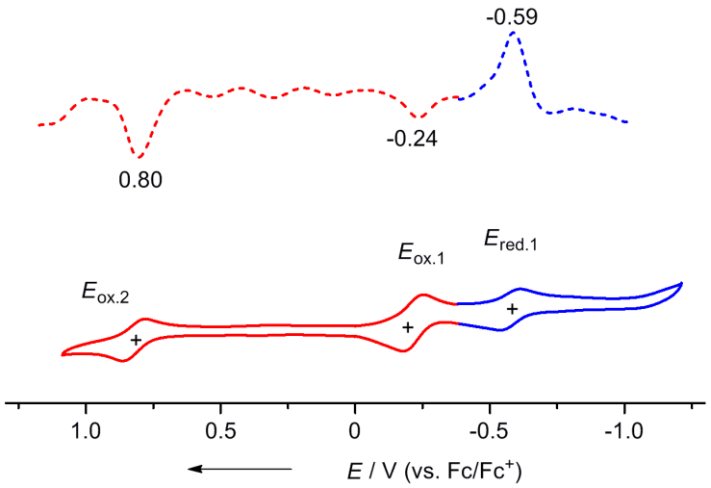

Figure S4-15. Cyclic voltammogram and differential pulse voltammogram of **14-ox**.

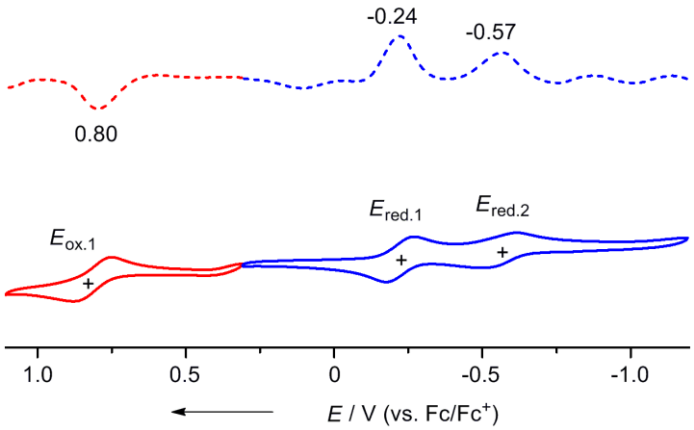

Figure S4-16. Cyclic voltammogram and differential pulse voltammogram of **15**.

Table S2-1. Summary of the electrochemical potentials (V) and HOMO-LUMO gaps (eV).

Compound	$E_{ox.4}$	$E_{ox.3}$	$E_{ox.2}$	$E_{ox.1}$	$E_{red.1}$	$E_{red.2}$	$E_{red.3}$	ΔE_{HL}[b]
3a				0.52	-1.36	-1.83		1.88
3b				0.57[a]	-1.36[a]			1.93
4a	0.89	0.71	0.20	-0.24	-1.40	-1.78	-1.98	1.16
4b	0.75	0.63	0.19	-0.23	-1.54	-1.63	-2.06	1.31
5a				0.51	-1.33	-1.78		1.84
5b				0.65[a]	-1.40[a]	-1.86		2.05
6	0.86	0.75	0.25	-0.16	-1.36	-1.58	-1.99	1.20

[a]Irreversible peak; [b]Electrochemical HOMO-LUMO gap, ΔE_{HL} = e($E_{ox.1}$-$E_{red.1}$).

Table S2-2. Summary of the electrochemical potentials (V) and HOMO-LUMO gaps (eV).

Compound	$E_{ox.2}$	$E_{ox.1}$	$E_{red.1}$	$E_{red.2}$	$E_{red.3}$	ΔE_{HL}[b]
Ni-P		0.58[a]	-1.78			2.36
Ni-DAP		0.85	-1.32	-1.99		2.17
10	1.00	0.62	-0.42	-2.26	-2.42	1.04
12	0.77	0.61	-1.28	-1.79		1.89
12-ox	0.74	-0.32	-0.68			0.36
13		0.75	-0.28	-0.67		1.03
14		0.53[a]	-1.26	-1.77	-1.89	1.79
14-ox	0.80	-0.24	-0.59			0.35
15		0.80	-0.24	-0.57		1.04

[a]Irreversible peak; [b]Electrochemical HOMO-LUMO gap, ΔE_{HL} = e($E_{ox.1}$-$E_{red.1}$).

7. X-Ray Crystal Data

The crystals were wrapped in silicon oil and then were frozen. Data collections for all the crystals were performed on a SuperNova diffractometer using graphite-monochromated Cu Kα radiation (λ = 1.54184 Å). Using Olex2,[1] the structures of **3b** and **4b** were solved with the olex2.solve[2] structure solution program using Charge Flipping,[3] the structure of **6-Cl** was solved with the SIR2004[4] structure solution program, the structures of **3a**, **5a**, **5b** and **15** were solved with the ShelXT[5] structure solution program, the structure of **6** were solved with ShelXS[6] structure solution program. All of the above structures were refined with the ShelXL[7] refinement package using Least Squares minimization. Due to the highly disordered ^{t}Bu groups, DFIX restrains were applied to fix 1,2- and 1,3-distances between carbons atoms in ^{t}Bu groups of **5a**, **5b**, **6** and **6-Cl**. Disordered solvents in **3b**, **4b**, **5b**, **6**, **6-Cl** and **15** were squeezed by using Platon.[8]

Table S3-1. Crystal data and structure refinement for **3a**.

Identification code	3a
Empirical formula	$C_{205}H_{229}N_{14}Ni_3O$
Formula weight	3081.14
Temperature/K	99.9(5)
Crystal system	monoclinic
Space group	$P2_1/c$
a/Å	33.0120(7)
b/Å	17.7275(3)
c/Å	30.1749(5)
α/°	90
β/°	91.719(2)
γ/°	90
Volume/Å^3	17651.0(6)
Z	4
ρ_{calc}g/cm^3	1.159
μ/mm^{-1}	0.806
F(000)	6596.0
Crystal size/mm^3	0.3 × 0.3 × 0.02
Radiation	CuKα (λ = 1.54184)
2Θ range for data collection/°	7.32 to 133.2
Index ranges	$-39 \leq h \leq 34$, $-21 \leq k \leq 15$, $-35 \leq l \leq 35$
Reflections collected	117754
Independent reflections	31164 [R_{int} = 0.0777, R_{sigma} = 0.0746]
Data/restraints/parameters	31164/301/2124
Goodness-of-fit on F^2	1.022
Final R indexes [I>=2σ (I)]	R_1 = 0.0613, wR_2 = 0.1478
Final R indexes [all data]	R_1 = 0.0832, wR_2 = 0.1625
Largest diff. peak/hole / e Å^{-3}	0.91/-0.53

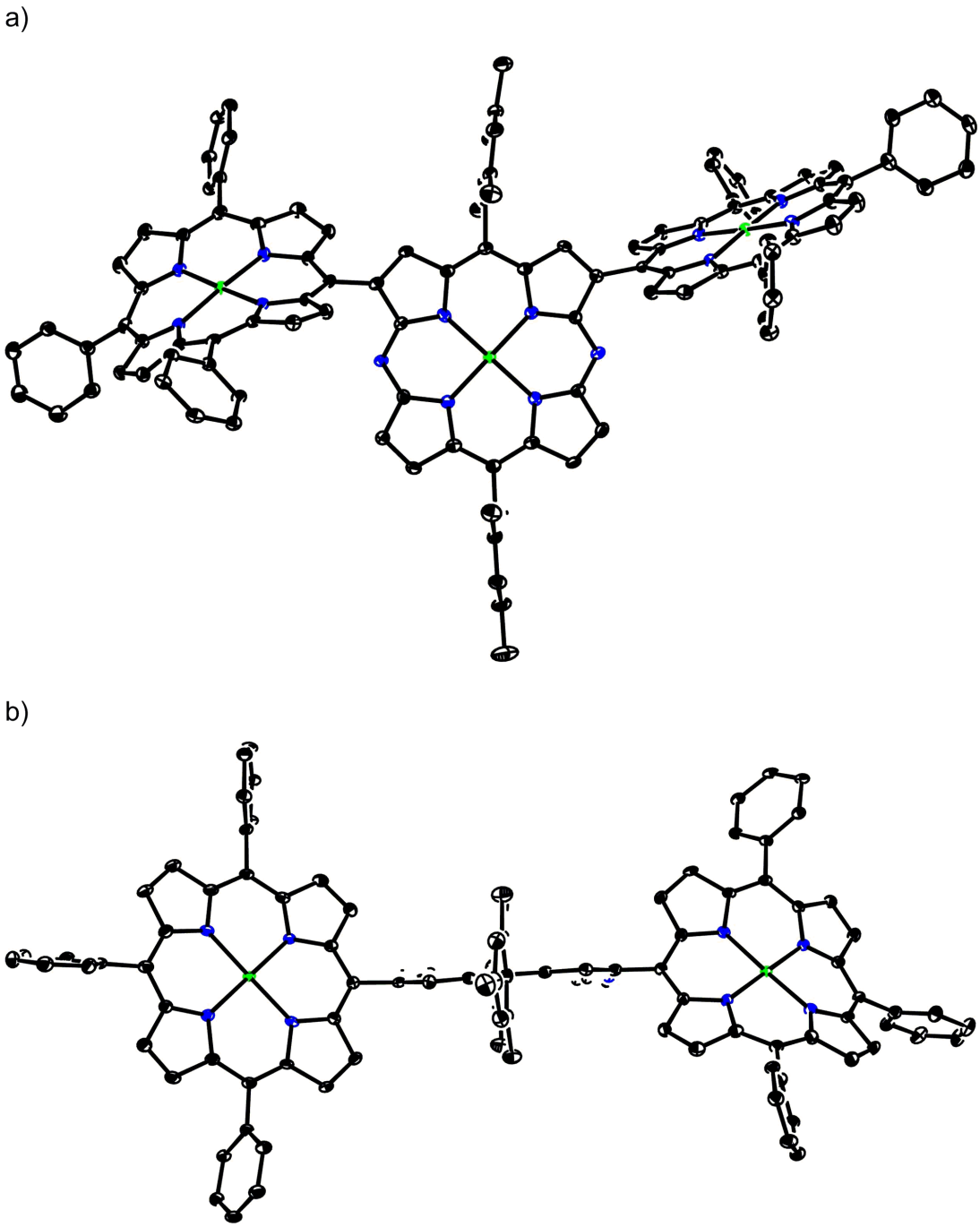

Figure S5-1. X-ray crystal structure of **3a**. a) Top view and b) side view. The thermal ellipsoids are scaled to 50% probability level. Solvent molecules, *tert*-butyl groups of *meso*-aryl substituents, and all hydrogen atoms are omitted for clarity.

Table S3-2. Crystal data and structure refinement for **3b**.

Identification code	3b
Empirical formula	$C_{160}H_{170}N_{14}Ni_3$
Formula weight	2465.22
Temperature/K	100.01(10)
Crystal system	triclinic
Space group	P-1
a/Å	12.1732(4)
b/Å	15.6437(3)
c/Å	24.1466(4)
α/°	72.6545(16)
β/°	80.455(2)
γ/°	79.266(2)
Volume/Å^3	4282.51(18)
Z	1
ρ_{calc}g/cm^3	0.956
μ/mm^{-1}	0.728
F(000)	1312.0
Crystal size/mm^3	0.2 × 0.2 × 0.1
Radiation	CuKα (λ = 1.54184)
2Θ range for data collection/°	9.95 to 133.196
Index ranges	-13 ≤ h ≤ 14, -18 ≤ k ≤ 18, -28 ≤ l ≤ 28
Reflections collected	61516
Independent reflections	15113 [R_{int} = 0.0566, R_{sigma} = 0.0475]
Data/restraints/parameters	15113/102/882
Goodness-of-fit on F^2	1.018
Final R indexes [I>=2σ (I)]	R_1 = 0.0604, wR_2 = 0.1527
Final R indexes [all data]	R_1 = 0.0729, wR_2 = 0.1605
Largest diff. peak/hole / e Å^{-3}	0.83/-0.43

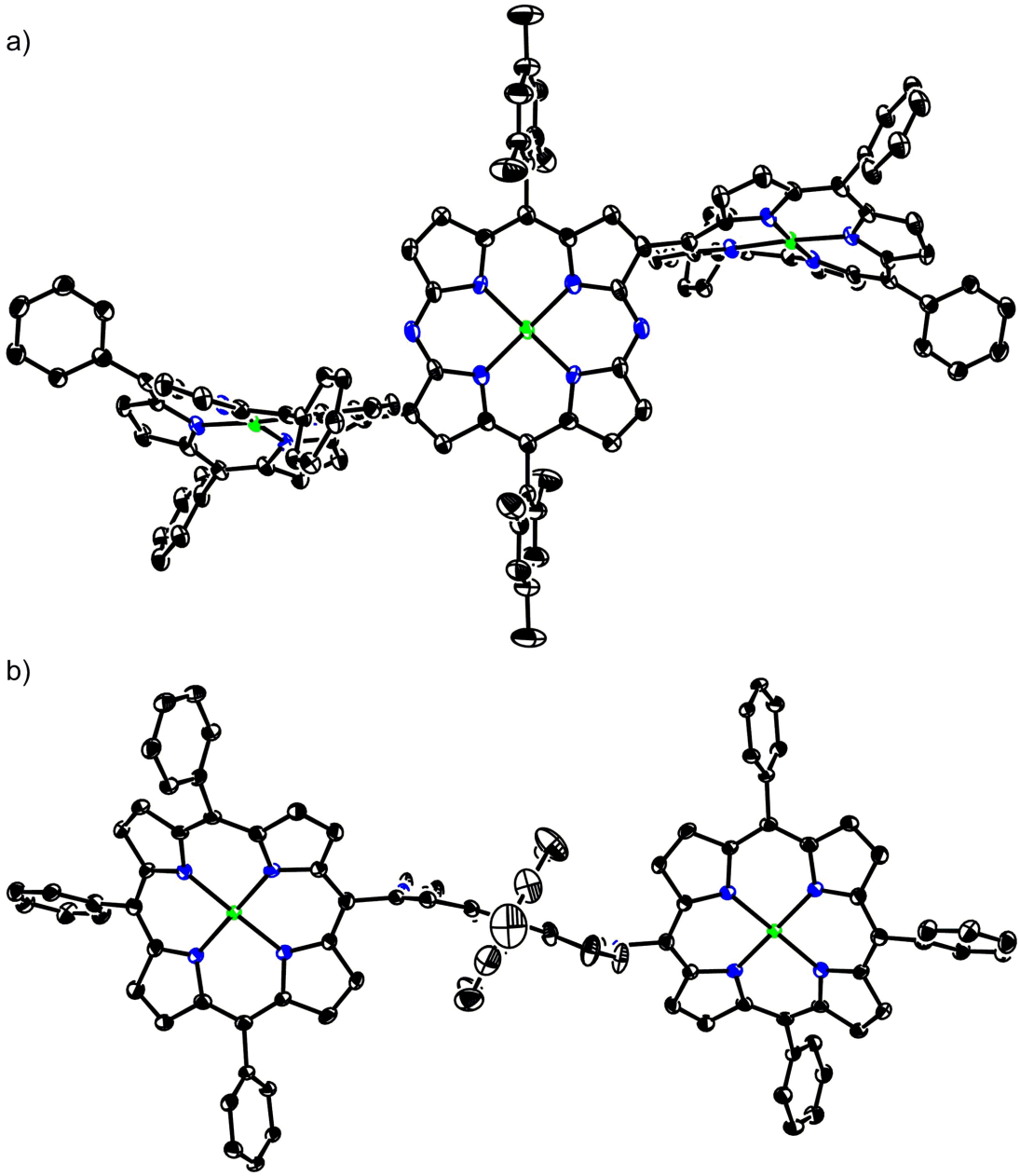

Figure S5-2. X-ray crystal structure of **3b**. a) Top view and b) side view. The thermal ellipsoids are scaled to 50% probability level. Solvent molecules, *tert*-butyl groups of *meso*-aryl substituents, and all hydrogen atoms are omitted for clarity.

Table S3-3. Crystal data and structure refinement for **4b**.

Identification code	4b
Empirical formula	$C_{160}H_{168}N_{14}Ni_3$
Formula weight	2463.20
Temperature/K	100.2(5)
Crystal system	monoclinic
Space group	P2/n
a/Å	16.4956(3)
b/Å	19.5137(8)
c/Å	27.9638(6)
α/°	90
β/°	98.4471(18)
γ/°	90
Volume/Å^3	8903.6(4)
Z	2
ρ_{calc}g/cm^3	0.919
μ/mm^{-1}	0.701
F(000)	2620.0
Crystal size/mm^3	0.2 × 0.05 × 0.02
Radiation	CuKα (λ = 1.54184)
2Θ range for data collection/°	7.062 to 133.198
Index ranges	-20≤ h≤ 20, -23≤ k≤ 23, -34≤ l≤ 33
Reflections collected	15742
Independent reflections	15742 [R_{int} = 0.0733, R_{sigma} = 0.0468]
Data/restraints/parameters	15742/0/818
Goodness-of-fit on F^2	1.126
Final R indexes [I>=2σ (I)]	R_1 = 0.0939, wR_2 = 0.2850
Final R indexes [all data]	R_1 = 0.1191, wR_2 = 0.3089
Largest diff. peak/hole / e Å^{-3}	2.00/-0.93

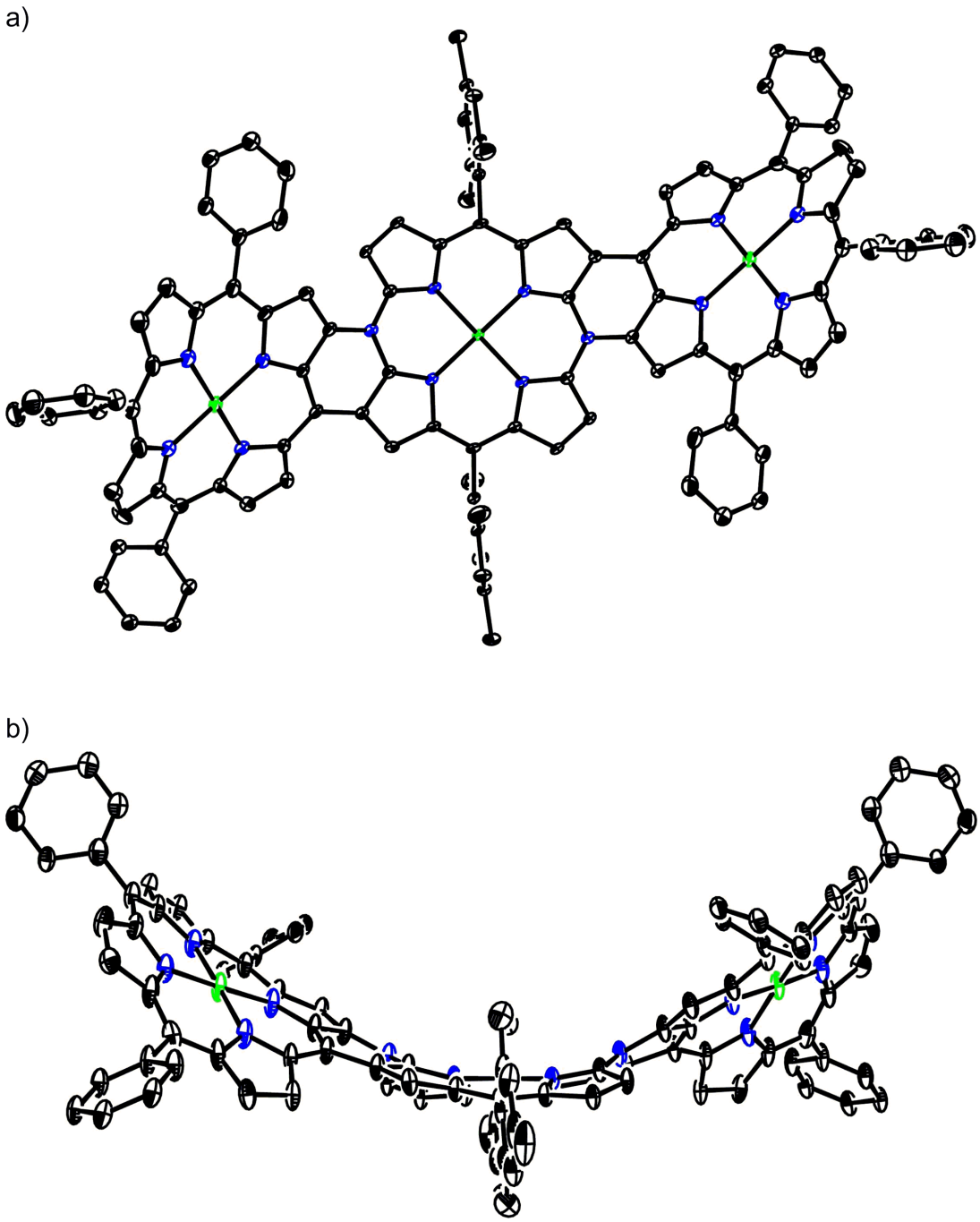

Figure S5-3. X-ray crystal structure of **4b**. a) Top view and b) side view. The thermal ellipsoids are scaled to 30% probability level. Solvent molecules, *tert*-butyl groups of *meso*-aryl substituents, and all hydrogen atoms are omitted for clarity.

Table S3-4. Crystal data and structure refinement for **5a**.

Identification code	5a
Empirical formula	$C_{160}H_{170}N_{14}Ni_3$
Formula weight	2465.22
Temperature/K	100.0(2)
Crystal system	monoclinic
Space group	$P2_1/n$
a/Å	20.2235(11)
b/Å	30.1037(7)
c/Å	27.7552(7)
α/°	90
β/°	108.649(4)
γ/°	90
Volume/Å^3	16010.2(11)
Z	4
ρ_{calc}g/cm^3	1.023
μ/mm^{-1}	0.779
F(000)	5248.0
Crystal size/mm^3	0.2 × 0.03 × 0.03
Radiation	CuKα (λ = 1.54184)
2Θ range for data collection/°	7.15 to 133.202
Index ranges	$-23 \leq h \leq 24$, $-20 \leq k \leq 35$, $-33 \leq l \leq 33$
Reflections collected	105696
Independent reflections	28255 [R_{int} = 0.0970, R_{sigma} = 0.0963]
Data/restraints/parameters	28255/321/1724
Goodness-of-fit on F^2	1.077
Final R indexes [I>=2σ (I)]	R_1 = 0.1127, wR_2 = 0.3239
Final R indexes [all data]	R_1 = 0.1710, wR_2 = 0.3921
Largest diff. peak/hole / e Å^{-3}	0.73/-0.59

a)

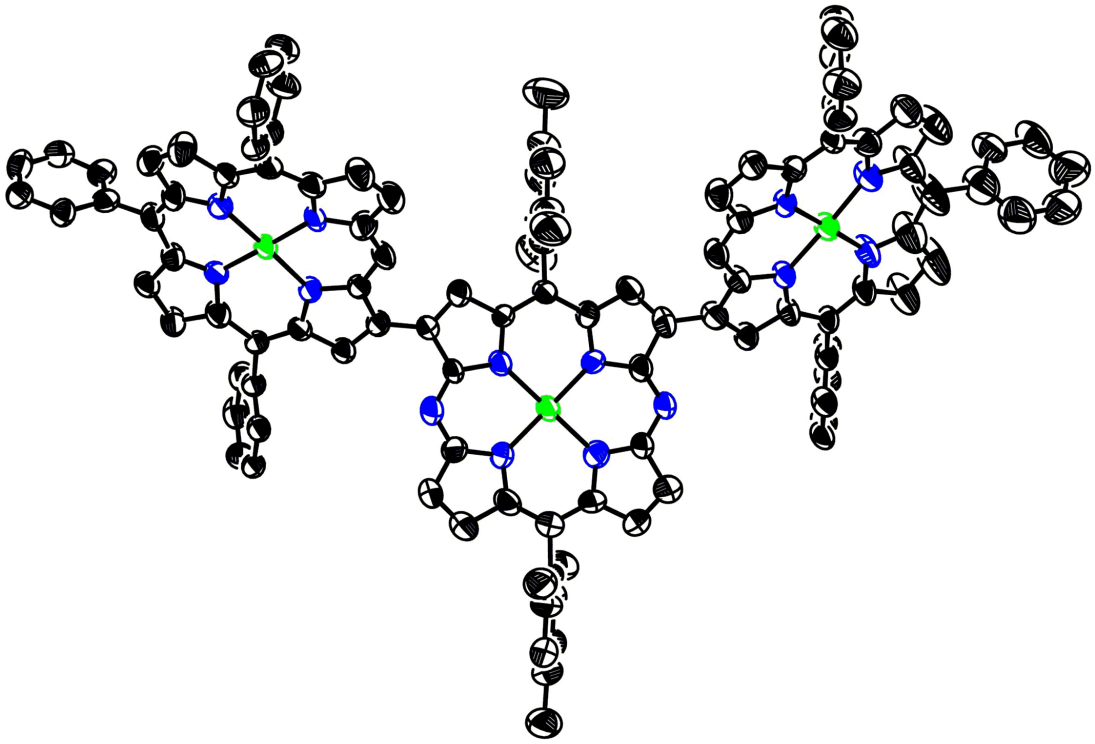

b)

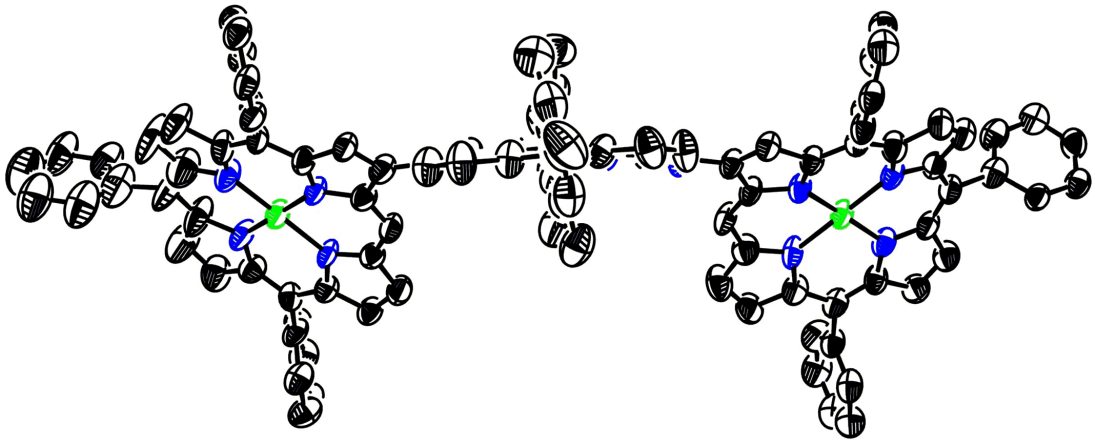

Figure S5-4. X-ray crystal structure of **5a**. a) Top view and b) side view. The thermal ellipsoids are scaled to 50% probability level. Solvent molecules, *tert*-butyl groups of *meso*-aryl substituents, and all hydrogen atoms are omitted for clarity.

Table S3-5. Crystal data and structure refinement for **5b**.

Identification code	5b
Empirical formula	$C_{160}H_{170}N_{14}Ni_3$
Formula weight	2465.22
Temperature/K	101(2)
Crystal system	triclinic
Space group	P-1
a/Å	11.99689(17)
b/Å	15.9669(2)
c/Å	23.9854(3)
α/°	73.5180(12)
β/°	89.4513(11)
γ/°	80.3482(12)
Volume/Å^3	4339.82(11)
Z	1
ρ_{calc}g/cm^3	0.943
μ/mm^{-1}	0.719
F(000)	1312.0
Crystal size/mm^3	0.3 × 0.2 × 0.05
Radiation	CuKα (λ = 1.54184)
2Θ range for data collection/°	7.48 to 133.2
Index ranges	$-13 \leq h \leq 14$, $-19 \leq k \leq 19$, $-28 \leq l \leq 28$
Reflections collected	61951
Independent reflections	15306 [R_{int} = 0.0450, R_{sigma} = 0.0328]
Data/restraints/parameters	15306/272/931
Goodness-of-fit on F^2	1.094
Final R indexes [I>=2σ (I)]	R_1 = 0.0625, wR_2 = 0.1625
Final R indexes [all data]	R_1 = 0.0658, wR_2 = 0.1652
Largest diff. peak/hole / e Å^{-3}	0.72/-0.53

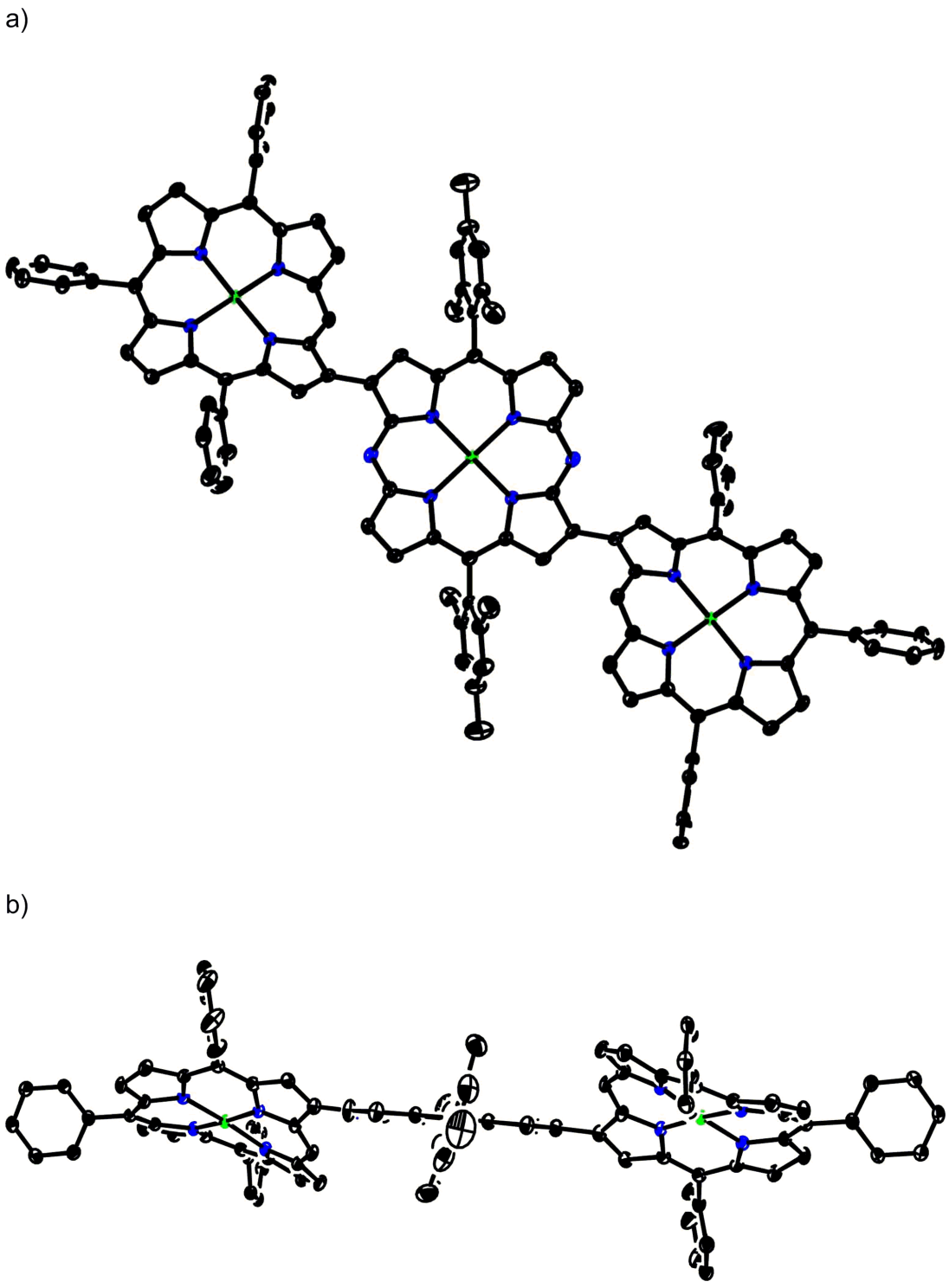

Figure S5-5. X-ray crystal structure of **5b**. a) Top view and b) side view. The thermal ellipsoids are scaled to 50% probability level. Solvent molecules, *tert*-butyl groups of *meso*-aryl substituents, and all hydrogen atoms are omitted for clarity.

Table S3-6. Crystal data and structure refinement for **6**.

Identification code	6
Empirical formula	$C_{160}H_{164}N_{14}Ni_3$
Formula weight	2459.17
Temperature/K	100.27(10)
Crystal system	triclinic
Space group	P-1
a/Å	19.5178(5)
b/Å	27.7250(9)
c/Å	28.7677(6)
α/°	104.436(2)
β/°	95.669(2)
γ/°	104.971(3)
Volume/Å^3	14340.6(7)
Z	3
ρ_{calc}g/cm^3	0.854
μ/mm^{-1}	0.653
F(000)	3918.0
Crystal size/mm^3	0.1 × 0.04 × 0.03
Radiation	CuKα (λ = 1.54184)
2Θ range for data collection/°	8.658 to 134.16
Index ranges	$-14 \leq h \leq 23$, $-33 \leq k \leq 33$, $-34 \leq l \leq 34$
Reflections collected	82935
Independent reflections	50539 [R_{int} = 0.0761, R_{sigma} = 0.1492]
Data/restraints/parameters	50539/195/2449
Goodness-of-fit on F^2	0.984
Final R indexes [I>=2σ (I)]	R_1 = 0.0983, wR_2 = 0.2607
Final R indexes [all data]	R_1 = 0.1492, wR_2 = 0.3045
Largest diff. peak/hole / e Å^{-3}	1.02/-0.65

a)

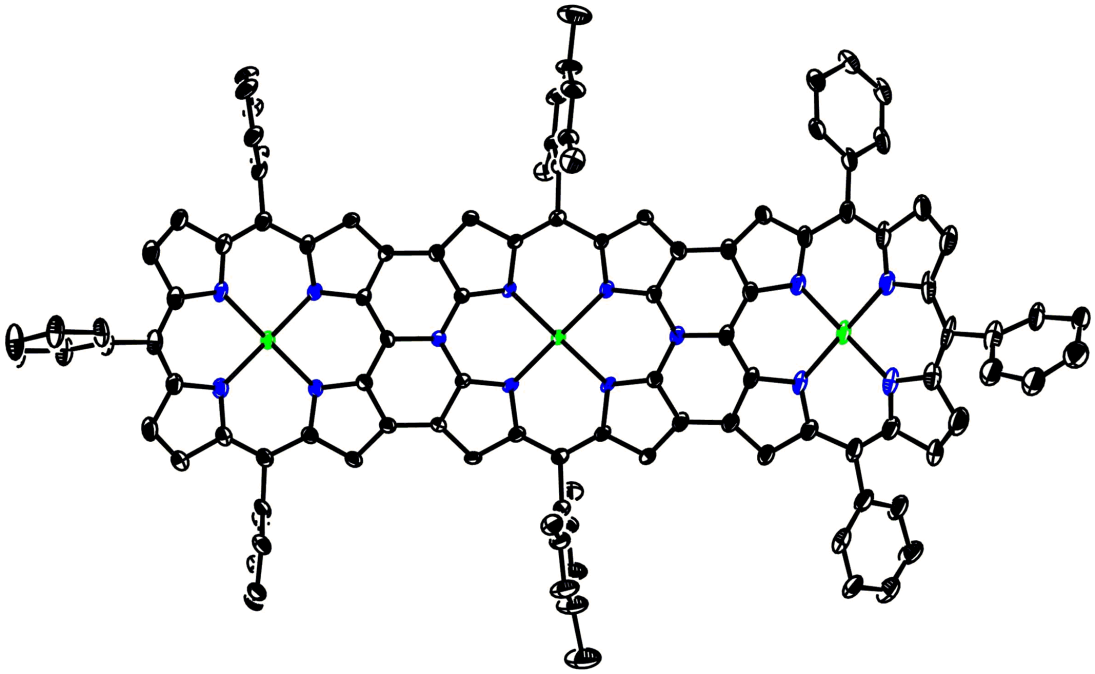

b)

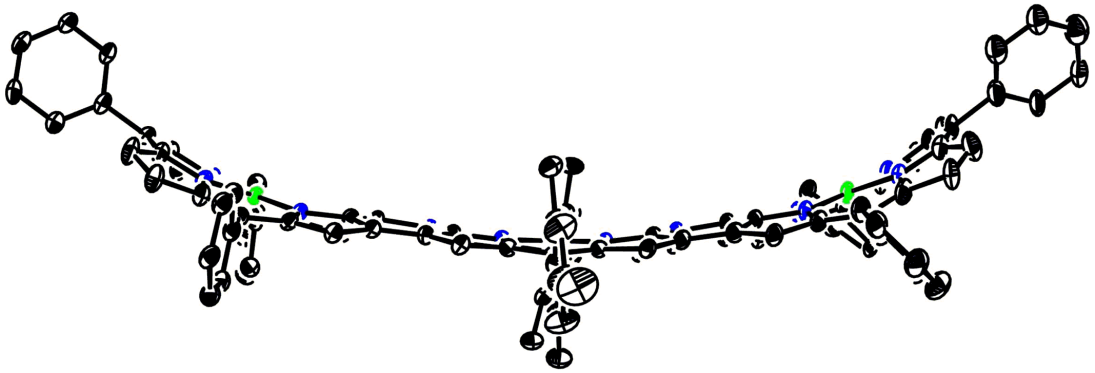

c)

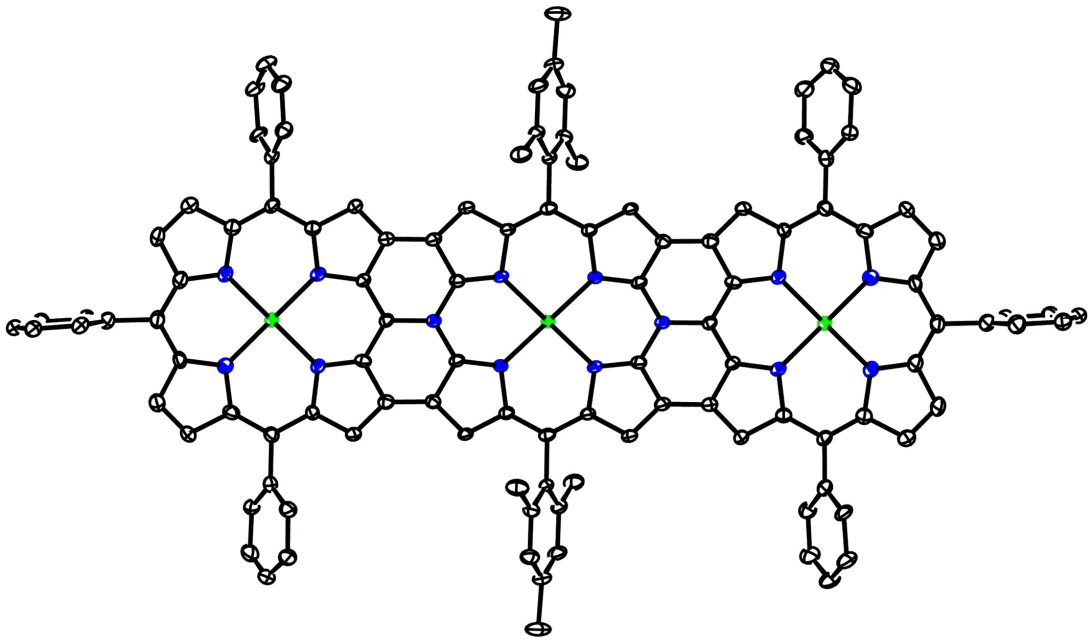

d)

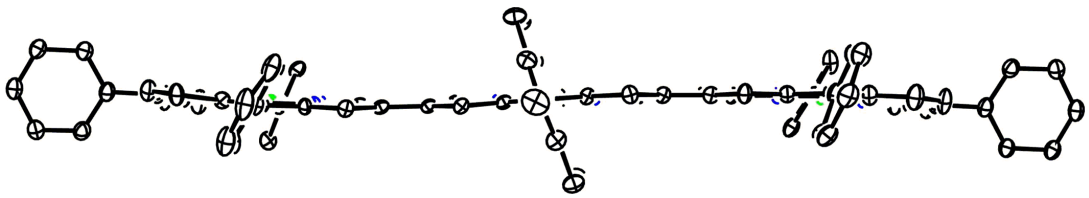

Figure S5-6. X-ray crystal structure of **6**. a) Top view and b) side view for one configuration of **6**; c) top view and d) side view for another configuration of **6**. The thermal ellipsoids are scaled to 30% probability level. Solvent molecules, *tert*-butyl groups of *meso*-aryl substituents, and all hydrogen atoms are omitted for clarity.

Table S3-7. Crystal data and structure refinement for **6-Cl**.

Identification code	6-Cl
Empirical formula	$C_{480}H_{487}Cl_3N_{42}Ni_9$
Formula weight	7478.83
Temperature/K	100.01(10)
Crystal system	triclinic
Space group	P-1
a/Å	19.8298(3)
b/Å	27.6668(4)
c/Å	28.8267(4)
α/°	104.2487(11)
β/°	96.2653(12)
γ/°	105.3083(13)
Volume/Å^3	14526.0(4)
Z	1
ρ_{calc}g/cm^3	0.855
μ/mm^{-1}	0.773
F(000)	3964.0
Crystal size/mm^3	0.3 × 0.08 × 0.08
Radiation	CuKα (λ = 1.54184)
2Θ range for data collection/°	8.202 to 133.202
Index ranges	$-23 \leq h \leq 23$, $-32 \leq k \leq 32$, $-34 \leq l \leq 34$
Reflections collected	302803
Independent reflections	51221 [R_{int} = 0.0734, R_{sigma} = 0.0668]
Data/restraints/parameters	51221/426/2621
Goodness-of-fit on F^2	0.959
Final R indexes [I>=2σ (I)]	R_1 = 0.0982, wR_2 = 0.2645
Final R indexes [all data]	R_1 = 0.1384, wR_2 = 0.2935
Largest diff. peak/hole / e Å^{-3}	1.15/-0.58

a)

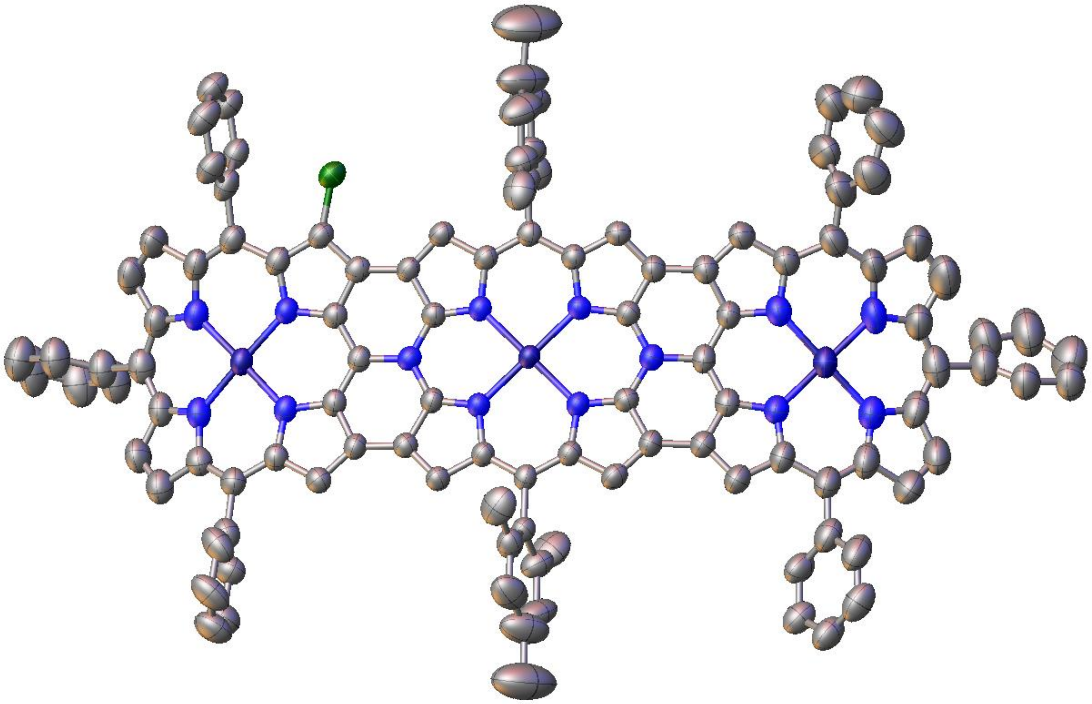

b)

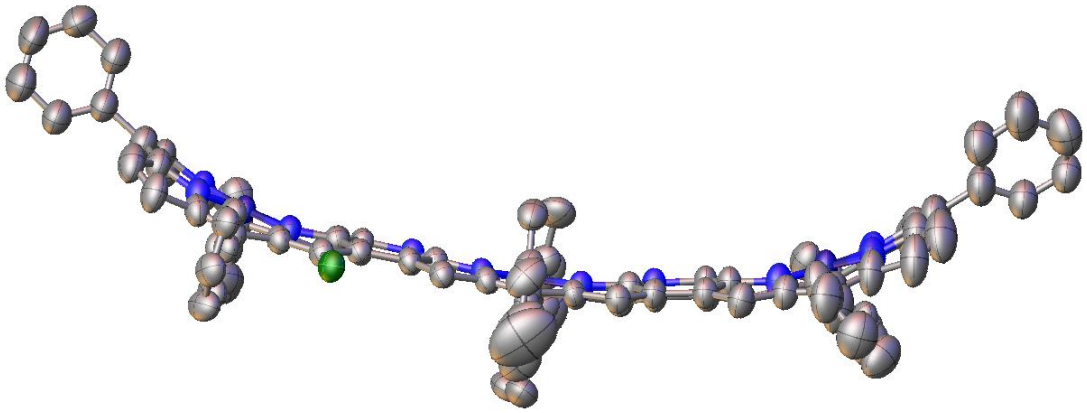

Figure S5-7. X-ray crystal structure of **6-Cl**. a) Top view and b) side view for one configuration of **6-Cl**. The thermal ellipsoids are scaled to 50% probability level. Solvent molecules, *tert*-butyl groups of *meso*-aryl substituents, and all hydrogen atoms are omitted for clarity.

Table S3-8. Crystal data and structure refinement for **15**.

Identification code	15
Empirical formula	$C_{128}H_{122}Cl_5F_6N_{10}Ni_2Sb$
Formula weight	2330.77
Temperature/K	100.01(10)
Crystal system	triclinic
Space group	P-1
a/Å	16.6924(4)
b/Å	19.0219(5)
c/Å	21.9272(6)
α/°	80.695(2)
β/°	71.430(2)
γ/°	72.720(2)
Volume/Å^3	6284.6(3)
Z	2
ρ_{calc}g/cm^3	1.232
μ/mm^{-1}	3.485
F(000)	2412.0
Crystal size/mm^3	0.3 × 0.3 × 0.3
Radiation	CuKα (λ = 1.54184)
2Θ range for data collection/°	4.878 to 133.2
Index ranges	$-19 \leq h \leq 15$, $-22 \leq k \leq 21$, $-26 \leq l \leq 22$
Reflections collected	41474
Independent reflections	22203 [R_{int} = 0.0480, R_{sigma} = 0.0711]
Data/restraints/parameters	22203/542/1462
Goodness-of-fit on F^2	1.033
Final R indexes [I>=2σ (I)]	R_1 = 0.1035, wR_2 = 0.2774
Final R indexes [all data]	R_1 = 0.1193, wR_2 = 0.2938
Largest diff. peak/hole / e Å^{-3}	3.85/-2.76

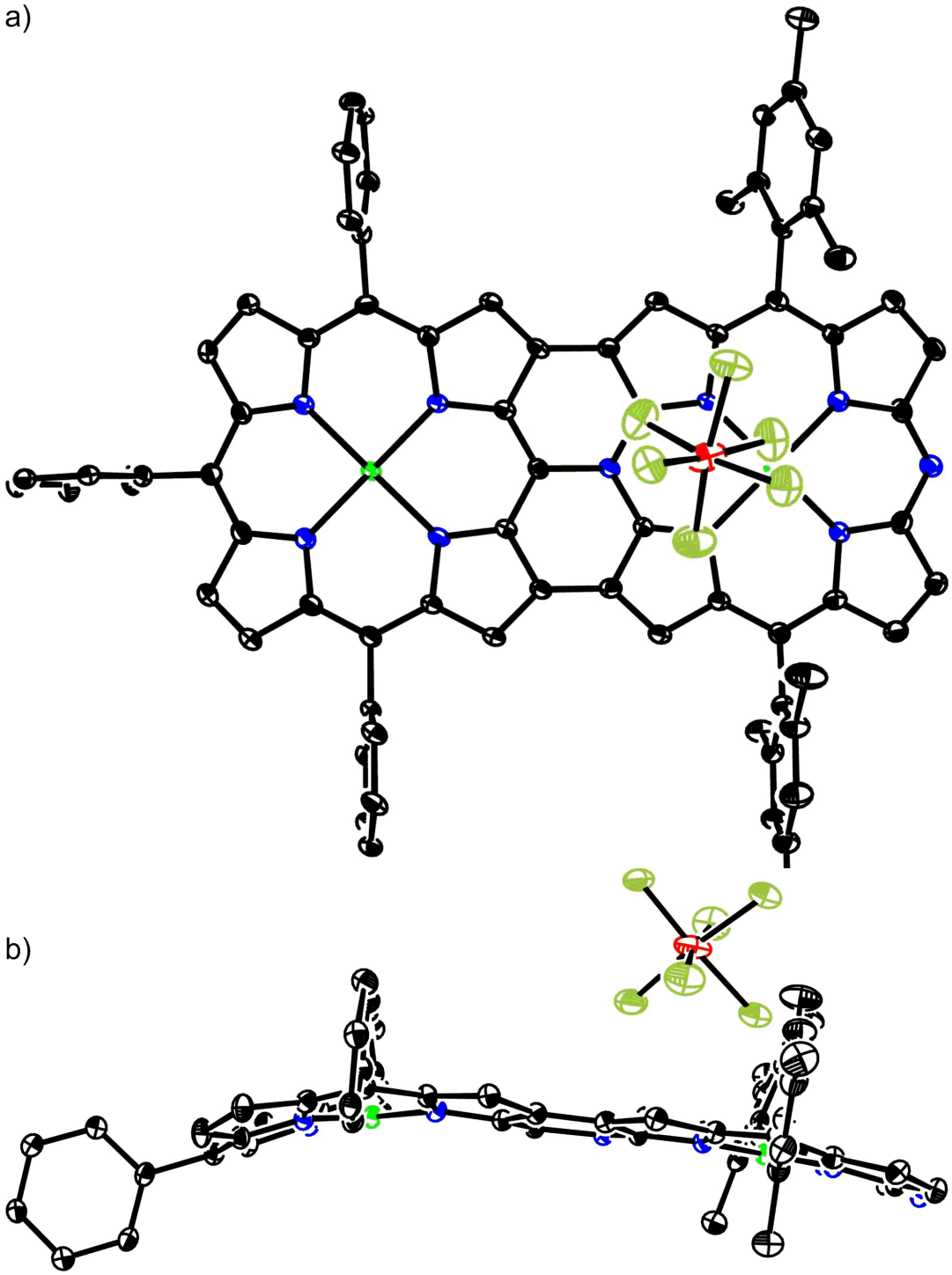

Figure S5-8. X-ray crystal structure of **15**. a) Top view and b) side view. The thermal ellipsoids are scaled to 30% probability level. Solvent molecules, *tert*-butyl groups of *meso*-aryl substituents, and all hydrogen atoms are omitted for clarity.

8. DFT Calculations

All calculations were carried out using the Gaussian 09 program.[9] Initial geometries of **4a**, **4b**, **6** and **10** were from corresponding X-ray structures. Structures were optimized without any symmetry restriction. Geometry optimizations in the ground state were performed by the density functional theory (DFT) with B3LYP (Becke's three-parameter hybrid exchange functionals and the Lee-Yang-Parr correlation functional)[10] level employing a basis set of 6-31G(d) for all of the atoms. The nucleus independent chemical shifts (NICS) values were obtained with the GIAO method based on the optimized structures. All of the Bq atoms (noted as A-Z) were placed in the geometrical center of the five- or six-membered rings.

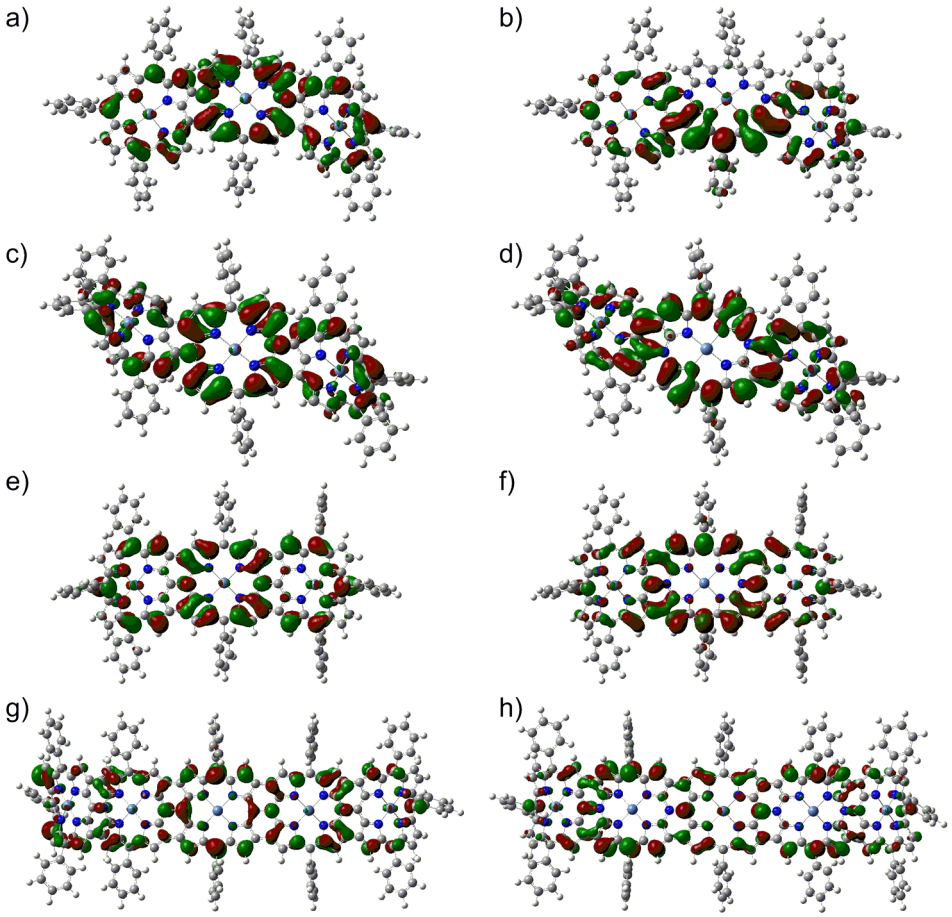

Figure S6-1. Molecular orbital diagrams of **4a**, **4b**, **6** and **10**. a) HOMO and b) LUMO of **4a**; c) HOMO and d) LUMO of **4b**; e) HOMO and f) LUMO of **6**; g) HOMO and h) LUMO+1 of **10**. 3,5-Di-*tert*-butylphenyl and 2,4,6-trimethylphenyl are replaced by phenyl for simplification.

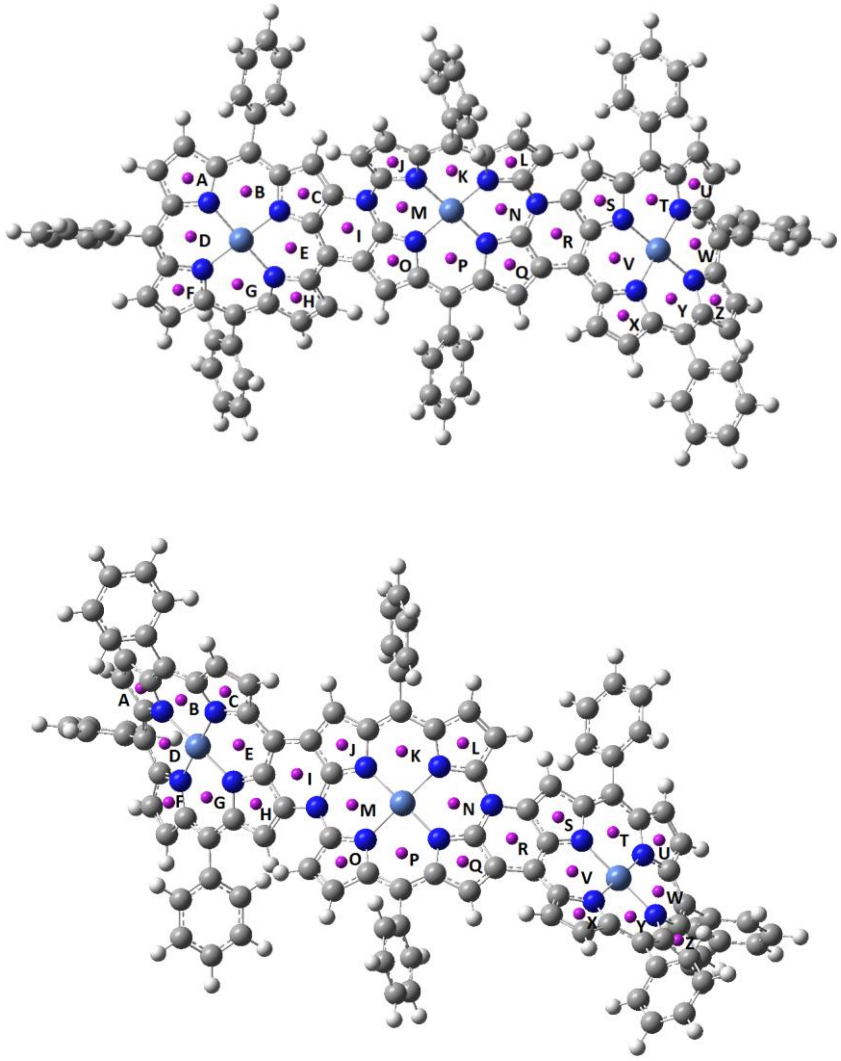

	A	B	C	D	E	F	G	H	I	J	K	L	M
4a	-5.51	-17.23	-10.34	-16.73	-16.42	-6.32	-16.39	-6.98	-1.00	-5.07	-1.96	-5.17	1.47
4b	-6.23	-16.61	-7.00	-16.81	-16.51	-5.56	-17.29	-10.53	-0.97	-5.99	1.58	-4.25	0.82
	N	**O**	**P**	**Q**	**R**	**S**	**T**	**U**	**V**	**W**	**X**	**Y**	**Z**
4a	1.06	-5.03	2.13	-4.62	-0.89	-9.89	-17.10	-5.79	-16.37	-16.86	-6.94	-16.38	-6.11
4b	0.88	-4.16	1.59	-5.89	-1.07	-10.55	-17.21	-5.57	-16.61	-16.83	-6.97	-16.72	-6.43

Figure S6-2. Calculated NICS(0) values of **4a** and **4b**.

9. References

[1] O. V. Dolomanov, L. J. Bourhis, R. J. Gildea, J. A. K. Howard and H. Puschmann, *J. Appl. Cryst.*, 2009, **42**, 339.

[2] L. J. Bourhis, O. V. Dolomanov, R. J. Gildea, J. A. K. Howard and H. Puschmann, *Acta Cryst.*, 2015, **A71**, 59.

[3] L. Palatinus and G. Chapuis, *J. Appl. Cryst.*, 2007, **40**, 786.

[4] M. C. Burla, R. Caliandro, M. Camalli, B. Carrozzini, G. L. Cascarano, L. De Caro, C.

Giacovazzo, G. Polidori and R. Spagna, *J. Appl. Cryst.*, 2005, **38**, 381.
[5] G. M. Sheldrick, *Acta Cryst.*, 2015, **A71**, 3.
[6] G. M. Sheldrick, *Acta Cryst.*, 2008, **A64**, 112.
[7] G. M. Sheldrick, *Acta Cryst.*, 2015, **C71**, 3.
[8] A. L. Spek, *Acta Cryst.*, 2009, **D65**, 148.
[9] Gaussian 09, Revision D.01, M. J. Frisch, G. W. Trucks, H. B. Schlegel, G. E. Scuseria, M. A. Robb, J. R. Cheeseman, G. Scalmani, V. Barone, B. Mennucci, G. A. Petersson, H. Nakatsuji, M. Caricato, X. Li, H. P. Hratchian, A. F. Izmaylov, J. Bloino, G. Zheng, J. L. Sonnenberg, M. Hada, M. Ehara, K. Toyota, R. Fukuda, J. Hasegawa, M. Ishida, T. Nakajima, Y. Honda, O. Kitao, H. Nakai, T. Vreven, J. A. Jr. Montgomery, J. E. Peralta, F. Ogliaro, M. Bearpark, J. J. Heyd, E. Brothers, K. N. Kudin, V. N. Staroverov, T. Keith, R. Kobayashi, J. Normand, K. Raghavachari, A. Rendell, J. C. Burant, S. S. Iyengar, J. Tomasi, M. Cossi, N. Rega, J. M. Millam, M. Klene, J. E. Knox, J. B. Cross, V. Bakken, C. Adamo, J. Jaramillo, R. Gomperts, R. E. Stratmann, O. Yazyev, A. J. Austin, R. Cammi, C. Pomelli, J. W. Ochterski, R. L. Martin, K. Morokuma, V. G. Zakrzewski, G. A. Voth, P. Salvador, J. J. Dannenberg, S. Dapprich, A. D. Daniels, O. Farkas, J. B. Foresman, J. V. Ortiz, J. Cioslowski, D. J. Fox, Gaussian, Inc., Wallingford CT, 2013.
[10] (a) A. D. Becke, *J. Chem. Phys.*, 1993, **98**, 1372. (b) C. Lee, W. Yang and R. G. Parr, *Phys. Rev. B*, 1998, **37**, 785.